

Review

# Photocatalytic TiO<sub>2</sub>-Based Nanostructures as a Promising Material for Diverse Environmental Applications: A Review

Maria-Anna Gatou <sup>1,\*</sup>, Athanasia Syrrakou <sup>1</sup>, Nefeli Lagopati <sup>2,3</sup>  and Evangelia A. Pavlatou <sup>1,\*</sup> 

<sup>1</sup> Laboratory of General Chemistry, School of Chemical Engineering, National Technical University of Athens, Zografou Campus, 15772 Athens, Greece; a\_syrrakou@mail.ntua.gr

<sup>2</sup> Laboratory of Biology, Department of Basic Medical Sciences, Medical School, National and Kapodistrian University of Athens, 11527 Athens, Greece; nlagopati@med.uoa.gr

<sup>3</sup> Biomedical Research Foundation, Academy of Athens, 11527 Athens, Greece

\* Correspondence: mgatou2@mail.ntua.gr (M.-A.G.); pavlatou@chemeng.ntua.gr (E.A.P.); Tel.: +30-210-7724034 (M.-A.G.); +30-210-7723110 (E.A.P.)

**Abstract:** Contemporary technological and industrial advancements have led to increased reliance on chemicals for product innovation, leading to heightened contamination of water sources by traditional pollutants (organic dyes, heavy metals) and disease-causing microorganisms. Wastewater treatment processes now reveal “emerging pollutants”, including pharmaceuticals, endocrine disruptors, and agricultural chemicals. While some are benign, certain emerging pollutants can harm diverse organisms. Researchers seek cost-effective water purification methods that completely degrade pollutants without generating harmful by-products. Semiconductor-based photocatalytic degradation, particularly using titanium dioxide (TiO<sub>2</sub>), is popular for addressing water pollution. This study focuses on recent applications of TiO<sub>2</sub> nanostructures in photocatalysis for eliminating various water pollutants. Structural modifications, like doping and nanocomposite formation, enhance photocatalyst performance. The study emphasizes photocatalytic elimination mechanisms and comprehensively discusses factors impacting both the mechanism and performance of nano-TiO<sub>2</sub>-based photocatalysts. Characteristics of TiO<sub>2</sub>, such as crystal structure and energy band-gap, along with its photocatalytic activity mechanism, are presented. The review covers the advantages and limitations of different TiO<sub>2</sub> nanostructure production approaches and addresses potential toxicity to human health and the environment. In summary, this review provides a holistic perspective on applying nano-TiO<sub>2</sub> materials to mitigate water pollution.

**Keywords:** titanium dioxide; nanostructures; synthesis methods; photocatalytic mechanism; dyes; heavy metals; pesticides; microbes; environmental applications; toxicity



**Citation:** Gatou, M.-A.; Syrrakou, A.; Lagopati, N.; Pavlatou, E.A. Photocatalytic TiO<sub>2</sub>-Based Nanostructures as a Promising Material for Diverse Environmental Applications: A Review. *Reactions* **2024**, *5*, 135–194. <https://doi.org/10.3390/reactions5010007>

Academic Editors: Annalisa Volpe, Caterina Gaudiuso and Maria Chiara Sportelli

Received: 4 January 2024

Revised: 19 January 2024

Accepted: 29 January 2024

Published: 1 February 2024



**Copyright:** © 2024 by the authors. Licensee MDPI, Basel, Switzerland. This article is an open access article distributed under the terms and conditions of the Creative Commons Attribution (CC BY) license (<https://creativecommons.org/licenses/by/4.0/>).

## 1. Introduction

The World Water Development Report (2020) [1] underscores the critical environmental priority of protecting water reserves amidst global climate change challenges. Currently, natural aquatic environments face vulnerability to various hazardous substances from multiple sources, including civic society, the public sector and, notably, industrial activities.

Various industries (textile, pharmaceutical, agricultural, papermaking, printing, cosmetics, and food processing) generate extensive wastewater laden with diverse organic pollutants, such as pharmaceuticals, dyes, heavy metals, endocrine disruptors (EDCs), pesticides, and herbicides, leading to contamination. Additionally, water contamination results from a multitude of microorganisms thriving in raw household sewage, containing fecal matter and other decomposable substances. This conducive environment for microbial proliferation contributes to the onset and transmission of diseases. Notably, prevalent waterborne bacteria, like *Escherichia coli*, originating from the excrement of both farm animals and humans, cause ailments like diarrhea, renal failure, colitis, and hemolytic uremic syndrome [2]. *Salmonella*, inducing illnesses such as typhoid fever and salmonellosis [3],

and cholera, caused by *Vibrio cholera*'s cholera toxin production [4], are severe diseases. Bacterial pathogens, like *Pseudomonas aeruginosa*, contribute to conditions like diarrhea and Shanghai fever [5], while Legionella, a primary agent in transmitting Legionnaire's disease [6], can proliferate in water sources.

Several treatment methods, including chemical precipitation, separation, adsorption, coagulation, biological treatment, and Fenton oxidation techniques, are currently employed [7]. Despite their application, these methods often result in partial pollutant degradation, transferring contaminants between phases and producing secondary by-products requiring additional treatment [8,9]. Biological treatment, reliant on microbial metabolism [10–12], is reliable, cost-effective, and safe but exhibits lower efficacy in suspended solids removal, necessitating improved operational management. Coagulation and precipitation methods form flocs using polymer or inorganic coagulants (e.g., Fe, Al), aiding pollutant coagulation for subsequent removal through water-soluble metal salts, pH adjustment, or polymer coagulants producing sludge flocs to effectively precipitate or separate solids from wastewater [13–15]. While these techniques enhance treatment effectiveness, chemical use raises environmental concerns, and the resulting biological sludge contributes to pipe blockages and water quality deterioration. Fenton oxidation, leveraging Fenton's reagent for oxidative capabilities, generates hydroxyl radicals ( $\bullet\text{OH}$ ) through hydrogen peroxide and iron salt reactions [16–20]. This involves minimal additional device use compared to other oxidation methods, making it easy to implement. However, drawbacks include significant sludge generation and increased operating expenses for subsequent processing.

Currently, there is a growing emphasis on advanced oxidation processes (AOPs) utilizing semiconductor materials as a promising alternative to conventional methods [21]. These processes offer advantages, such as simplified equipment requirements, indiscriminate oxidation, straightforward operational management, cost efficiency, and comprehensive decomposition of organic dyes into harmless byproducts [22]. A unique aspect of AOPs involves the generation of reactive species, like  $\bullet\text{OH}$  radicals, enabling rapid and indiscriminate oxidation of organic, inorganic, and biological contaminants. Heterogeneous photocatalysis, employing oxide-based nanomaterials, is particularly effective in eliminating water-soluble pollutants from both water and wastewater under light exposure [23].

Metal oxide semiconductors, like titanium dioxide ( $\text{TiO}_2$ ), demonstrate enhanced adsorption ability and act as effective catalysts due to increased reactivity, high photosensitivity, extensive specific surface area, cost-efficiency, non-toxicity, and biocompatibility [24].  $\text{TiO}_2$ , notably one of the most widely used photocatalysts, owes its extensive utilization to advantageous characteristics, including heightened photocatalytic activity, chemical stability, cost-effectiveness, and abundance [25,26]. Existing in crystal structures, like anatase and rutile,  $\text{TiO}_2$  exhibits distinct band-gaps and surface attributes, significantly influencing its photocatalytic activity and selectivity. Anatase  $\text{TiO}_2$  is generally recognized as the most active among these structures [26,27]. Given their widespread application and exploration,  $\text{TiO}_2$ -based nanostructures have undergone diverse means of optimization and chemical modifications to enhance efficiency and broaden their application scope. Efforts have particularly focused on improvement in  $\text{TiO}_2$ 's absorption of visible light through doping with non-metal or transition metal ions, combination with other semiconductor materials or deposition of noble metal nanoparticles with a surface plasmonic resonance (SPR) effect [28–30].

This review comprehensively summarizes recent advancements in applying  $\text{TiO}_2$  nanostructures for photocatalytic water and wastewater remediation. It specifically explores the photocatalytic remediation of various pollutants commonly found in urban water and wastewater samples, highlighting the mechanisms involved, and addressing a breadth of pollutants not extensively covered in recent reviews. Additionally, the present review elucidates the benefits and drawbacks of common synthetic approaches to fabricating  $\text{TiO}_2$  nanostructures and provides insights into the overall characteristics of titanium dioxide. Lastly, the toxicity mechanism of titanium dioxide nanostructures is thoroughly discussed.

## 2. Overview of TiO<sub>2</sub>'s Characteristics

### 2.1. Structural Properties

Titanium dioxide encompasses eight crystal phases: rutile, anatase, brookite, TiO<sub>2</sub>-B (monoclinic) [31], TiO<sub>2</sub>-R (ramsdellite) [32], TiO<sub>2</sub>-H (hollandite) [33], TiO<sub>2</sub>-II (columbite) [34], and TiO<sub>2</sub>-III (baddeleyite) [35–37]. Rutile, anatase, and brookite have primarily attracted attention in research and applications due to their natural occurrence under atmospheric pressure [38,39]. While other phases have been investigated, their formation involves high pressure, limiting practical significance [40,41]. Each crystal structure features distinct atomic arrangements, with titanium atoms in anatase, rutile, and brookite forming an octahedral coordination with oxygen [42]. Despite similarities, the configuration of TiO<sub>6</sub> octahedra varies across phases (Figure 1).

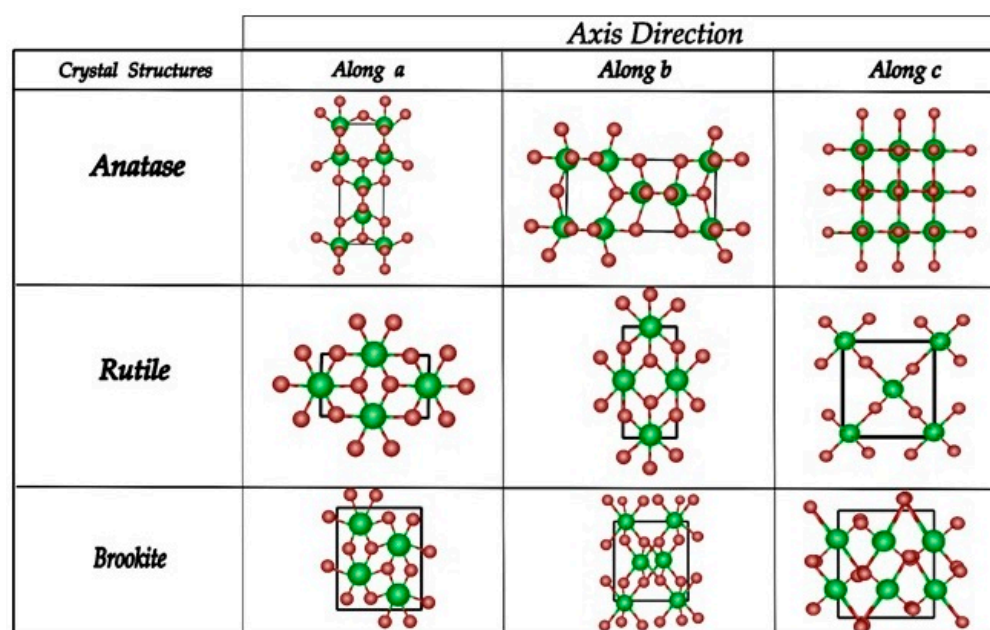


**Figure 1.** Anatase, rutile and brookite TiO<sub>2</sub> crystal structure along a, b and c axis directions. Green is used to indicate Ti atoms, while red is utilized for O atoms [43].

Anatase, with a tetragonal lattice in the I4<sub>1</sub>/Amd space group (space group number 141), exhibits lattice parameters  $a = b = 3.785 \text{ \AA}$  and  $c = 9.514 \text{ \AA}$ . Despite the lowest thermodynamic stability among the three TiO<sub>2</sub> polymorphs, anatase's TiO<sub>6</sub> octahedra form a 3D framework, with O atoms positioned at the vertices through corner-sharing. As a result, a corner-sharing pattern is established as each O atom is shared between two octahedra. Rutile, the most robust for unit sizes  $> 14 \text{ nm}$  [44], adopts a tetragonal lattice (P4<sub>2</sub>/mm space group, space group number 136) with lattice parameters  $a = b = 4.593 \text{ \AA}$  and  $c = 2.958 \text{ \AA}$ . Its TiO<sub>6</sub> units with a slight orthorhombic distortion [45], and in an edge-sharing configuration, form chains along the c-axis, interconnected by shared vertices, thus constructing a 3D network. This leads to a more densely packed structure than that of anatase. Brookite, less prevalent, has an orthorhombic lattice (Pbc2<sub>1</sub> space group, space group number 29) with lattice parameters  $a = 5.502 \text{ \AA}$ ,  $b = 8.942 \text{ \AA}$ , and  $c = 5.144 \text{ \AA}$ . Similar to rutile, brookite's TiO<sub>6</sub> octahedra connect via edge-sharing, forming chains along the c-axis. However, brookite displays a more distorted arrangement and decreased symmetry compared to rutile [43].

XRD is commonly utilized by researchers to identify the prevalent TiO<sub>2</sub> polymorphs. Anatase shows characteristic peaks at  $\theta$  values (diffraction angles) of 12.65°, 18.9°, and 24.05°. Rutile's peaks appear at  $\theta = 13.75^\circ$ , 18.1°, and 27.2°, and brookite's peaks are located at  $\theta$  values of 12.65°, 12.85°, 15.4°, and 18.1° [46].

## 2.2. Energy Band-Gap ( $E_g$ )

A scholarly discourse is taking place concerning the band-gap characteristics of the three as-mentioned  $\text{TiO}_2$  polymorphs, due to various imperfections. The band-gap within titanium dioxide originates from the arrangement of electrons in both Ti and O atoms. Across all three polymorphs of titanium dioxide, the valence band (VB) mainly comprises O 2p orbitals, while the conduction band (CB) primarily consists of Ti 3d orbitals [47,48]. The most increased point of the VB resides at the  $\Gamma$  point within the Brillouin zone, while the lowest point of the CB sits at the X point. The band-gap of titanium dioxide is termed 'direct', indicating that the transition of an  $e^-$  from the VB to the CB does not require a conservation of momentum. However, there are suggestions in some studies of the indirect character of the  $\text{TiO}_2$ 's band-gap, possibly due to the separation of O 2p and Ti 3d orbitals brought about by the crystal field from six O atoms [42,49]. This separation leads to a displacement of the CB, concerning momentum in relation to the VB. In all three titanium dioxide polymorphs, defects, as well as foreign elements, can create specific points inside the band-gap, influencing the material's electronic characteristics. For instance, O vacancies may incorporate states close to the CB in anatase titanium dioxide, consequently heightening its photocatalytic capability. Correspondingly, the inclusion of transition metals can incorporate states adjacent to the VB or CB, thereby modifying the material's electronic features [50,51]. Moreover, the characteristics of  $\text{TiO}_2$ 's electrons are notably impacted by defects and foreign elements, such as oxygen vacancies that contribute to the material's n-type doping. These anomalies additionally have the potential to alter the band-gap properties, with indications supporting the notion that oxygen vacancies may generate specific points inside the band-gap in anatase, as well as in rutile titanium dioxide [52–54].

Despite the fact that it is widely acknowledged that anatase titanium dioxide possesses a direct band-gap ranging from 3.2 to 3.26 eV, conflicting studies exist regarding the band-gap's nature (ranging from 2.8 to 3.0 eV) in rutile titanium dioxide. Absorption thresholds are observed at 384 nm for anatase and 410 nm for rutile [55]. Some research studies have indicated an indirect band-gap in rutile  $\text{TiO}_2$ , while others propose the presence of a direct band-gap transition close to 3 eV. The brookite phase exhibits a barely decreased band-gap ( $\approx 2.9$  eV). Additionally, the absorption thresholds differ among these phases, as the anatase phase absorbs light within the UV region, whereas the rutile and brookite phases tend to absorb light within the visible region [56].

## 2.3. Robustness and Phase Shift

In comparison to other phases, rutile stands as the most robust form of  $\text{TiO}_2$ , displaying exceptional resistance to decomposition or phase alterations, even under extremely increased temperatures. Nevertheless, metastable phases, like anatase and brookite, are able to transform into the more thermodynamically robust rutile through calcination at specific temperatures. Numerous studies have delved into the mechanism behind  $\text{TiO}_2$  phase transitions during calcination. According to [57], the transition process from anatase to rutile involves nucleation and subsequent growth. Initially, rutile nuclei form on the surface of anatase, progressively expanding into the bulk. Given the substantial differences between anatase and rutile, the transformation necessitates the breakage and reformation of bonds [58]. As anatase transitions to rutile, the {112} planes of anatase persist as the {100} planes in inaugurally formed rutile. This transition involves rearranging Ti and O atoms within these planes through the relocation of Ti atoms to form rutile by the rupture of two Ti–O bonds in the  $\text{TiO}_6$  octahedron. Consequently, the creation of O vacancies accelerates the transformation, while Ti interstitials impede it. This shift from anatase to rutile represents a non-equilibrium phase transition, typically occurring within a certain temperature range (400–1000 °C). The calcination temperature significantly impacts product impurities, size of particles, and the specific surface area during this transformation process. The presence of impurities and the processing atmosphere notably affect defect structures, influencing both temperature and phase transition rate. In general, impurities such as Li, K, Na, Fe, Ce, and Mn oxides tend to stimulate phase transformation through the enhancement

of oxygen vacancies, whereas impurities such as S, P, and W tend to hinder it. Reductive atmospheres, like H<sub>2</sub> and Cl<sub>2</sub>, facilitate the transformation, while conducive atmospheres restrain it by promoting the formation of Ti interstitials [58].

The artificial synthesis process is instrumental in producing anatase nanoparticles, particularly when synthesizing TiO<sub>2</sub> in an aqueous solution [59]. This choice is influenced by the close energy levels among the aforementioned titanium dioxide phases. When nanoparticles are sufficiently small (<13 nm), their minimal surface free energy becomes crucial in determining phase transformations [60]. Anatase remains the most stable phase for nano-TiO<sub>2</sub> crystals <11 nm, while the rutile phase demonstrates thermodynamic stability for nanocrystals larger than 35 nm. Brookite, positioned between anatase and rutile, exhibits intermediate stability. Functioning as a metastable phase, brookite shares physical attributes that fall between those of anatase and rutile [60].

#### 2.4. Other Features

The anatase phase exhibits elevated charge carrier concentrations, as opposed to the rutile and brookite phases, credited to its larger specific surface area, as well as increased quantity of O vacancies. Normally, the charge carrier concentration within titanium dioxide falls approximately between 10<sup>16</sup> and 10<sup>21</sup> cm<sup>-3</sup> [61–64]. These distinct characteristics render each phase appropriate for diverse applications. More specifically, the anatase phase finds common use in photocatalysis, while the rutile phase is preferred in solar cells, given its effective charge transfer abilities.

Rutile's refractive index (≈2.6) is marginally higher than that of anatase (≈2.48), indicating the denser nature of the rutile phase, leading to increased radiation absorption. Anatase typically exhibits a dielectric constant  $\epsilon$  ranging from 31 to 51, whereas rutile's dielectric constant falls within the range 110 to 117 [50,51,65–67]. The aforementioned values are approximations for crystalline titanium dioxide thin films, while deviations may occur in amorphous thin films. The basic features of anatase, rutile and brookite TiO<sub>2</sub> crystal structures are detailed in Table 1.

**Table 1.** Basic features of anatase, rutile and brookite TiO<sub>2</sub> crystal structures [42,48,50,51,61,65,67–70].

Feature	Anatase	Rutile	Brookite
Crystal structure	Tetragonal I4 <sub>1</sub> /Amd (141)	Tetragonal P4 <sub>2</sub> /mnm (136)	Orthorhombic Pbc2 <sub>1</sub> (29)
Lattice parameters a, b, c (Å)	a = b = 3.785 c = 9.514	a = b = 4.593 c = 2.958	a = 5.502 b = 8.942 c = 5.144
Lattice volume (Å <sup>3</sup> )	136.25	62.07	257.38
Specific Gravity (g/cm <sup>3</sup> )	3.8–3.9	≥4.2	3.9–4.1
Hardness (Mohs scale)	5.5–6.0	5.5–6.0	5.5–6.0
Density (kg/m <sup>3</sup> )	3830	4240	4170
Refractive index	n <sub>g</sub> = 2.5688, n <sub>p</sub> = 2.6584	n <sub>g</sub> = 2.9467, n <sub>p</sub> = 2.6506	n <sub>g</sub> = 2.809, n <sub>p</sub> = 2.677
Band-gap (eV)	3.2–3.26	2.8–3.0	2.9
Absorption band-gap (eV)	2.04	1.78	2.20
Ti-O bond length (Å)	1.92–1.95	1.91–1.94	1.87–2.04
O-O bond length (Å)	2.43	2.43	2.49

### 3. Methods Utilized in the Synthesis of Nanoparticles

Typically, various metal and metal oxide nanoparticles can be synthesized using two primary methods: top-down and bottom-up approaches. Top-down techniques encompass the disintegration of larger or bulk substances to create the desired nanomaterials. Conversely, bottom-up strategies involve the assembly of individual atoms and molecules to form larger nanomaterials, as illustrated in Figure 2. The diversity of physical, chemical, and environmentally friendly approaches employed in synthesizing different nanoparticles aligns with either of these two approaches.

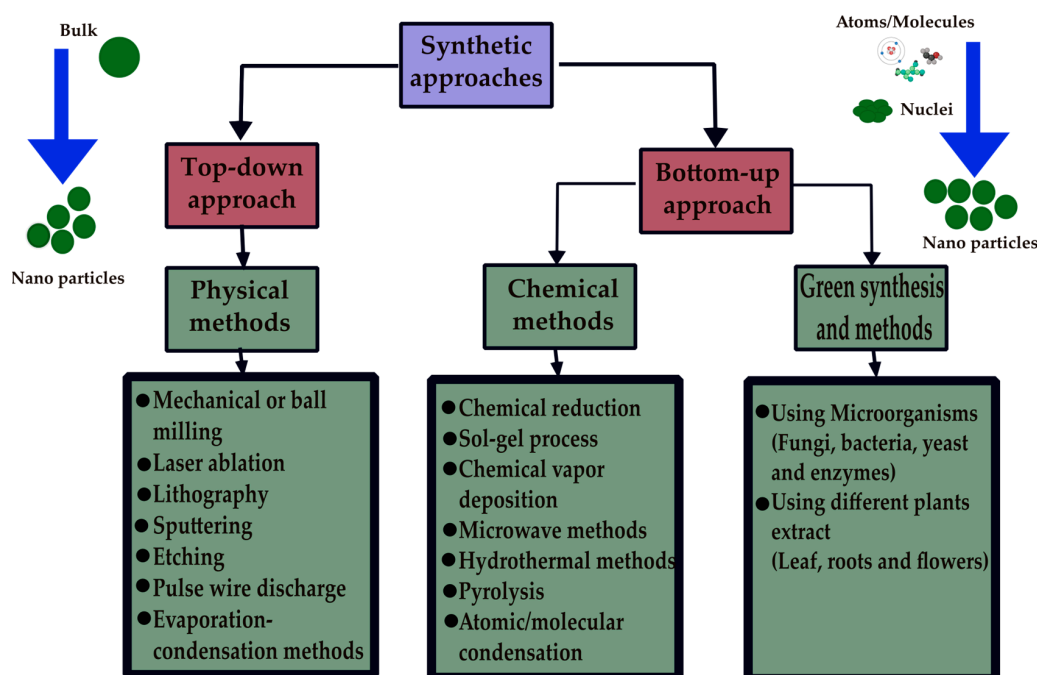


**Figure 2.** Various synthetic approaches for the production of nanoparticles.

### 3.1. Physical Methods

All physical methods utilized for synthesizing nanoparticles have been identified as top-down approaches. These physical techniques, including mechanical or ball milling, laser ablation, lithography, sputtering, etching, and pulse wire discharge, operate within the framework of a top-down approach, breaking down large molecules into smaller ones [71–76]. Among these methods, lithography stands out for nanoparticle synthesis effectiveness but necessitates high energy input. Despite the substantial energy employed, this method is almost unsuitable for producing symmetrical nanoparticles [77].

The fundamental drawback of the top-down techniques lies in generating nanoparticles with an imprecise surface structure. It is believed that the conventional top-down approach induces significant crystallographic damage to the resulting structures [78]. Although the physical route is simple, swift, and direct, it yields nanoparticles of inferior quality, characterized by flawed surface morphology and unintended impurities [79]. Hence, scientists have been exploring an alternative approach, namely the bottom-up method, aiming to synthesize high-quality and high-purity nanoparticles.

### 3.2. Chemical Methods

The chemical methodology utilized in nanoparticle production predominantly adopts a bottom-up technique. This bottom-up approach involves the combination of small molecules or atoms to create larger molecules through self-assembly mechanisms. Bottom-up methods mirror agglomeration processes and stand in contrast to top-down approaches. Several chemical methods, like sol-gel processes [80], hydrothermal methods, chemical vapor deposition [81], physical vapor deposition [82], solvothermal [83], co-precipitation [84], chemical reduction [85] and microwave-assisted approaches [86], are included in the bottom-up strategies for nanoparticle production [87].

### 3.3. Green/Biosynthesis Methods

Traditional methods have long been employed for nanoparticle synthesis, yet recent research underscores the superiority of green approaches over conventional methods, due to several benefits, including reduced failure rates, cost-effectiveness, and simplified characterization. Green synthesis, or biosynthesis, involves the utilization of biomolecules to facilitate nanoparticle formation by diminishing the titanium precursor. These biomolecules serve not only as reducing agents but also as capping agents, curbing nanoparticle agglomeration. Pro-

teins, polysaccharides, organic acids, enzymes, flavonoids, terpenoids, and phenols, among others, can serve as these biomolecules. Additionally, green nanoparticle synthesis demonstrates greater environmental friendliness compared to physical and chemical synthesis, notably lowering emissions of harmful chemicals. Leveraging the manifold advantages of green synthesis, it has found successful applications across various fields [88]. In Table 2, the benefits and drawbacks of the methods utilized in synthesizing nanoparticles are summarized.

**Table 2.** Benefits and drawbacks of synthetic methods.

Synthetic Method	Benefits	Drawbacks
Physical	<ul style="list-style-type: none"> <li>No capping reagents are required.</li> <li>Absence of by-products.</li> <li>Size distribution and shape are uniform.</li> </ul>	<ul style="list-style-type: none"> <li>Enhanced cost.</li> <li>Sophisticated facilities needed.</li> <li>Extreme conditions.</li> </ul>
Chemical	<ul style="list-style-type: none"> <li>High controlled size distribution and shape.</li> <li>Cost efficient.</li> </ul>	<ul style="list-style-type: none"> <li>Noxious capping reagents are needed.</li> <li>Toxic emissions.</li> <li>Long-lasting reactions.</li> </ul>
Green/biosynthesis	<ul style="list-style-type: none"> <li>Eco-friendly.</li> <li>Facile process.</li> <li>Cost efficient.</li> <li>No capping reagents are needed.</li> </ul>	<ul style="list-style-type: none"> <li>Wide particle size distribution.</li> <li>Nanoparticles' aggregation.</li> <li>Potential contamination.</li> </ul>

### 3.4. Synthesis of Nano-TiO<sub>2</sub> Materials

The synthetic approach with titanium dioxide can be customized to generate diverse crystal structures, sizes, and shapes, all of which can significantly impact its sensing capabilities. Various synthetic techniques, such as sol-gel, hydrothermal, and vapor phase methods, have been utilized to craft TiO<sub>2</sub> nanomaterials with distinct characteristics. The sol-gel synthetic approach is initiated by hydrolyzing titanium alkoxides in the presence of H<sub>2</sub>O and alcohol, subsequent to a condensation reaction, which results in the formation of a robust gel precursor. The hydrothermal synthetic method entails subjecting Ti precursors to high pressure and temperature in an aqueous solution, yielding nanocrystalline titanium dioxide with distinct morphologies. Vapor phase synthesis comprises the thermal breakdown of Ti precursors in a gaseous phase, yielding high-purity titanium dioxide nanoparticles with controlled particle size. This segment offers an overview of hydrothermal, sol-gel, and green synthetic approaches, alongside chemical vapor deposition, physical vapor deposition, as well as other approaches. Table 3 summarizes and compares several synthetic routes, delineating their respective benefits and limitations.

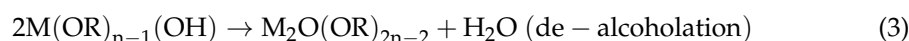
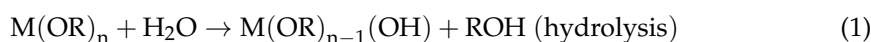
In general, the bottom-up synthetic approaches, such as sol-gel, hydrothermal, CVD and PVD, have gained interest and constitute the most common ways for producing TiO<sub>2</sub> nanostructures, due to their advantage in controlling particles' size and structural attributes during synthesis. However, the aforementioned approaches are costly, time- and energy-consuming, requiring increased temperature and pressure conditions. Additionally, noxious and volatile reagents are utilized that can harm both the environment and human life, while mass production is limited. All these characteristics promote limitations in their manufacturing, as well as potential environmental applications [89]. Hence, an eco-friendly and cost-efficient approach is needed to synthesize TiO<sub>2</sub> nanostructured materials on a larger scale with fewer hazards [90]. Consequently, green synthesis has been proposed as an alternative approach for TiO<sub>2</sub> nanostructure synthesis. Green synthesis is a naturally adaptable, environmentally benign and non-toxic approach that uses less expensive chemicals and requires low energy for cost-efficient production [91,92]. Biological extracts can operate as both stabilizing and reducing agents and the same reducing agent can be employed to develop a variety of metallic nanoparticles [93], while water-soluble metabolites are mostly involved in the reduction process [91]. Moreover, nanostructures with better morphology and stability have also been reported through a green synthetic approach [91].

**Table 3.** Comparison of the most commonly utilized methods for the production of TiO<sub>2</sub> nanoparticles.

Synthetic Method	Benefits	Drawbacks
Sol-gel	<ul style="list-style-type: none"> <li>• Cost-efficient.</li> <li>• Low temperature needed.</li> <li>• Increased control.</li> <li>• Enhanced specific surface area.</li> <li>• Eco-friendly.</li> </ul>	<ul style="list-style-type: none"> <li>• Sensitivity to reaction conditions.</li> <li>• Post-treatment needed.</li> </ul>
Hydrothermal	<ul style="list-style-type: none"> <li>• Variable control.</li> <li>• Enhanced specific surface area.</li> </ul>	<ul style="list-style-type: none"> <li>• Need of increased temperature and pressure.</li> <li>• Time-consuming.</li> <li>• Concentrated chemicals are used.</li> </ul>
Chemical Vapor Deposition (CVD)	<ul style="list-style-type: none"> <li>• Enhanced purity.</li> <li>• Exceptional control of film thickness and morphology.</li> </ul>	<ul style="list-style-type: none"> <li>• Complex infrastructure.</li> <li>• Increased cost.</li> <li>• Expertise required.</li> <li>• Non-eco-friendly.</li> </ul>
Physical Vapor Deposition (PVD)	<ul style="list-style-type: none"> <li>• Increased purity.</li> <li>• Precise control of film thickness and morphology.</li> <li>• Eco-friendly.</li> </ul>	<ul style="list-style-type: none"> <li>• Increased cost of equipment and maintenance.</li> <li>• Enhanced energy requirements.</li> </ul>
Green/biosynthesis	<ul style="list-style-type: none"> <li>• Eco-friendly.</li> <li>• Cost-efficient.</li> <li>• No capping and stabilizing reagents required.</li> <li>• No complex infrastructure required.</li> <li>• Ease in handling.</li> <li>• Reduced agglomeration.</li> </ul>	<ul style="list-style-type: none"> <li>• Control of size may be challenging.</li> </ul>

### 3.4.1. Sol-Gel Synthetic Approach

The sol-gel approach stands as a widely adopted method in the fabrication of titanium dioxide. In comparison to alternative methods, this approach allows operation at lower temperatures and provides precision in regulating the size and morphology of TiO<sub>2</sub> particles. TiO<sub>2</sub> can be generated in various forms, such as powder, aerogel, fiber spinning, and thin films. The precursors commonly fall into two categories: (a) metal alkoxides and (b) inorganic metal salts [94–96]. The primary steps involve hydrolysis, condensation, aging, drying, and heat treatment. When metal alkoxides serve as precursors, hydrolysis takes place by substituting the OR group of metal oxide M-O-R with water's hydroxyl group, forming a molten gel. With time, the metal alcoholates of hydroxide coalesce to construct a 3D network, eventually resulting in gel formation as the solvent diminishes. Through tailoring the primary precursor's chemical structure and meticulously controlling processing variables, nanocrystalline products characterized by enhanced chemical purity can be attained. The typical process of preparing titanium dioxide via sol-gel procedures entails hydrolysis and polycondensation reactions of Ti(OR)<sub>n</sub> (titanium alkoxides), culminating in the creation of oxo-polymers that subsequently transition into an oxide network. The sol-gel technique is advanced based on the subsequent equations (Equations (1)–(4)):



The hydrolysis and condensation processes happen concurrently, resulting in the creation of a sol or a colloidal suspension containing nanoparticles within a liquid phase. This sol undergoes aging and drying phases, leading to the formation of a gel, which is then subjected to enhanced temperature calcination, in order to eliminate organic residues and attain the desired crystalline configuration for titanium dioxide. Through modulation of synthesis parameters, like pH, temperature, and precursor concentration, the as-mentioned approach offers precise manipulation of the dimensions, structure, and crystalline nature of titanium dioxide nanoparticles. Furthermore, this method is comparatively straightforward, cost-efficient, and adaptable for large scale production.

Studies concerning this technique predominantly concentrate on manipulating various factors within the procedure to enhance the characteristics of  $\text{TiO}_2$ . These influential factors encompass the molar ratio of precursor: $\text{H}_2\text{O}$ , solution's pH, precursor type, catalyst type, annealing temperature and time. This review particularly delves into the impact of the precursor: $\text{H}_2\text{O}$  molar ratio, the pH value of the solution, and annealing duration and temperature. The detailed process of the sol-gel method is depicted in Figure 3.

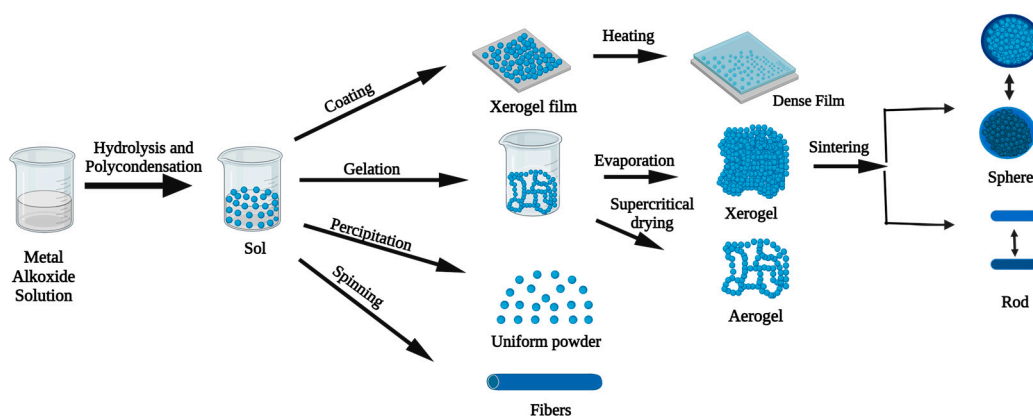


**Figure 3.** Schematic illustration of the sol-gel synthetic approach for the production of distinct  $\text{TiO}_2$  nanostructures.

#### Precursor: $\text{H}_2\text{O}$ Molar Ratio

In the initial hydrolysis stage of the sol-gel procedure, the quantity of  $\text{H}_2\text{O}$  utilized plays a pivotal role. In cases where the  $\text{H}_2\text{O}$  volume is insufficient, additional substances, like alcohol compounds, might not dissolve entirely. In [97], it was proposed that the precursor: $\text{H}_2\text{O}$  ratio ( $R_w$ ) should not fall below 2.5, emphasizing that adequate water content enhances the hydrolysis rate. According to another study [98], the  $R_w$  value yields three potential outcomes. Firstly, a  $R_w$  value that is too small may result in incomplete alcoholate dissolution. Secondly, at a moderate  $R_w$  value, water engages with monomer molecules. Finally, an excessively large  $R_w$  value, surpassing the critical value, might expedite hydrolysis completion within a brief period.

#### Solution's pH

The solution's pH value during synthesis significantly influences the production of  $\text{TiO}_2$ . It holds the ability to impact both the shape and the comprehensive structure of the resulting titanium dioxide nanoparticles. In previous research [99], a highly acidic titanium tetrachloride solution subjected to high-temperature aging resulted in the synthesis of small, finely-tuned particle sizes. The study revealed that pH value not only influenced particle's morphology, but also affected the robustness of the colloid. Studies suggest that an escalation in particle size occurs because of an abundance of  $\text{H}^+$  ions within the solution that substantially disrupt both nucleation and growth processes.

### Annealing Procedure's Time and Temperature

Temperature and duration are pivotal elements in the annealing process of titanium dioxide powder synthesized through the sol-gel technique. Managing these variables allows for the modification of TiO<sub>2</sub>'s structure and properties. In a study by Castrejon-Sanchez [100], TiO<sub>2</sub> created via the sol-gel approach underwent annealing at 475 °C for times ranging from 35 to 200 min. Observations revealed a structural shift in the sample from 100% anatase to 0% rutile, indicating a transition in TiO<sub>2</sub> structure from anatase to rutile as the annealing time increased. Additionally, Kim and co-researchers [101] investigated temperature's impact on titanium dioxide thin films and noted that, at 400 °C, TiO<sub>2</sub> maintained an anatase structure, while a transformation to rutile occurred at temperatures approaching 1000 °C.

### Other Parameters

Additionally to titanium dioxide nanoparticles and coatings, ordered mesoporous titanium dioxide stands out as a distinctive TiO<sub>2</sub> material due to its exclusive porous configuration, drawing significant interest recent decades for potential applications across various domains, like photocatalysis, energy storage, and drug delivery. The synthetic procedure for ordered mesoporous titanium dioxide generally includes the utilization of surfactants acting as templates, in order to regulate the material's pore size and structure. One prevalent approach constitutes the sol-gel method, where the precursor is dissolved in a surfactant template-containing solvent, leading to subsequent hydrolysis and condensation reactions that yield the ordered mesoporous structure. Alternatively, the hard templating route employs rigid inorganic templates, like SiO<sub>2</sub> or Al<sub>2</sub>O<sub>3</sub>, to create the mesoporous framework, subsequently filled with the titanium dioxide precursor and subjected to enhanced temperature calcination for eliminating the template. Other methodologies encompass the utilization of block copolymer templates, the microwave-assisted synthetic approach, electrospinning, etc. [98,99,102–104]. The development of ordered mesoporous titanium dioxide remains an active realm of exploration, characterized by continual endeavors directed towards optimizing the conditions of synthesis and tailoring the material's attributes for specific applications.

### 3.4.2. Hydrothermal Synthetic Approach

The hydrothermal approach is a frequently utilized method for manufacturing titanium dioxide, wherein the manipulation of process conditions facilitates regulation of the particles' size and configuration. This technique involves the utilization of water as a solvent, combined with an appropriate solute to create the initial substance. The reaction transpires within a steel pressure container, occasionally using a PTFE (polytetrafluoroethylene) liner. The reaction's temperature and pressure levels depend on the concentration of the solution. Within the pressure vessel, dissolution and crystallization reactions take place, resulting in the creation of titanium dioxide.

The critical variables influencing the hydrothermal process encompass temperature, solution pH, and reaction duration. Hashemi and his team [105] accomplished the creation of 3D heterogeneous structures comprising ZnO nanowires specifically grown on TiO<sub>2</sub>/ZnO composite nanofibers through a combined approach employing electrospinning and the hydrothermal technique. Additionally, Aditya and Basanta [106] adopted an alternate solvent method, distinct from the hydrothermal approach, employing a precursor mixture of TiCl<sub>4</sub> and distilled water to fabricate TiO<sub>2</sub> thin films.

Moreover, Prathan and colleagues conducted a study that introduced a hydrothermal technique to produce vertically-aligned TiO<sub>2</sub> nanorods on a fluorine-doped tin oxide glass substrate, employing minimal amounts of harmful substances [107]. Through optimized conditions, they achieved enhanced crystalline orientations across the [001] axis, predominantly exposing (002) facets, resulting in excellent visible light transmittance and effective electron pathways. The as-mentioned low-cost method exhibits promise for cultivating well-aligned titanium dioxide single-crystal nanorods appropriate for solar cell applications, while reducing the utilization of precursors and HCl. In a separate investigation, Ibrahim and co-researchers [108] varied hydrothermal reaction times between 1 to 5 h and observed some influence on TiO<sub>2</sub> charac-

teristics and performance, albeit not distinctly evident. Furthermore, researchers like Reilly and his team [109] utilized porous glass microbeads as a substrate for titanium dioxide growth, reducing  $\text{TiO}_2$  wear rates. In addition, Hameed and Abdulrahman [110] utilized titanium isopropoxide and potassium hydroxide as precursors, heating the solution and subjecting it to a magnetic field, resulting in  $\text{TiO}_2$  with enhanced antibacterial activity compared to samples without magnetic treatment. The experimental process is illustrated in Figure 4.

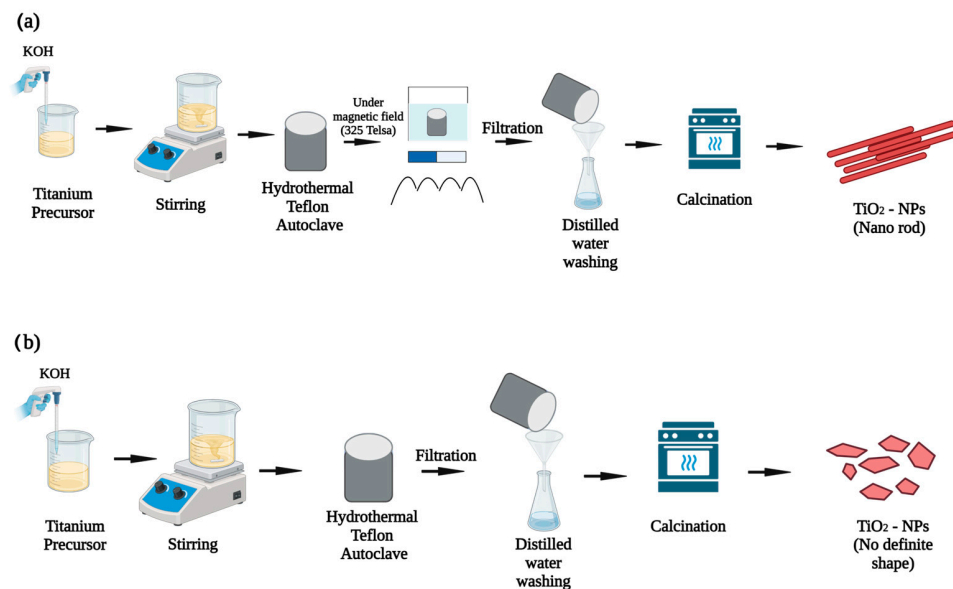


**Figure 4.** Diagram of the experimental procedure employing hydrothermal method: (a) hydrothermal approach incorporating magnetic field and (b) hydrothermal technique devoid of magnetic field [110].

#### 3.4.3. Chemical Vapor Deposition (CVD) Synthetic Approach

In the production of  $\text{TiO}_2$  through chemical vapor deposition, the initial substance changes from a solid to a gas form, then onto the substrate, where it undergoes pyrolysis or chemical reactions to create thin titanium dioxide films. Key factors influencing this process include precursor concentration, deposition temperature, and substrate morphology. Previous research employing chemical vapor deposition often utilized titanium isopropoxide as a precursor, also termed metal–organic chemical vapor deposition. For instance, Ahn and colleagues [111] employed titanium isopropoxide as a precursor, comparing plasma enhanced chemical vapor deposition (PECVD) and low-pressure chemical vapor deposition (LPCVD) processes for  $\text{TiO}_2$  fabrication. The deposition rate of PECVD was observed to be three times faster than that of LPCVD. Similarly, Djerdja and his team [112] utilized  $\text{TiCl}_4$  as a precursor, in order to deposit  $\text{TiO}_2$  films at lower temperatures, noting that substrate properties significantly influenced the quality of the resulting titanium dioxide films. Astinchap and co-researchers [113] examined the impact of substrate temperature and the quantity of precursor used on thin films of titanium dioxide.

In a separate study, Zhang and Li [114] innovatively utilized titanium isopropoxide as the precursor, employing atomizing chemical vapor deposition technology for the first time. An ultrasonic transducer atomized the precursor, successfully depositing  $\text{TiO}_2$  films onto the substrate. Observations indicate that, as the temperature rises, there is a corresponding increase in the surface roughness of the sample, along with an augmentation in the anatase diffraction peak. Moreover, it is suggested that elevating both the substrate temperature and precursor concentration contributes to enhanced film crystallinity. Additionally, the rate of deposition demonstrated an initial rise followed by a decrease as the precursor concentration increases.

#### 3.4.4. Physical Vapor Deposition (PVD) Synthetic Approach

Physical vapor deposition is a method that converts the precursor into a gaseous form before applying it onto the substrate. In contrast to chemical vapor deposition, this

technique does not entail any chemical reactions. PVD technology encompasses two main approaches for deposition based on the target object: cathode arc and magnetron sputtering. Esparza-Contro and his team [82] effectively modified the chemical characteristics of a titanium dioxide film. This was accomplished by regulating the oxygen partial pressure, while coating a Fe wire on the film, employing PVD technology.

Then, Ghufran and co-researchers [115] utilized cathode arc and magnetron sputtering technologies to apply TiO<sub>2</sub> thin films. They analyzed both the surficial morphology, as well as the chemical composition, of the as-mentioned thin films utilizing SEM/EDX analysis. This evaluation aimed to study the adhesion characteristics of these thin films. The research findings concluded that a higher roughness in the deposited TiO<sub>2</sub> film correlated with increased adhesion. While the majority of the studies involving PVD-based titanium dioxide film preparation concentrate on altering the deposition process-impacting factors, such as the crystal structure, oxygen flow rate during deposition, grain size, target surface roughness, distance from the matrix, and deposition power, there are also investigations focused on enhancing the entire PVD apparatus.

Moreover, Artoshina and his team [116] enhanced the conventional magnetron sputtering apparatus and employed AFM and XRD techniques for characterizing the Ag@TiO<sub>2</sub> and Tm-Ag@TiO<sub>2</sub> samples. The use of an inverted DC measuring and controlling tube increased material density when sputtering onto the substrate, resulting in more stable equipment parameters during operation compared to traditional methods.

Furthermore, Supriad and colleagues [117] utilized electrolytic polishing technology, in order to treat the deposited target material. Their findings indicated that substrates with decreased surface roughness facilitated the plating of titanium dioxide film, and smoother substrate surfaces led to better adhesion of the film.

Finally, in another study [118], magnetron sputtering technology was employed to deposit TiO<sub>2</sub>/SnO<sub>2</sub> and TiO<sub>2</sub>/CuO films.

#### 3.4.5. Green Synthetic Approach

Chemical vapor deposition, physical vapor deposition, and the sol-gel synthetic approaches are part of both physical and chemical methodologies. In general, these techniques involve increased temperatures and pressures, posing potential harm to the environment. In contrast, the green synthetic approach, utilizing plants and microorganisms, is characterized by a reduced environmental impact and is considered as more eco-friendly. This approach falls into two categories: plant synthesis, using plant extracts, and microbial synthesis, employing bacteria, fungi, yeast, and enzymes. Subsequent sections will delve into progress and developments within both these methods.

#### Synthesis of TiO<sub>2</sub> Nanoparticles Using Microorganisms

The synthesis of titanium dioxide nanoparticles through microorganism-mediated processes surpasses conventional chemical and physical methods in creating stable, cost-effective, and environmentally friendly nanoparticles. Various microorganisms, like fungi, yeast, and bacteria, are utilized, given a composition rich in proteins, polysaccharides, organic acids, and enzymes [119]. These microorganisms aid in metal ions' reduction to metal nanoparticles via hydrolysis and reduction processes [120]. Enhancing nanoparticle stability is achievable by coating them with nanoparticles, a process facilitated by the bioactive components present in microorganisms. Utilizing microorganisms in the green pathway for nanoparticle production is more feasible for large scale manufacturing, due to their resilience to agitation and pressure compared to plant-based methods [121]. Moreover, manipulating the metabolism of microorganisms allows for the acquisition of nanoparticles with favorable properties, achieved through the optimization of various operational conditions.

The microorganism approach extensively employs intracellular and extracellular methods [122]. Intracellular nanoparticle formation involves introducing metal precursors into the culture, leading to their uptake by microbial cells. Consequently, the resulting nanoparticles are somewhat challenging to extract, necessitating further steps, such as chemical

treatments, centrifugation, and filtration, to disrupt cells and extract the nanoparticles. Conversely, the extracellular method involves trapping metal ions onto the surface of microbial cells, followed by the reduction of these ions into nanoparticles through bioactive precursors within the microbial cells (Figure 5). Many researchers favor this method for nanoparticle production, due to the lack of additional extraction steps.

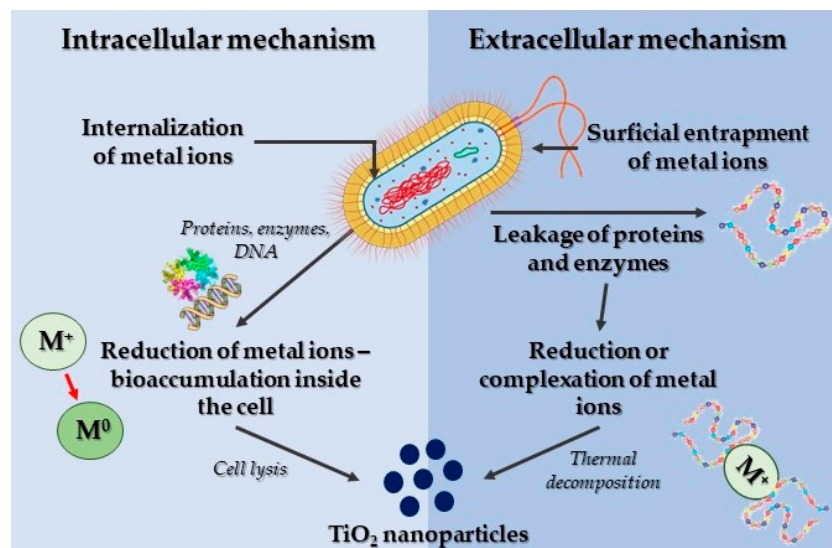


**Figure 5.** Schematic representation of the procedure of TiO<sub>2</sub> nanoparticle formation through microorganisms, involving the two potential mechanisms (extracellular and intracellular).

Bacteria exhibit promising potential, due to their abilities in mobilizing and immobilizing metals, particularly in the reduction of metal ions for nanoparticle generation. While the exact mechanism behind nanoparticle generation through bacteria remains incompletely explored, achieving the desired morphology is attainable through optimization of operational parameters [123]. Babitha and co-researchers [124] conducted research utilizing *Propionibacterium jensenii* and TiO(OH)<sub>2</sub>, leading to the production of crystalline anatase titanium dioxide nanoparticles with sizes ranging from 15 to 80 nm, as verified through XRD and FE-SEM analyses.

Furthermore, Salman and co-workers [125] examined TiO<sub>2</sub> nanoparticle synthesis using *Lactobacillus crispatus* without employing calcination. These nanoparticles, displaying anatase as the crystalline phase, were characterized by a particle size equal to 70.98 nm, showcasing both spherical and oval shapes. In addition, Órdenes and his team [126] employed a non-pathogenic soil bacilli (*Bacillus mycoides*) and TiO(OH)<sub>2</sub> in their research. Notably, an organic substance layer was observed on the TiO<sub>2</sub> nanoparticles, speculated to be an extracellular matrix produced by the bacterium. The as-developed organic substance played a role in green synthesis by assisting in capping and stabilizing the nanoparticles, while it appeared to be a peptide or carbohydrate through FTIR analysis. Moreover, Sunkar and his team utilized *B. cereus* and titanium dioxide, in order to produce pure anatase TiO<sub>2</sub> nanoparticles [127]. Their research highlighted nanoparticle production, due to the bacteria's negative electrokinetic potential. Additionally, the hydrolysis of TiO<sub>2</sub> nanoparticles was facilitated by *B. cereus*' extracellular proteins, as certified by FTIR study.

In addition, Suriyaraj et al. [128] utilized Ti(OH)<sub>4</sub> along with extremophilic and radiation-resistant *B. licheniformis* to produce nanoparticles, measuring 16.3 nm and displaying sphere-shaped morphology. Optimal conditions revealed the pH value of the as-mentioned nanoparticles as equal to 4.5. TEM analysis showcased the production of nanoparticles on the cell wall surface of the bacterial species after treatment with Ti(OH)<sub>4</sub>. In addition, other research using the same bacteria and TiO<sub>2</sub> as raw materials synthesized irregular, as well as spherical nanoparticles [129]. Employing the intracellular approach, the process was characterized by a longer oxidation duration (96 h), causing a delay. On the contrary, titanium dioxide nanoparticles were extracellularly synthesized within 48 h

using *Lactobacillus* species [130]. The aforementioned nanoparticles varied in size (8–35 nm) and were identified to possess rutile and anatase crystalline phases, as verified through TEM and XRD analyses, respectively. Similar to other bacterial species, these species attracted titanium cations, due to negative electrokinetic potential. Additionally, the slightly acidic pH and decreased oxi-red potential activated oxidoreductase enzymes bound by the membrane, thus leading to nanoparticles generation.

TiO<sub>2</sub> nanoparticles were created at 37 °C by utilizing *Halomonas elongata* and TiO(OH)<sub>2</sub>, leading to anatase TiO<sub>2</sub> nanoparticles [131]. Mixing the *H. elongata* supernatant with TiO(OH)<sub>2</sub>, followed by incubation at 37 °C, resulted in the production of titanium dioxide nanoparticles within the white precipitate. Although this approach seemed straightforward, it exhibited a delay, taking 96 h to complete. FTIR analysis identified various functional groups, such as alkyl halides, alkenes, alkynes, and alcohols. Further research involved synthesizing titanium dioxide nanoparticles from the supernatant of *Streptomyces* species HC1, using TiO(OH)<sub>2</sub> as Ti precursor [132]. White clusters of TiO<sub>2</sub> nanoparticles were obtained by subjecting a solution with pH=5 to a steam bath at 60 °C for 30 min in this research. XRD data confirmed these nanoparticles to be in the anatase phase, characterized by spherical shapes with sizes ranging from 43 to 67 nm, as observed in SEM images.

Fungi and yeast present distinct advantages compared to bacteria, due to their high metal tolerance, convenience in handling, isolation, culture, and maintenance, without the necessity of additional intricate or costly equipment (Figure 6). In the synthesis of TiO<sub>2</sub> nanoparticles utilizing *Fusarium oxysporum* fungi and K<sub>2</sub>TiF<sub>6</sub> as raw materials, the extracellular method was employed [133]. The resulting TiO<sub>2</sub> nanoparticles exhibited spherical shapes, ranging in size from 6 to 13 nm, and were found to exist in both brookite and rutile phases. Another innovative approach involved investigating a novel approach using *Aspergillus flavus* mycelia and titanium dioxide [134]. Surficial analysis unveiled that, although these nanoparticles were agglomerated, they exhibited stability without direct aggregation, indicating that the conversion of titanium dioxide into titanium dioxide nanoparticles occurred at the surface. Additionally, it was observed that immobilized *Aspergillus flavus* mycelia were more efficient in binding TiO<sub>2</sub> nanoparticles.

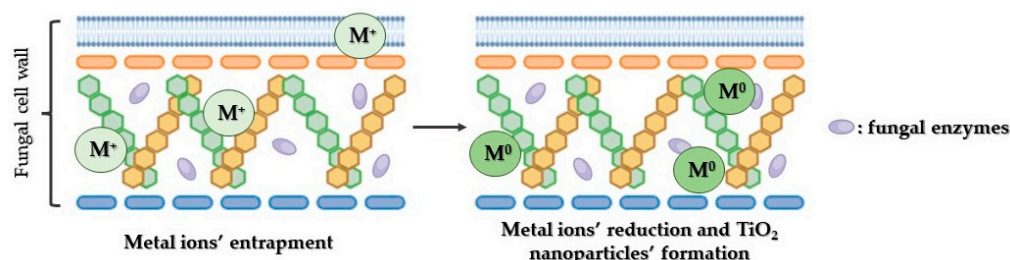


**Figure 6.** Proposed process outlining the formation of TiO<sub>2</sub> nanoparticles using fungal extracts [135].

Another study investigated the utilization of *Trichoderma viride* [136]. The obtained nanoparticles were crystalline, displaying a size equal to 74.4 nm. These nanoparticles possessed a spherical shape and high purity. In other research [137], TiO<sub>2</sub> nanoparticles were synthesized utilizing the wild mushroom *Fomitopsis Pinicola* and titanium isopropoxide, showing rutile phase formation with reduced crystallinity. FTIR studies confirmed the involvement of reducing and capping agents, like polyphenols and flavonoids, throughout the entire nanoparticles' synthesis process. Recently, TiO<sub>2</sub> nanoparticles were produced utilizing *Trichoderma citrinoviride* and titanium isopropoxide [138]. The research team employed an extracellular approach in an acidic environment followed by calcination at 450 °C for 2 h. Nevertheless, XRD analysis indicated a mixture of two phases in these nanoparticles, namely rutile and anatase.

*Saccharomyces cerevisiae* was combined with TiO(OH)<sub>2</sub> that served as the TiO<sub>2</sub> precursor [130]. Baker's yeast consists of various compounds, such as methoxy and hydroxyl derivatives of quinones, benzoquinones, and tolu-quinones, which proved highly effective in producing TiO<sub>2</sub> nanoparticles. In another investigation, baker's yeast was utilized alongside TiCl<sub>3</sub> as the TiO<sub>2</sub> precursor for intracellular generation of TiO<sub>2</sub> nanoparticles [139].

Notably, this method resulted in the production of highly pure anatase crystalline phase without any presence of the rutile phase. SEM and TEM analyses of the nanoparticles emphasized the spherical nature of the nanoparticles, ranging in diameter from 3.6 to 12 nm, while surface analysis revealed a relatively simple lamellar structure.

Enzymes play pivotal roles as reducing agents, catalysts, and stabilizers in the enzyme-mediated synthesis of titanium dioxide nanoparticles. Consequently, several research teams have employed specific enzymes in the production of titanium dioxide nanoparticles. Nevertheless, this method of creating titanium dioxide nanoparticles has received limited attention, due to its dependence on specific substrates and controlled growth parameters. Enzymes utilization may not be economically feasible concerning commercialization prospects. In a study by Sumerel and his team [140], silicatein and Ti-bis(ammonium lactate)di-hydroxide (BALDH) were utilized to fabricate TiO<sub>2</sub> nanoparticles, resulting in the production of both amorphous and crystalline forms. Subsequent XRD study verified the transformation of the amorphous TiO<sub>2</sub> nanoparticles into the anatase phase upon heating to 427 °C. Further elevation of the temperature to 827 °C led to the crystallization of titanium dioxide nanoparticles into the rutile phase.

In addition, Johnson and co-researchers [141] detailed the production of TiO<sub>2</sub> nanoparticles utilizing Ti-BALDH and urease enzymes as the initial components, in order to study the impact of incubation temperature and reaction duration on the crystal phases of TiO<sub>2</sub> nanoparticles. Regardless of the experimental conditions, XRD analysis confirmed that the acquired nanoparticles were consistently in the anatase crystalline phase. Altering the incubation temperatures and reaction times had minimal influence on the surficial morphology of the obtained titanium dioxide nanoparticles.

#### Synthesis of TiO<sub>2</sub> Nanoparticles Using Plants

The fabrication of titanium dioxide nanoparticles through plant-mediated means offers several advantages in comparison to microorganism-mediated synthesis. This method is more convenient, cost-effective, yields higher outputs, is easily manageable, requires less time, and does not necessitate the maintenance of cell cultures [142]. Moreover, this approach holds additional value by utilizing plant waste, such as fruit peels, seeds, and stems, enhancing sustainability. Plants contain various metabolites and phytochemicals that serve as effective reducing agents during nanoparticle synthesis.

Although diverse parts of plants have been employed in plant-moderated titanium dioxide nanoparticle fabrication, utilizing leaves from different plants could emerge as a promising approach due to their availability, in contrast to roots, stems, and seeds. Additionally, leaves' treatment is cost and energy effective, as stems, seeds, and roots are challenging to finely crush for phytochemical extraction. Furthermore, flowers are less preferable, given their usage in perfume manufacturing and for decorative purposes. The graphical representation of plant-moderated synthesis, particularly using leaf extracts, for nanoparticle production is depicted in Figure 7.

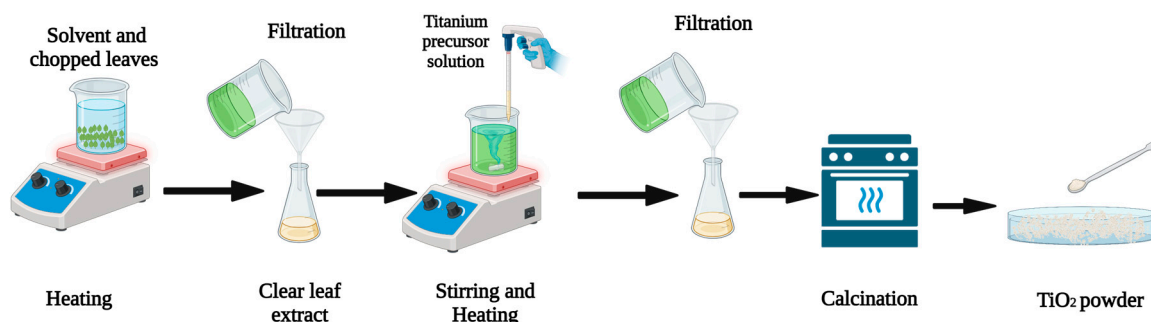


**Figure 7.** Illustration of the plant-mediated synthetic approach for the fabrication of nano-TiO<sub>2</sub> particles.

The initial phase of plant-mediated synthesis involves acquiring plant extracts from any plant part, which are subsequently boiled in an appropriate solvent, usually distilled

water or ethanol, after a thorough cleaning process. The obtained filtered solution, recognized as the plant extract, serves as the reducing agent required for the Ti precursor [143]. With continuous stirring and suitable conditions, the plant extract undergoes gradual addition of an appropriate titanium precursor. A noticeable alteration in the solution's color indicates the initial formation of amorphous TiO<sub>2</sub> nanoparticles. After filtration, these amorphous titanium dioxide nanoparticles are washed using a proper solvent, in order to prohibit contact with the plant extract. Ultimately, the filtered titanium dioxide nanoparticles are dried and subjected to calcination at 500 °C, leading to the formation of crystalline titanium dioxide nanoparticles.

Gowri and his team [144] utilized *Nyctanthes arbour-tristis* leaves as the primary plant extract, along with titanium isopropoxide, as the titanium precursor for their initial experimentation. Upon XRD analysis, it was discerned that these nanoparticles possessed pure, crystalline anatase TiO<sub>2</sub> phases. Furthermore, Sethy and co-workers [145] fabricated titanium dioxide nanoparticles demonstrating a notably enhanced specific surface area (105 m<sup>2</sup>/g) and a significant pore diameter equal to 10.50 nm. For this research, *Syzygium cumini* leaves had been chosen as plant extract source, as well as capping agent, leading to the production of irregularly shaped nanoparticles with non-uniform characteristics. Remarkably, the as-mentioned nanoparticles presented a decreased zeta potential equal to −18.7 mV, contributing to a moderately stable behavior.

In the synthesis involving *Mentha* aquatic leaf extract, titanium isopropoxide served as the titanium source [146]. The resulting nanoparticles displayed a sphere-shaped morphology and possessed a stable anatase TiO<sub>2</sub> crystalline phase, which was attributed to the high content of phenols and flavonoids found in *Mentha* aquatic leaves. These significant discoveries have spurred further investigations into plant extracts.

Pushpamalini and his team [147] fabricated titanium dioxide nanoparticles under heat treatment at 400 °C, in order to entirely remove biomolecules and prevent agglomeration. Utilizing different plant species (*Piper betel*, *Ocimum tenuiflorum*, *Moringa oleifera* and *Coriandrum sativum*) they obtained titanium dioxide nanoparticles exhibiting the anatase TiO<sub>2</sub> phase in total and characterized by sizes equal to 6.6 nm, 7.0 nm, 6.6 nm and 6.8 nm, respectively. The FTIR analysis suggested nearly complete elimination of biomolecules at 400 °C, a conclusion further verified through TEM analysis, which revealed subtle clustering of the acquired TiO<sub>2</sub> nanoparticles.

Moreover, Subhapiya and co-researchers [92] utilized TiOSO<sub>4</sub> and *Trigonella foenum-graecum* for the development of titanium dioxide nanoparticles, displaying strong light absorption at a wavelength equal to 400 nm. *Aloe barbadensis*, commonly known as aloe vera, is recognized for its abundant minerals, vitamins, amino and fatty acids, terpenoids, and flavonoids. The as-mentioned plant extract was incorporated into two research projects using TiCl<sub>4</sub> as the Ti source. The research of [148] documented a calcination procedure to synthesize TiO<sub>2</sub> nanoparticles, yielding anatase-phase nanoparticles within the size range of 60–80 nm. Conversely, [149] omitted the calcination process, resulting in mixed phases of titanium dioxide nanoparticles, including anatase, brookite, and rutile, within a size range equal to 20–50 nm, while displaying a sphere-shaped morphology. The use of calcination within the methodology facilitated the production of pure single-crystalline TiO<sub>2</sub> nanoparticles.

Furthermore, Hameed and his team [150] synthesized TiO<sub>2</sub> nanoparticles utilizing banana peel extract and titanium dioxide. The subsequent AFM analysis verified an average diameter equal to 88.45 nm for the as-prepared TiO<sub>2</sub> nanoparticles, while the XRD analysis confirmed a volume of 31.5 nm. Finally, Ali and co-researchers [151] conducted a novel fabrication process of TiO<sub>2</sub> quantum dots using watermelon peel waste. The resultant composite exhibited an average particle size equal to 7 nm and manifested a polycrystalline crystal structure. Notably, it displayed effective inhibitory properties against various pathogenic bacteria, such as *Bacillus subtilis*, *Escherichia coli*, *Cryptococcus neoformans*, *Candida albicans*, *Aspergillus niger* and *Pseudomonas fumigatum*. The synthetic procedure of the as-mentioned composite is illustrated in Figure 8.

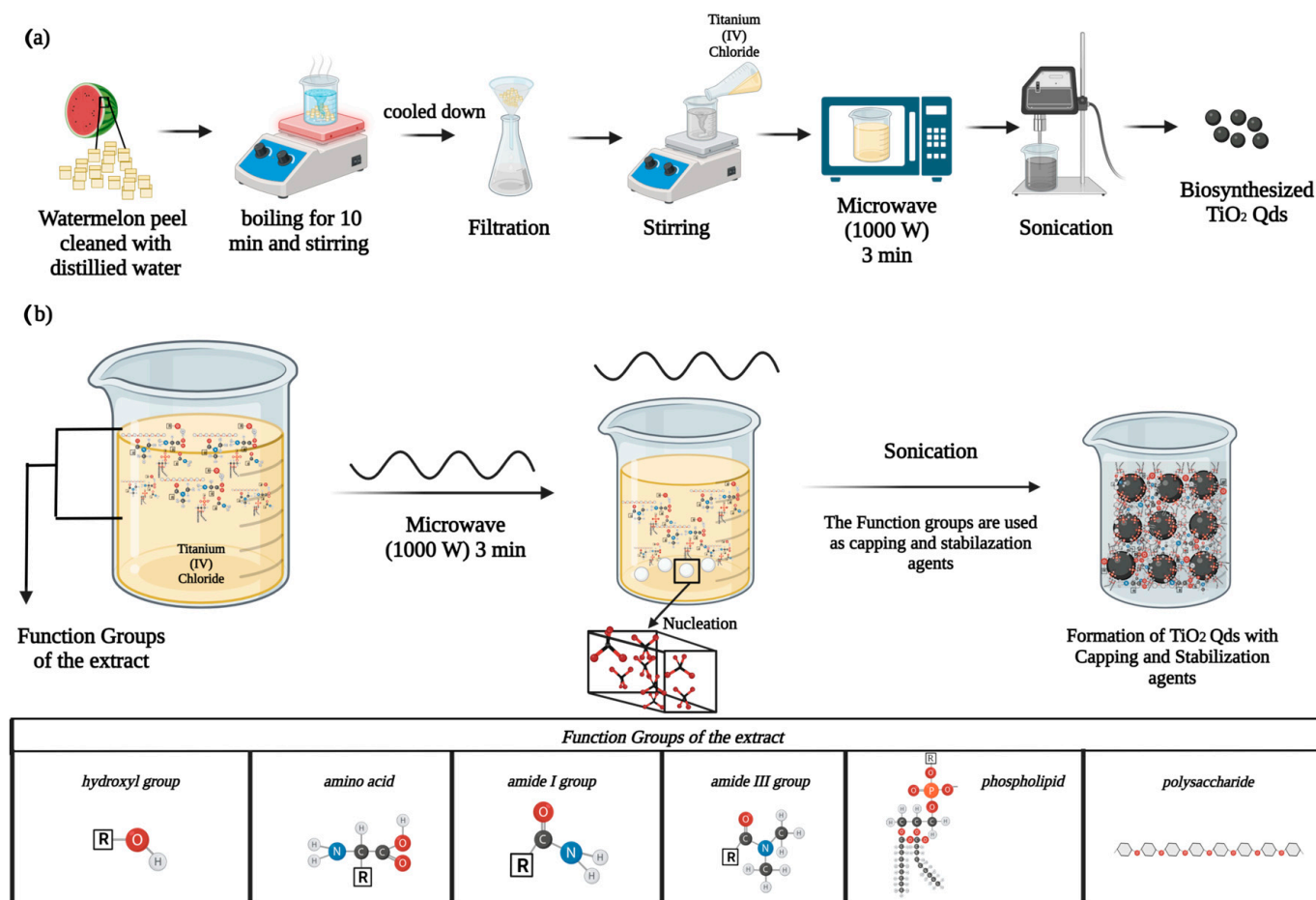


**Figure 8.** (a) Biosynthesis of  $\text{TiO}_2$  quantum dots utilizing watermelon peel extract and (b) mechanism of formation of the as-mentioned quantum dots.

Madadi and his team [152] synthesized  $\text{TiO}_2$  nanoparticles using titanium butoxide as the Ti precursor combined with *Glycyrrhiza glabra* root extract. The resulting nanoparticles exhibited an increased size range (60–70 nm) compared to previously reported nanoparticles. In a separate study, titanium N-tetra-butoxide was employed as the Ti precursor in an ethanolic root extract of *Kniphofia foliosa* [153]. Rather than utilizing heat, precipitation of titanium dioxide nanoparticles occurred by employing a NaOH solution. Variations in the precursor:plant extract volume ratios (1:2, 1:1 and 2:1) were investigated for characterization purposes. XRD analysis indicated that produced samples with volume ratios equal to 1:1 and 2:1 yielded crystalline titanium dioxide nanoparticles featuring an anatase  $\text{TiO}_2$  phase, while the 1:2 sample exhibited fewer crystalline nanoparticles. Excessive plant extract presence led to reduced crystallinity. These nanoparticles showcased stability even at temperatures surpassing 500 °C, exhibiting sizes in the range of 8.2–10.2 nm. Additionally, FTIR analysis confirmed the presence of significant phytochemicals within the root extract.

In addition, Al-Shabib and co-researchers [154] used *Withania somnifera* root extract in conjunction with bulk titanium dioxide during the synthetic process. *Withania somnifera* root extract is comprised of various elements, such as withanolide, flavonoid, amino acid, alkaloid, and phenolic derivatives. The aforementioned constituents played a crucial role in reducing bulk titanium dioxide for  $\text{TiO}_2$  nanoparticles, ensuring their stabilization as well. Notably, the resulting nanoparticles were found to possess mixed crystalline phases of anatase and brookite without undergoing calcination. Also, TEM analysis confirmed the presence of nanoparticles exhibiting sphere- and square-shaped morphologies, ranging in size between 50 and 90 nm. Moreover, zeta potential measurements indicated the exceptional stability of the as-prepared nanoparticles, possessing a value equal to  $-24$  mV.

Flower extracts have been a subject of interest for synthesizing titanium dioxide nanoparticles. Marimuthu and his team [155] synthesized TiO<sub>2</sub> nanoparticles utilizing *Calotropis gigantea* flower extract and TiO(OH)<sub>2</sub>. However, XRD analysis revealed impurities in the fabricated TiO<sub>2</sub> nanoparticles, because of the presence of bioorganic molecules, as well as residual TiO(OH)<sub>2</sub> on the nanoparticles' surface. Similarly, Aravind and co-researchers [156] employed jasmine flower extract for the production of TiO<sub>2</sub> nanoparticles. Devikala and his team [157] achieved the production of nano-TiO<sub>2</sub> particles using *Caesalpinia pulcherrima* flower extract and TiOSO<sub>4</sub>. XRD analysis showcased the anatase TiO<sub>2</sub> phase and tetragonal structure of the obtained nanoparticles, while SEM and TEM analysis revealed asymmetrical sphere-shaped nanoparticles within a size range of 20–25 nm. Nanoparticle agglomeration was also observed in SEM analysis. Furthermore, EDX analysis was conducted to determine atomic percentage and identify impurities, confirming the purity of the acquired TiO<sub>2</sub> nanoparticles, without the presence of any impurities.

There is a growing inclination towards utilizing seed extracts as an alternative means for synthesizing TiO<sub>2</sub> nanoparticles, thus circumventing the utilization of noxious chemicals and organic solvents. An aqueous flax seed extract was employed to convert titanium isopropoxide into nano-TiO<sub>2</sub> particles [158]. A comparative investigation was conducted within this research, both in the presence and absence of flax seed extract, to obtain TiO<sub>2</sub> nanoparticles. The nano-TiO<sub>2</sub> particles produced utilizing the seed extract exhibited minimal agglomeration, smaller size, and greater visibility compared to those produced without seed extract. Moreover, the particles generated in the presence of seed extract displayed notably high porosity. These findings indicate that the seed extract, including both reducing and stabilizing agents, proved highly efficient in synthesizing nano-TiO<sub>2</sub> particles with regulated shape and size. Lately, Aslam and co-researchers [159] synthesized nano-TiO<sub>2</sub> particles using *Abelmoschus esculentus* seed extract, due to its high flavonoid content. The resulting particles displayed uniform distribution with minimal agglomeration compared to commercially available TiO<sub>2</sub> nanoparticles. EDS analysis indicated no impurity peak, signifying the total decomposition of reducing and capping agents during the calcination process, ensuring that the obtained TiO<sub>2</sub> nanoparticles possessed an anatase phase.

Taking into consideration the aforementioned literature, extensive and notable investigations have focused on fabricating TiO<sub>2</sub> nanoparticles through green synthesis methods, aiming to address challenges linked with the traditional approaches [160]. Additionally, Table 4 presents a breakdown of the benefits and drawbacks associated with the different green synthetic approaches for nanoparticle production. Analysis in the same table (Table 4) indicates that employing various plant extracts for nanoparticles' synthesis emerges as a more viable option compared to utilizing microorganisms from several perspectives.

**Table 4.** Benefits and drawbacks of the distinct green synthetic approaches.

Green Synthetic Method	Benefits	Drawbacks
Microorganism-assisted method	<ul style="list-style-type: none"> <li>• Effective production.</li> <li>• Enhanced stability.</li> <li>• Resistive nature to agitation and pressure</li> <li>• Adjustable culture parameters for achieving desired nanoparticles' physical properties.</li> </ul>	<ul style="list-style-type: none"> <li>• Requirement of cell culture development.</li> <li>• Decreased yield.</li> <li>• Longer synthesis times.</li> <li>• Potential contaminations.</li> </ul>
Plant-assisted method	<ul style="list-style-type: none"> <li>• More convenient.</li> <li>• Cost-efficient.</li> <li>• Increased yield.</li> <li>• Facile process.</li> <li>• Utilization of plants waste.</li> <li>• Shorter synthesis times.</li> </ul>	<ul style="list-style-type: none"> <li>• Nanoparticles' aggregation.</li> <li>• Crushing of harder parts of plants (such as roots or stems) may be difficult.</li> </ul>

### Other Approaches

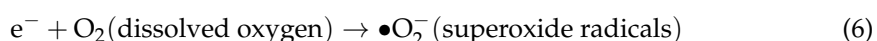
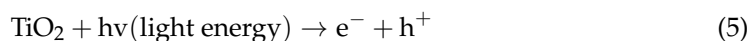
Apart from the well-known methods, like sol–gel, hydrothermal, chemical vapor deposition, physical vapor deposition, and green approaches, various other approaches exist for fabricating TiO<sub>2</sub> nanoparticles. One such method is the sono-chemical synthetic approach, utilizing ultrasound waves to expedite nanoparticle synthesis. This technique proves advantageous by enabling swift nanoparticle production at low temperatures and pressures, offering a cost-effective process. Microwave-assisted synthesis, another method utilizing microwave radiation, is capable of yielding highly uniform nanoparticles at significant rates. The utilization of microwaves facilitates prompt heating, minimizing the total duration of the synthetic procedure [161–163]. The template-assisted synthetic approach presents an additional approach for creating ordered mesoporous TiO<sub>2</sub> nanoparticles [164–166]. By employing a material as a template, this method guides the growth of TiO<sub>2</sub>, forming a well-organized mesoporous structure, beneficial for tailor-making materials characterized by specific pore sizes, as well as shapes.

Additionally, the plasma-assisted method stands out as a promising synthesis technique, employing plasma discharge in order to generate reactive species reacting with Ti precursors for creating nanoparticles. This approach enables nanoparticle synthesis at relatively decreased temperatures and pressures, offering the capability of producing nanoparticles with distinctive properties and morphologies [167–169].

Finally, the solvothermal technique stands as one more viable method for synthesizing TiO<sub>2</sub> nanoparticles. In this approach, a solvent-dissolved Ti precursor undergoes heating under elevated pressure, fostering nanoparticle creation. The aforementioned approach is notably advantageous for nanoparticle generation, characterized by enhanced crystallinity and purity, while allowing control over size and structure. For instance, Sugahara and his team [170] achieved both dendritic, as well as spherical, morphologies of titanium dioxide nanostructures utilizing two precursors and specific decreased temperature conditions, employing the metal–organic decomposition (MOD) method.

### 4. Photocatalytic Activity Mechanism of TiO<sub>2</sub>

Because TiO<sub>2</sub> acts as a semiconductor, it possesses a relatively narrow E<sub>g</sub> between its VB and CB. When exposed to visible or ultra-violet light, particularly in the UV-A range with wavelengths between 315–400 nm [171], the surface of the semiconductor absorbs this light, prompting electrons (e<sup>−</sup>) in the VB to acquire energy and to transition to the CB. Consequently, these excited e<sup>−</sup> can interact with adsorbates, resulting in the surficial generation of positively and negatively charged species [172]. However, the observed photonic effectiveness for photocatalysis with TiO<sub>2</sub> remains notably low, typically <1% [173]. TiO<sub>2</sub> possesses an E<sub>g</sub> spanning 3–3.2 eV as previously mentioned, with its maximum absorption wavelength (λ<sub>max</sub>) at ≈400 nm. Figure 9 illustrates the process of exciting e<sup>−</sup> from the VB to the CB in TiO<sub>2</sub>. When exposed to light at this wavelength, the TiO<sub>2</sub> surface heats up significantly, reaching temperatures as high as 30,000 °C. As a result, the prevailing reaction is commonly an oxidation process that leverages dissolved oxygen in water to decompose pollutants (Equations (5)–(7)).



The hydroxyl radical, derived from this process, plays a pivotal role in breaking down contaminants in water by functioning as an oxidizing agent. To maintain the particles' electro-neutrality, specific measures are necessary, ensuring simultaneous reduction of O and pollutants' oxidation. This prevents the inhibition of the recombination procedure by oxygen [174].

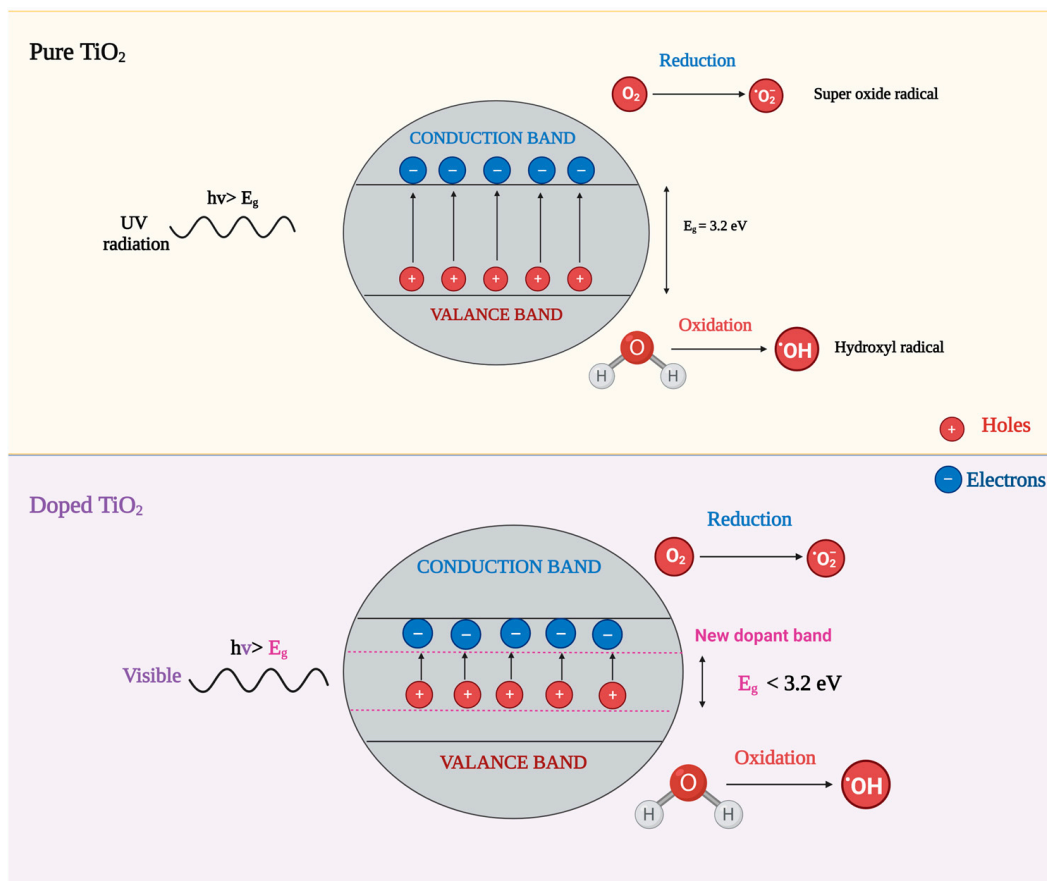


**Figure 9.** Energy levels and band-gaps comparison for pure and doped TiO<sub>2</sub>.

According to research, superoxide radicals ( $\bullet\text{O}_2^-$ ) can at times surpass hydroxyl radicals ( $\bullet\text{OH}$ ) in the preference for a photo-degradation mechanism [175]. These superoxide radicals might endure protonation to generate the hydroxy-peroxyl radical ( $\bullet\text{HO}_2$ ). This radical possesses the capability to eliminate undesired radical products, thus postponing the electron/hole recombination, as elucidated in prior studies (Equation (8)) [176].



The sequence of steps involved in heterogeneous photocatalysis using TiO<sub>2</sub> comprises five stages: (i) moving molecules destined for degradation to the photocatalyst's surface through mass transfer [176], (ii) binding these molecules to the active sites of TiO<sub>2</sub>, followed by the excitation of  $e^-$  in the VB, due to light exposure [177], (iii) the adsorbed molecules' degradation through photocatalysis, (iv) releasing the degradation products by desorption, and (v) transporting these products away from the TiO<sub>2</sub> surface. This mechanism aligns with advanced oxidation processes (AOPs), a category of those water treatment techniques devised as alternatives to traditional methods, like chemical precipitation and biological treatment [178]. AOPs involve degrading pollutants using in situ generated  $\bullet\text{OH}$  and other reactive oxygen species (ROS) [179], enabling the breakdown of compounds resistant to conventional treatments [180]. The non-specific nature of these radicals often leads to scavenging, where free radicals remove undesirable molecules [181]. Evaluation of the corresponding Gibbs free energy values for this mechanism demonstrates the overall process as thermodynamically favorable and spontaneous [182].

Following photocatalytic degradation, five primary types of products emerge: (i) dehalogenation products, recognized for their slow formation alongside hydroxylation, (ii) alkyl chain oxidation products, (iii) isomerization and cyclization products preserving atomic structures, (iv) products from aromatic ring opening, and (v) decarboxylation products [183].

## 5. Environmental Applications of TiO<sub>2</sub>-Based Photocatalytic Nanostructures

### 5.1. TiO<sub>2</sub>-Based Photocatalysts for Effective Elimination of Pharmaceutical Pollutants from Water and Wastewater

During the last few years, numerous new organic pollutants have emerged in the environment [184–186]. Various sources contribute to the environmental occurrence of drug residuals, including hospital and manufacturing wastewater, as well as landfill leachates [187,188]. The rapid increase in human population, accelerated industrialization, as well as increased pharmaceutical dependence, have remarkably enhanced environmental pollution [189,190]. Even though the release of pharmaceutical remnants into the environment may seem negligible initially, they tend to accumulate over time and pose severe threats to humans and both terrestrial and aquatic organisms. Such compounds have been detected in multiple origins, as hospital effluents, municipal wastewater treatment plants, groundwater, surficial water, as well as drinking water [191]. Due to their robust nature, these compounds resist degradation through the typical biological procedures used in municipal wastewater treatment plants. As a consequence, they remain untreated for prolonged periods, posing hazards to ecosystems [192]. Previous studies have indicated that even at extremely low concentrations (50 ng/L), the occurrence of pharmaceutical agents in surficial water and groundwater systems implies a significant risk to humans and animals by contaminating their main source of drinking water [193]. In addition, the increase in various types of antibiotics notably adds to the escalation of resistance among bacteria and microbes against medicinal substances, consequently raising the likelihood of increased risk to human populations [194]. Pharmaceutical substances enter aquatic environments, like wastewater, through various mechanisms subsequent to their usage, whether in their original state or as by-products of metabolism. The illustration in Figure 10 depicts the pathways through which these substances are released during the phase of drug administration.

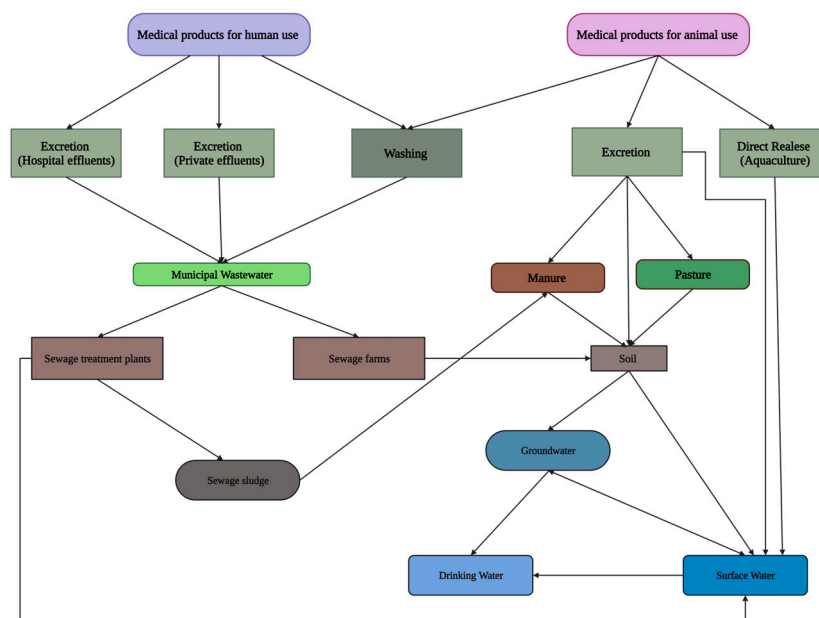


**Figure 10.** Distribution pathways of medical products/pharmaceutical substances into the environment.

The utilization stage in the pharmaceuticals' lifecycle significantly contributes to their environmental release. Distinguishing if residuals found within the environment originate from human or veterinary usage can be challenging, particularly when certain products are used by both, due to specific product characteristics or misuse. The primary avenue for pharmaceuticals entering the environment during consumption is through human and agricultural animal waste, like urine and feces, which consistently find their way into sewage or soil. Despite the fact that excretion constitutes the predominant approach,

substantial amounts of products administered topically, like anti-inflammatory gels, can be rinsed away during bathing. As a result, the quantity and nature of drug residuals discharged post-consumption vary based on parameters, like the quantity and type of substance ingested, administration method and metabolic degree [195].

Up to now, a variety of methods have been utilized for eliminating pharmaceutical substances from water and wastewater effluents. These techniques encompass activated sludge treatment, membrane reactors, algal and microbial reactors, alongside other biological procedures, like biological aerated filters, sequencing batch reactors, trickling filters, rotating biological contactors, biofilm reactors, membrane bioreactors, constructed wetlands, biological activated carbon filters, anaerobic digestion, bio-electrochemical systems, and phytoremediation [196,197]. Several crucial parameters, entailing physical and chemical properties, contaminants' biodegradability, solubility, robustness, as well as operational conditions (such as temperature, pH, and duration), significantly influence the fate of pharmaceutical pollutants in water bodies. Furthermore, attempts have been undertaken to utilize indirect optical decomposition methods employing  $\bullet\text{OH}$ , produced via sunlight-mediated activation of nitrate and humic acid, acting as light sensitizers [198]. The decay of optical properties in wastewater treatment processes depends on various parameters, like intensity of solar irradiation, geographical location, depth of water, climate, and water's organic composition. High turbidity levels caused by increased sludge concentration limit light penetration, minimizing optical degradation within traditional wastewater treatment plants [199]. In these facilities, impurity removal primarily relies on absorption facilitated by particulate matter and microbial degradation. However, the effectiveness of adsorption in eliminating pharmaceutical compounds is limited. Adsorption efficacy depends on factors like electrostatic interactions, hydrophobic drug properties, and their interactions with biological substances, like microorganisms. Additionally, factors like the type of reactor (fixed bed or continuous system), flow rate, and adsorbent concentration play significant roles. The literature suggests that acidic drugs (e.g., Ibuprofen, Clo-fibric acid, Phenopfen, and Bezafibrate) with  $\text{pK}_a$  ranging between 3.6 and 4.9 have minimal adsorption capacity to activated sludge [200]. While some drugs partially degrade and get removed from water and wastewater, others undergo complete degradation, forming various by-products [201]. Biodegradation includes the use of anaerobic or aerobic digestion by varied microorganisms found in sewage sludge, typically used for handling it. This process facilitates the breakdown of pharmaceutical substances present within the sludge. However, some medications may persist without changing, leading to potential contamination of water bodies, like surface or groundwater. Additionally, the membrane process is being considered as a biological treatment method. Ongoing research is exploring various biological approaches to eliminate pharmaceutical pollutants. For instance, a previous study found that activated sludge had the capability to remove steroid hormone E2 at a percentage equal to  $\approx 70\text{--}80\%$  [202].

Given the limitations of traditional techniques in eliminating pharmaceutical pollutants, such as low effectiveness, substantial energy usage, and the generation of detrimental by-products, researchers have introduced advanced oxidation processes as an auspicious and efficient alternative approach [203]. AOP methods include ozonation, photocatalysis and Fenton/photo-Fenton approaches. The aforementioned methods aim to thoroughly degrade and mineralize various pharmaceutical compounds, as per the available literature [204]. AOPs involve generating extremely reactive species as free radicals ( $\bullet\text{O}_2^-$ ,  $\bullet\text{OH}$  and  $\bullet\text{HO}_2$ ), focusing particularly on  $\bullet\text{OH}$ . The as-mentioned radicals, especially  $\bullet\text{OH}$ , possess significant ability in eliminating pollutants' molecules [205]. Based on the drug effluent's characteristics, as well as the preferred treatment goal, AOPs are able to be utilized either separately or along with other biological and physical processes [206]. Among AOP methods,  $\text{TiO}_2$ -based photocatalysis has arisen as a hopeful and effective method for eradicating pharmaceutical contaminants from water-based settings [207,208].

Manasa and his team investigated the effectiveness of four distinct titanium dioxide photocatalysts doped with boron and cerium (0.1 wt.% and 1 wt.% Ce- $\text{TiO}_2$ , as well as

1 wt.% and 2 wt.% B-TiO<sub>2</sub>), prepared via the EDTA-citrate approach, for breaking down typical fluoroquinolone-based antibiotics (ciprofloxacin and norfloxacin) using sunlight irradiation. The observed band-gap values ranged from 2.5 to 2.9 eV, indicating the presence of a new energy level towards efficient charge separation and recombination's decrease. At optimized conditions, 1 wt.% Ce-TiO<sub>2</sub> and 1 wt.% B-TiO<sub>2</sub> exhibited superior photocatalytic performance, potentially because of enhanced cerium adsorption rate and the boron occupying interstitial lattice positions, along with a reduced band-gap. These catalysts showcased 93% decomposition for both ciprofloxacin and norfloxacin, coupled with increased disinfection effectiveness of the order of 95–99.99% [209]. Conversely, Suwanarung and co-researchers investigated the impact of several N-doping concentrations on surficial features, crystalline phase structure, optical and textural attributes, chemical state, and photocatalytic performance of N-doped titanium dioxide nano-rice particles. Under the examined parameters, the highest and lowest decomposition percentages of ciprofloxacin were 94.3% and 70% for 12.5 wt.% N and 1 wt.% N, respectively, upon UV irradiation for 4 h, indicating an enhancement of photocatalytic activity with increasing nitrogen dopant concentrations [210].

Furthermore, Martins and co-researchers examined the decomposition of ciprofloxacin through photocatalysis upon UV and visible light irradiation, utilizing high-efficiency Au@TiO<sub>2</sub> photocatalytic nanostructures. They achieved this by refining synthetic factors, adjusting photocatalysis parameters, and employing computational modeling. They observed that the resulting nanocomposites absorbed 40–55% more irradiation within the visible spectrum compared to pure TiO<sub>2</sub>. Experimental assessments revealed a higher decomposition of ciprofloxacin (91%) under UV light irradiation, while a percentage equal to 49% was achieved under visible light irradiation [211]. In another study, Cabrera-Reina and colleagues investigated the elimination of the antibiotics imipenem and meropenem from various aqueous solutions (distilled water, river water, and simulated wastewater treatment plant effluents) using TiO<sub>2</sub> photocatalysis at a pilot plant scale. They demonstrated favorable decomposition rates under the specific experimental conditions employed [212].

Moreover, Truppi and his team developed a photocatalytic nanocomposite (Au@TiO<sub>2</sub> nanorods) via a co-precipitation approach, followed by calcination at ascending temperatures (250–650 °C). Their research focused on investigating the photocatalytic efficiency of the as-mentioned nanocomposites in degrading an antibiotic molecule (nalidixic acid) utilizing visible light irradiation [213]. Notably, nanocomposites calcined at 450 °C exhibited degradation rates up to 3.2 times more rapid than that of TiO<sub>2</sub> Evonik P25, a commercially available reference material, towards decomposing the targeted compound.

In addition, Gomez-Aviles and co-researchers achieved total decomposition of acetaminophen using C-TiO<sub>2</sub> nanotubes calcined at 400 and 500 °C under solar light irradiation in 1 h. They utilized lignin as a carbon precursor, in order to alter the anatase TiO<sub>2</sub> lattice via a hydrothermal process followed by thermal treatment. The hydrothermal method allowed the production of TiO<sub>2</sub> nanotubes possessing a relatively well-developed surface area, while the resulting C-TiO<sub>2</sub> exhibited an E<sub>g</sub> value equal to 2.95 eV, given the existence of the lignin-derived material [214]. Lately, Penas-Garzon and co-researchers studied activated carbon-TiO<sub>2</sub> heterostructures prepared via different methods (solvothermal, microwave-assisted, and sol-gel) utilizing lignin as the carbon source. Among these methods, the microwave-assisted route demonstrated superior performance towards the photocatalytic degradation of acetaminophen, ibuprofen and antipyrine upon solar light irradiation [215].

Additionally, Ahmadpour and colleagues showcased the efficacy of a TiO<sub>2</sub>@Zn-Fe<sub>2</sub>O<sub>4</sub>/Pd photocatalyst produced via the photo-deposition method. They optimized pH, catalyst concentration, and diclofenac's initial concentration, demonstrating its excellent performance in degrading this pharmaceutical substance under solar light exposure. The catalyst exhibited super magnetic properties, facilitating its magnetic separation for facile recovery from the reaction mixture [189].

In a pioneering effort, the same researchers developed ZnFe<sub>2</sub>O<sub>4</sub>@TiO<sub>2</sub>/Cu nanocomposites for naproxen removal, achieving an 80.7% degradation efficiency under sunlight irradiation. DRS analysis of the nanocomposites revealed heightened light absorption in the visible spectrum, resulting in reduced electron-hole recombination. Copper's inclusion, possessing an enhanced specific surface area, fostered increased Cu-semiconductor charge and energy transfer. The nanocomposites displayed notable stability and recyclability, maintaining a 72.3% removal rate after 5 cycles of catalyst use [187].

Then, Murgolo and his team investigated a photocatalyst composed of hydroxyapatite and TiO<sub>2</sub> for eliminating diclofenac in water. Their findings indicated a remarkable 95% degradation of the targeted compound within 24 h using the as-mentioned catalyst under UV light exposure [216].

In a separate study, Czech and colleagues examined novel TiO<sub>2</sub> nanocomposites integrating pristine carbon nanotubes (MWCNTs) at varying concentrations (0.15–8.78 wt.%) for the removal of acetaminophen from water. The most effective photocatalytic performance was observed with the nanocomposite containing 1.72 wt.% MWCNTs, enabling 81.6% elimination of acetaminophen from water [217].

Payan and his team also conducted a synthesis of Cu-doped TiO<sub>2</sub> functionalized with SWCNTs using a novel process combining sol-gel and hydrothermal methods. The characterization analysis confirmed the successful integration of Cu ions into the TiO<sub>2</sub> structure and surficial attachment of nanoparticles onto SWCNTs without altering the TiO<sub>2</sub> lattice structure. Regarding photocatalytic performance, total decomposition of sulfamethazine was accomplished under a pH value equal to 7, 10 wt.% SWCNT content, 4 wt.% Cu content, sulfamethazine concentration equal to 30 mg/L and duration of reaction equal to 135 min [218].

Furthermore, Abdelraheem and colleagues carried out a comprehensive study involving the solar light-mediated remediation of domestic wastewater effluents using N,B-co-doped TiO<sub>2</sub>. This study focused on the decomposition of bisphenol A, ibuprofen, triclosan, diclofenac, and estrone in double distilled water and various treated wastewater samples. The investigation also considered the impact of typical wastewater components, such as NO<sub>3</sub><sup>-</sup>, Cl<sup>-</sup>, Br<sup>-</sup> and HCO<sub>3</sub><sup>-</sup> characterized by recognized ROS quenching attributes. The obtained data demonstrated the successful removal of all examined compounds from individual and combined systems, even in the occurrence of naturally present, typical inorganic quenching agents [219].

Carbuloni and his team explored metformin's decomposition using TiO<sub>2</sub>@ZrO<sub>2</sub> nanocomposites upon UV light irradiation. Their study revealed the effective removal of metformin from water under optimized conditions of pH and concentration of the utilized catalyst. The enhanced performance of the TiO<sub>2</sub>@ZrO<sub>2</sub> nanocomposites towards the photocatalytic degradation of the model pharmaceutical pollutant was linked to the textural and structural characteristics' alteration, like increased specific surface area, reduced size of the particles, enhanced anatase phase concentration and E<sub>g</sub> variations [220].

Additionally, Escudeiro de Oliveira and colleagues employed nanotubes developed on a Ti-0.5 wt.% W alloy for eliminating estrone (E1) and 17 $\alpha$ -ethinylestradiol (EE2), which constitute important drugs listed in the EU Watch List, upon both UV and visible light irradiation. Based on their results, the doped samples presented enhanced photocatalytic activity in comparison to samples without doping, as well as other semiconductors, when subjected to both types of light irradiation. This superiority was attributed to reduced recombination rates of photo-produced charges and a flat-band potential's shift towards more negative values [221].

Finally, Gurung and his team investigated the elimination of typically utilized pharmaceuticals (carbamazepine and diclofenac) utilizing a Ag<sub>2</sub>O@TiO<sub>2</sub> (P25) photocatalyst. Optimal removal percentages of the order of 89.10% for carbamazepine and 93.5% for diclofenac were achieved after 180 min under UV irradiation and a photocatalyst dose equal to 0.4 g/L in distilled water [222].

It is widely accepted that the formation of a Schottky heterojunction through the combination of noble metals with TiO<sub>2</sub> can effectively boost photocatalytic activity [223]. To elaborate, the majority of noble metals possess Fermi levels lower than TiO<sub>2</sub>'s conduction band, leading to the suppression of charge carrier recombination [224]. Simultaneously, the surface plasmon resonance (SPR) effect exhibited by nano-sized metals, such as Cu, Ag, and Au, enhances the material's absorption of visible light [225]. This SPR effect is characterized by the collective oscillation of electrons on the surface of nano-sized metals, and the controllable manipulation of SPR further augments photocatalytic activity [226]. More precisely, semiconductors loaded with plasmonic metals can significantly boost the generation of photogenerated carriers while concurrently elevating the concentration of superoxide or hydroxyl radicals on the semiconductor's surface. Consequently, this results in a robust capability to degrade various pollutants [227].

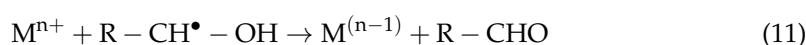
Generally, it is proposed that plasmonic metals share common features in their ability to enhance semiconductors through three mechanisms. Initially, metal nanoparticles exhibit a robust light absorption capacity within the visible spectrum and possess a significant scattering cross-section at the resonant wavelength. Both these characteristics substantially amplify the catalytic efficiency of proximal semiconductors. Secondly, the presence of metal nanoparticles on semiconductors results in a more potent electromagnetic field when subjected to localized surface plasmon resonance (LSPR) excitation compared to individual nanoparticles. This intensification facilitates the generation and separation of photogenerated electron-hole pairs within the semiconductor. Finally, the LSPR absorption wavelength of metal nanoparticles can be adjusted by manipulating particle size and shape. Consequently, catalyst performance can be enhanced by modifying the metal composition, morphology, and the contact interface between semiconductors [227].

Kaur and his team [228] fabricated Ag-modified TiO<sub>2</sub> catalysts with distinct morphologies and examined the effect on salicylic acid degradation. It was proposed that the morphological variations led to the difference in both interface and contact areas, which affected the performance of the catalyst.

Moreover, Gang and co-researchers [229] synthesized Ag nanoparticles of 24, 27 and 30 nm through a controlled chemical reduction and these were subsequently loaded onto TiO<sub>2</sub>. The Ag/TiO<sub>2</sub> plasmonic photocatalysts displayed superior stability and exceptionally improved the photocatalytic efficiency for visible-light degradation of tetracycline. Ag nanoparticles played a significant role and indicated size-dependent SPR effects, while Ag nanoparticles of 30 nm presented the highest photocatalytic efficiency (90 %) within 90 min.

### 5.2. TiO<sub>2</sub>-Based Photocatalysts for Effective Elimination of Heavy Metals from Water and Wastewater

Metal ions present in water can undergo reduction to their lower energy state when electrons generated via TiO<sub>2</sub> photo-excitation are available, particularly when the reduction potentials align favorably (Equation (9)). Alternatively, enhancing the reductive elimination of metallic ions can occur indirectly by introducing sacrificial electron donors, like methanol or formaldehyde (Equations (10) and (11)). Moreover, under specific circumstances where the existing oxidation state of the metal ions is not the highest attainable, they can be further oxidized to higher states through the influence of •OH or h<sup>+</sup> (holes) (Equation (12)) [230].



Heavy metals are typically characterized by their increased atomic weight and density, far surpassing that of H<sub>2</sub>O. Due to their relatively lower reactivity and strong properties,

they have been extensively utilized across various industries. Nevertheless, noxious heavy metals, like Pb, tend to accumulate swiftly in the environment, proving resistant to biological degradation [231]. Extensive reports highlight the severe toxicity of heavy metals to various human organs, leading to severe consequences, like mutations and cancer [232]. It is crucial to note that, while heavy metals are essential for proper bodily functions in specific quantities, their excess presence can be detrimental. Studies indicate significant adverse effects of heavy metals on plants, involving decreased uptake of nutrients and reduced productivity, when grown in soil where these metals are present [233]. Titanium dioxide has emerged as a cost-effective and time-effective method for heavy metal removal, with primal research proposing their reduction to decreased oxidative states subsequent to their surficial deposition onto the photocatalyst [234].

Titanium dioxide has been effectively employed in the reduction of heavy metal ions through photocatalysis, such as  $\text{Ni}^{2+}$ ,  $\text{Cd}^{2+}$ ,  $\text{Pb}^{2+}$ , and  $\text{Cu}^{2+}$ , following first-order kinetics. Enhanced removal of these metals was observed in more acidic conditions, suggesting  $\text{TiO}_2$ 's adaptability to function in such environments. Research indicates that the mechanism primarily involved in heavy metal removal was adsorption, facilitated by the substantial specific surface area of the nano- $\text{TiO}_2$  particles [235]. These nano- $\text{TiO}_2$  particles demonstrated promise for reusability and operation under room temperature conditions. Their adsorption capacity conformed to established isotherms, like the Langmuir isotherm, showcasing  $\text{TiO}_2$  nanoparticles as a promising alternative for the removal of heavy metal ions from wastewater [236].

Moreover, titanium dioxide has exhibited effectiveness in photo-catalytically eliminating As from industrial wastewater. The material displayed capability for multiple cycles and retained its effectiveness after regeneration. Simultaneously, other heavy metal ions, like  $\text{Cu}^{2+}$ ,  $\text{Cd}^{2+}$ , and  $\text{Pb}^{2+}$ , also presented reduced concentrations, indicating the potential for simultaneous removal without sludge generation [237].

Ti nanotube arrays, altered with the coupling agent KH-570, proved highly effective in degrading  $\text{Pb}^{2+}$ ,  $\text{Cu}^{2+}$ , and  $\text{Cr}^{6+}$  present in water. The array's arrangement enhanced specific surface area, as well as photocatalytic effectiveness, while the coupling agent augmented interaction between Ti and the heavy metals' ions. Nevertheless, this altered photocatalyst necessitated UV irradiation for effective operation, while its performance was influenced by wastewater turbidity [238]. Despite these limitations, further evaluation of this catalyst is warranted due to its beneficial aspects.

Titanium dioxide has established a significant history in eliminating Hg ( $\text{Hg}^{2+}$  to  $\text{Hg}^0$ ) from wastewater, serving as both a photocatalyst [239] and an assisting agent [240]. Research indicates photocatalytic efficacy within a pH range of 3 to 7, notably highlighting the effectiveness of the sol-gel method in producing particles with substantial surface area. Enhancements in catalyst efficiency were observed when increasing pH levels in this range, displaying considerable kinetics [241].

$\text{TiO}_2$  nanotubes have proven remarkably efficient in eliminating  $\text{Cu}^{2+}$  ions from water while concurrently generating hydrogen. Their enhanced catalytic activity stems from the significantly larger surface area compared to traditional nanoparticles, attributed to their distinctive shape and structure. The volume of hydrogen produced correlates with the quantity of  $\text{Cu}^{2+}$ , with an initial concentration of 10 mol % of  $\text{Cu}^{2+}$  in titanium dioxide demonstrating optimal performance [242]. Furthermore, the transformation of  $\text{Cr}^{6+}$  ions to  $\text{Cr}^{3+}$  is achievable using doped  $\text{TiO}_2$  photocatalysts. Achieving >99% elimination effectiveness was possible by doping with Fe and exposing the catalyst to visible irradiation. Enhanced electron transfer among the doped titanium dioxide and the ions of heavy metal, compared to pure  $\text{TiO}_2$ , significantly contributed to the supreme performance [243].

Another method for  $\text{Cr}^{3+}$  ion removal involved doping  $\text{TiO}_2$  developed on graphene oxide with Mn. This process commences with electron transfer from  $\text{Cr}^{6+}$  towards the photocatalyst, yielding  $\text{Cr}^{3+}$ , accompanied by subsequent electron transfer resulting in  $\text{Cr}^0$  atoms [244]. The co-doping process involving Ag and Mn in  $\text{TiO}_2$  has demonstrated remarkable effectiveness in eliminating  $\text{Cr}^{6+}$  and  $\text{Cu}^{3+}$  ions from water using a thermody-

namically spontaneous adsorption mechanism. The as-mentioned photocatalyst exhibited the ability to eliminate even negligible quantities of these heavy metal ions [245]. Another approach, that of doping with Gd, also displayed positive outcomes in removing  $\text{Cr}^{6+}$  ions. However, the observations were not as encouraging as those acquired from Fe and Ag@Mn-co-doped  $\text{TiO}_2$  photocatalysts [246]. Furthermore, the elimination of  $\text{Cr}^{6+}$  from wastewater was attained by creating a composite material consisting of titanium dioxide with EDTA on a carbon sheet substrate, showcasing exceptional photodegradation efficiency. This composite exhibited enhanced coordination, while the carbon sheet substrate acted as a dispersion matrix both for nano- $\text{TiO}_2$  particles and EDTA molecules [247].

The inclusion of  $\text{MnO}_2$  alongside  $\text{TiO}_2$  remarkably enhanced the elimination of  $\text{Pb}^{2+}$  ions, despite a reduction in surface area. This alteration fostered appealing interactions between the dopant and ions, resulting in heightened ion adsorption by the photocatalyst [248]. Furthermore, the elimination of heavy metals present in nuclear wastes, like  $\text{Cs}^+$  and  $\text{Sr}^{2+}$ , was achieved through doping titanium dioxide nanotubes with chromium ions. The charged nanotubes significantly bolstered removal efficiency, capitalizing on the increased specific surface area [249,250]. In addition, studies indicate the effective reduction of arsenic, a common groundwater contaminant, through iron-doped  $\text{TiO}_2$ . The incorporation of Fe ions enabled both adsorption and photocatalytic activity under visible irradiation through decreasing the  $E_g$  value. Optimal results were achieved with 1 wt.% of Fe at a pH value equal to 7, showcasing its potential as a promising agent for As removal [251].

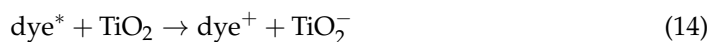
Nanocomposites have emerged as viable solutions for removing heavy metal ions from water. One proposed method towards the elimination of Pb from wastewater involved the utilization of  $\text{TiO}_2$  bio-nanocomposites, crafted through a procedure combining sol-gel fabrication of nano- $\text{TiO}_2$  particles and mixing with a polymeric solution. The as-proposed method presented a notable benefit, as it avoided introducing any by-pollutants into the treated water [252].

The photo-electrocatalytic elimination of  $\text{Cr}^{6+}$  was found to proceed nearly thrice faster compared to the conventional photocatalysis using  $\text{TiO}_2$ . Incorporating spherical nanostructures greatly expanded the reaction area, resulting in additional improvements [253]. Another effective approach for  $\text{Cr}^{6+}$  removal involved integrating  $\text{Ag}_3\text{PO}_4$  into  $\text{TiO}_2$  nanotube arrays, which exhibited equal efficacy in removing organic dyes [254].

The combination of mesoporous hollow  $\text{TiO}_2$  nanospheres with 3-aminopropyl triethoxysilane significantly enhanced the photodegradation effectiveness towards  $\text{Cu}^{2+}$ ,  $\text{Cd}^{2+}$ , and  $\text{Pb}^{2+}$ . The resulting composite demonstrated degradation efficiencies 12.7, 17.5, and 1.8 times higher, respectively, than those achieved by bare hollow nano- $\text{TiO}_2$  spheres [255]. Furthermore, the integration of reduced graphene oxide (rGO) with titanium dioxide nanospheres effectively removed  $\text{Ag}^+$  ions from water, where rGO contributed to increased charge carrier recombination. The maximum adsorption efficiency recorded was equal to 34.8 mg/g [256]. Additionally, a graphene-like  $\text{TiO}_2@\text{C}$  nanocomposite was utilized to eliminate  $\text{Pb}^{2+}$  ions from water, displaying an adsorption efficiency of the order of 331.7 mg/g [257].

### 5.3. $\text{TiO}_2$ -Based Photocatalysts for Effective Elimination of Organic Dyes from Water and Wastewater

A method of removing dyes from the water is photodegradation. There are two potential mechanisms that explain the process. One is the indirect path, where the dye molecule is excited by visible light energy, causing it to enter its triplet excited state. Subsequently, it is further transformed into a semi-oxidized radical by injecting electrons into the conduction band of titanium dioxide (Equations (13) and (14)) [258].



The second proposed mechanism is direct. In this process, dye molecules interact with the hydroxyl radicals produced, as well as with the electrons and holes formed due to excitation in

the conduction band. This interaction leads to the reduction and oxidation of the dyes, respectively [259]. The indirect mechanism is observed to predominate over the direct mechanism, and the photodegradation is higher and requires less time [260] (Figure 11).

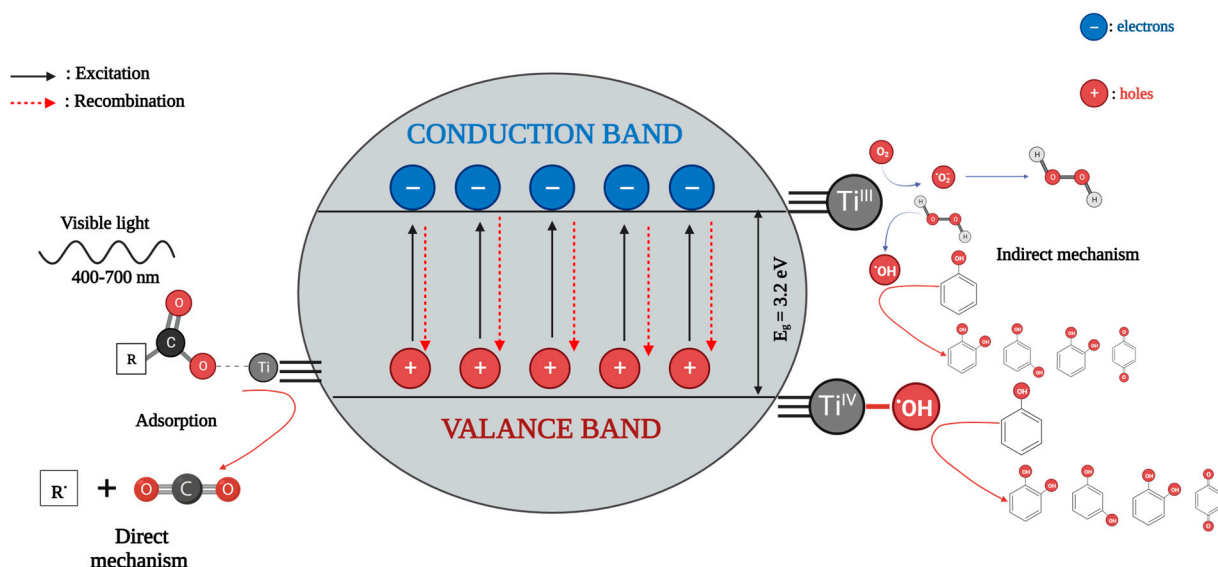


**Figure 11.** Schematic representation of the direct and indirect mechanism of the photocatalytic degradation of dyes using  $\text{TiO}_2$ .

The pollution of water sources by dyes has been increasing over the years, mainly because of industrial processes, endangering aquatic organisms and indirectly affecting humans. These dyes are frequently non-biodegradable, accumulating in the body over time [261]. Very often, industrial waste contains both dyes and heavy metals, which meaning that it is impractical to remove them with different processes [262]. It would be ideal to find an efficient and cost-effective way to remove both [263]. A type of dye that is dangerous and difficult to decay is azo [264]. Accumulation of dyes in the water and soil alter their characteristics, which presents a significant problem, being responsible for significant degradation of the water and soil.

Traditionally, techniques like flocculation, adsorption filtration, and dialysis have been employed to eliminate dye molecules from solution. Nevertheless, these techniques frequently lack consistency and reliability, often resulting in incomplete structural degradation and color removal. The discharge of inadequately processed waste into the environment contributes to higher pollution levels [265].  $\text{TiO}_2$  nanomaterials have also drawn attention, in the case of water pollution, as possible solution.

The immobilization of  $\text{TiO}_2$  nanomaterials on a matrix has been identified as an effective catalyst. Different azo dyes have been degraded with this type of catalyst. The process resulted in complete removal of color, with dye type AO10 being the easier to degrade. The concentration of organic carbon was significantly reduced in a few hours.  $\text{TiO}_2$  nanoparticles proved to be very promising for industrial waste degradation. The degradation is caused by the conversion of the double bond between two nitrogen atoms in the dye molecule to an  $\text{NH}_4^+$  ion [9].

Using Rhodamine blue as a pollutant, researchers tested the viability of a zeolite matrix containing  $\text{TiO}_2$ . They noted higher efficiency, while the composite was easier to recover and reuse [266]. Similar dyes, like methylene blue, have been used to test the difference between the use of micro-sized particles of  $\text{TiO}_2$  and nano-sized ones. As expected, the nanosized particles are much more efficient. There are also reports that solutions with higher pH are favorable for the degradation reaction [267]. A composite using a naturally sourced support matrix for the nanoparticles was synthesized using eggshells. The composite was tested on the same dyes as in the previous examples and had

positive results. The synthesis was based on the solvothermal method, which is found to play a role in the performance of the produced nanoparticles [268].

Simple TiO<sub>2</sub> nanoparticles have been used to degrade different dyes under sunlight. Solar radiation contains a percentage of UV light, making pure nanoparticles an effective option, if not the most efficient. Nevertheless, complete removal of the dyes was achieved [269]. Other nanostructures, like nanotubes, have also been tested yielding significant results. These can vary depending on the synthetic method and the target dye. For Orange II, the hydrothermal method had better results. Physical adsorption is the mechanism of degradation. Elevating the temperature lowered the time needed [270].

Doping is an easy method to increase the performance of the photocatalyst. Nickel and platinum as doping agents produce remarkable results. It should also be noted that, these metals make the nanoparticles magnetic, which helps recovery. They also proved to be very stable when they were reused [271]. Making the TiO<sub>2</sub> photocatalyst work effectively under visible light irradiation is often the point of the doping, by lowering the band-gap value. Manganese proved to be very effective as dopant, while zirconia and cobalt had negative results [272]. An increase in surface area with doping is also an important consideration. Metals like iron, copper and chromium have been tested. Doping with copper was found to be most effective at removing methylene blue. The surface area and the lower band-gap are both important factors in this result [273]. Reactive Red dye 198 was successfully degraded, using TiO<sub>2</sub> doped with Fe and N. A first-order reaction was observed, and the improved activity of the catalyst is attributed to the generation of superoxide species, as suggested by Kaur and colleagues [274]. Another doping element which has been tested is strontium. The doped TiO<sub>2</sub>, successfully degraded brilliant green, which is an antiseptic and antibacterial dye [275].

The incorporation of elements that are not metals, such as nitrogen and sulfur, has proven to enhance the photocatalytic efficiency of TiO<sub>2</sub>, improving the performance under visible light irradiation. The band-gap is reduced by the creation of N<sup>2+</sup> and S<sup>2+</sup> levels. A graphene matrix, containing TiO<sub>2</sub> nanoparticles co-doped with these, proved to be a very efficient catalyst for a number of different dyes [276,277].

Carbon doping has also been tested with TiO<sub>2</sub> nanorods. This resulted in a very efficient photocatalyst for dye removal, although the very high temperature requirements limit the potential for large scale applications [278]. The rare earth ytterbium, recovered from waste cathode ray tubes (CRT), was used to dope TiO<sub>2</sub> nanosheets. Recycling the material is an efficient way to make the process more environmentally friendly. The experiments proved that dye degradation is possible, while also degrading heavy metals (chromium) as reported by Zhang and his team [279].

MgO/TiO<sub>2</sub> nanocomposites are used in the photocatalytic methanation of CO<sub>2</sub> through reduction [280], as well as in the production of biodiesel [281]. These composites can be used in dye removal applications. Transition metals can also enhance the photocatalytic behavior of TiO<sub>2</sub>. Using sol-gel synthesis, TiO<sub>2</sub> nanoparticles doped with iron were produced and demonstrated high efficiency under visible light irradiation, at basic conditions [282].

Pure TiO<sub>2</sub> nanoparticles, which work under UV light irradiation, have been immobilized on polymer matrixes, retaining their efficiency, while exhibiting enhanced reusability. The incorporation is achieved using a dehydration reaction [283].

Electro-spinning has been used to synthesize nanofibers from TiO<sub>2</sub>/CuO. The photodegradation of an azo dye was tested, using the nanofibers. Enhanced adsorption capabilities and the ability to work under visible and UV light were noted. A TiO<sub>2</sub> nanocomposite with zinc sulfide has proven to be a potent photocatalyst. Even at small doses, it can degrade many different dyes when irradiated with ultra-violet light [284].

A TiO<sub>2</sub>/SiO<sub>2</sub> nanocomposite, characterized by a high anatase content, has been developed. There are many experiments using methylene blue which test this composite, with some studies using green synthetic methods [285].

Furthermore, a TiO<sub>2</sub>/SiO<sub>2</sub> nanocomposite, doped with copper, was created using a simple sol-gel technique. The presence of SiO<sub>2</sub> in the composite enhances the adsorption of organic compounds, while the addition of copper reduces the band-gap. High efficiency

in the degradation of Rhodamine B was reported [286]. In order to create  $\text{TiO}_2/\text{SiO}_2$  aerogels that work under visible light irradiation, researchers used tungsten and fluorine as doping agents. The high pore capacity and lower band-gap helped in the degradation of Rhodamine B [287]. Composites that use the same oxides, immobilized on the polymers polydimethylsiloxane and chitosan, have also been tested [288].

Phosphor-containing nanocomposites have been synthesized for UV and visible light photocatalysis. These  $\text{NaYF}_4:(\text{Gd}, \text{Si})/\text{TiO}_2$  nanocomposites exhibited enhanced absorption of UV/visible light and the separation of electron and hole pairs for efficient photocatalysis. Similar  $\text{NaYF}_4:\text{Yb}, \text{Tm}-\text{TiO}_2$  nanocomposites exhibit photocatalytic activity under near-infrared irradiation [289].

Palygorskite, a fibrous clay material, has also been used. Another usable clay is montmorillonite, a cheap and non-toxic way to add a support structure to  $\text{TiO}_2$  nanoparticles. Under ultra-violet light irradiation, the composite proved effective for dye degradation [290].

Other nanocomposites that have been tested are based on  $\text{TiO}_2@\text{SnO}_2$ . Their mesoporous structure and high surface area make them efficient catalysts for photodegradation [291]. Combining two catalysts often results in an improved composite material. Researchers also noted that this material exhibits anti-microbial activity [292]. The conditions of synthetic process can affect the properties of the resulting material. This was demonstrated by researchers using a microwave hydrothermal process to synthesize  $\text{CdS}/\text{CdTiO}_3-\text{TiO}_2$  nanocomposites [293].

A novel  $\text{TiO}_2$  composite consisting of anatase interacting with a rutile phase containing  $\text{Ti}^{3+}$  was synthesized by heating a mixture of  $\text{TiO}_2$  and  $\text{Ti}_2\text{O}_3$  at high temperatures. For this composite to degrade some dyes, requires other elements as co-catalysts, like Cu or Pt [294]. A nanocomposite that exhibited great photocatalytic performance under both UV and visible light irradiation was based on a zeolite matrix, which has the ability to adsorb dyes. The composite was made by  $\text{BiVO}_4/\text{TiO}_2-\text{NaY}$  [295].

Graphene nanoplates incorporated with  $\text{Ag}_2\text{O}/\text{TiO}_2$  were tested under visible light and UV conditions. Hydrogen peroxide was used to enhance the catalysis. Anions, like carbonate, nitrate, hydrogen phosphate, chloride, and sulfate, can affect the reaction [296].

$\text{TiO}_2$  was used to enhance the surface area of fly ash by a factor of ten. This novel material was used to successfully remove a heavy metal, a dye and a hazardous chemical used in detergents, under ultra-violet light irradiation [297].

Titanium dioxide immobilized onto electro-spun fibers from PVA was employed for the selective removal of methylene blue from a mixture of two dyes [298]. The polymer structures make possible the recovery and reuse of the nanoparticles. This composite demonstrated high photocatalytic efficiency in the decomposition of dye, attributed to the rapid swelling of the hydrogel in acidic conditions [299].

Enzymes have also been used alongside nanomaterials for water treatment. Researchers synthesized polydopamine tethered CPO/HRP- $\text{TiO}_2$  nanocomposites with high biocatalytic activity, stability and reusability. The synthetic method used was in situ polymerization along with an ultrasound bombardment size reduction technique. The enzyme is responsible for the biochemical degradation of the chromophore part of the dye. It has been employed in the degradation of aniline blue, crystal violet, and 2,4-dichlorophenol [300].

Multi walled carbon nanotubes have also been impregnated with  $\text{TiO}_2$  nanoparticles. The composite has similar positives as other immobilization matrixes [301].  $\text{TiO}_2$  nanoparticles have also been used in combination with activated carbon. This composite has been successful in degrading various dyes, in batches or with continuous flow [302]. Enhanced photocatalytic properties have also been achieved with silver doping on C- $\text{TiO}_2$  [303].

Graphene oxide (GO) has also been investigated when combined with  $\text{TiO}_2$ , as water filter, in order to remove dyes [304]. Higher presence of graphene oxide seems to positively affect the removal capabilities [305]. Reduced graphene oxide (rGO) has also been employed alongside  $\text{TiO}_2$  for dye degradation. Researchers utilized car bumpers as a recycled source of carbon, showcasing a method of upcycling waste into a novel and high-performance carbon-based photocatalyst. The technology holds the potential for improvement by

investigating the possibility of using different plastics for their carbon [306]. A hybrid rGO-TiO<sub>2</sub>/Co<sub>3</sub>O<sub>4</sub> nanomaterial was synthesized through co-precipitation and utilized for dye removal from wastewater. Reduced graphene oxide proved effective in narrowing the TiO<sub>2</sub>/Co<sub>3</sub>O<sub>4</sub> band-gap, allowing reaction under visible light. Furthermore, the rGO component inhibited electron-hole recombination, promoting dye degradation [307].

The g-C<sub>3</sub>N<sub>4</sub>/TiO<sub>2</sub> nanocomposite was able to perform under visible light irradiation. The nanotube-shaped nanomaterial exhibited the highest level of degradation compared to other structures and shapes derived from the experiments [308]. A graphitic carbon nitride-titanium dioxide-graphene aerogel was also an efficient catalyst under visible light irradiation [309,310]. A membrane made by g-C<sub>3</sub>N<sub>4</sub>/TiO<sub>2</sub>/PAA/PTFE was successfully used to filtrate waste under UV and visible light [311]. Another way to immobilize TiO<sub>2</sub> nanoparticles is on glass beads. These methods have been tested for dye and phenol removal [312,313].

Nanosheets of TiO<sub>2</sub>/g-C<sub>3</sub>N<sub>4</sub> with dispersed Fe<sub>3</sub>O<sub>4</sub> particles demonstrated high photocatalytic activity [314]. Similar results were observed for g-C<sub>3</sub>N<sub>4</sub>-TiO<sub>2</sub> composites independently [315]. Additionally, a composite of TiO<sub>2</sub> (MNTC nanosheets) formed from nanorods co-doped with Mo/N on carbon nanofibers was relatively successful [316]. Carbon nanosheets, similar to graphene with TiO<sub>2</sub>, demonstrated high adsorption capacity [257]. TiO<sub>2</sub> nanosheets also served as the foundation for a composite with Cu-biphenylamine, which achieved complete degradation of the dyes in under 3 h [317]. Another composite of TiO<sub>2</sub> nanosheets with silver completely removed the dye in 20 min [318].

Carbon dots are a zero-dimensional nanomaterial. SnO<sub>2</sub> carbon dots have been attached onto TiO<sub>2</sub> nanospheres to create a highly effective catalyst [319]. Three-dimensional nanomaterials containing nanorods have been used to create nanospheres of TiO<sub>2</sub> doped with platinum towards the visible light-assisted degradation of dyes [320].

Fe<sub>3</sub>O<sub>4</sub> has also been tested with TiO<sub>2</sub>. The experiments were performed under ultrasound to enhance performance [321]. In addition, the embedding of Fe<sub>3</sub>O<sub>4</sub> has been proven to be extremely useful, in order to provide TiO<sub>2</sub> with magnetic separation ability [322]. Moreover, the combination of oleic acid with TiO<sub>2</sub> was tested [323].

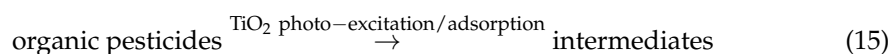
Photo-electrocatalysis has proven to be an efficient method for treating water containing methylene blue. Doping TiO<sub>2</sub> with fluorine enabled degradation under visible light and improved the generation of electron-hole pairs, enhancing performance [324]. In another study, met-anil yellow and Remazol red B dyes were successfully degraded through photo-electrocatalysis [325]. Furthermore, Pd-doped TiO<sub>2</sub> nanorods showed the ability to produce hydrogen as a byproduct during the removal of Rhodamine B through photo-electrocatalysis under solar irradiation. The unique structure of platinum atoms in the rod configuration contributed to its enhanced performance, particularly in retaining charges [326].

The use of TiO<sub>2</sub> as a photonic crystal has been demonstrated to enhance the degradation ability of catalysts in various studies. Titanium dioxide inverse opals have been proven to be effective in degrading dyes and phenols under ultra-violet light [327]. Photonic crystals coated with gold nanoparticles were able to remove phenols using visible light [328]. Inverse TiO<sub>2</sub> opal photonic crystals coupled with TiO<sub>2</sub>/poly(3-hexylthiophene) have demonstrated the ability to remove dyes with visible light sources [329]. TiO<sub>2</sub>@SiO<sub>2</sub> photonic crystals have been employed for the degradation of acetaldehyde and dyes [327,330]. An nc-TiO<sub>2</sub>/SnO<sub>2</sub> inverse opal composite membrane and Cu<sub>2</sub>O/TiO<sub>2</sub> have also been used as photocatalysts [331]. Inverse TiO<sub>2</sub>/Pt opals Schottky structures on the Ti substrate have proven effective in degrading phenols [332]. Additionally, a novel photonic crystal structural-induced Cu<sub>3</sub>SnS<sub>4</sub>/Ti<sup>3+</sup>-TiO<sub>2</sub> p-n coaxial heterojunction array was proved able to degrade dyes [333].

#### 5.4. TiO<sub>2</sub>-Based Photocatalysts for Effective Elimination of Pesticides from Water and Wastewater

The imperative need to remove pesticide residuals from water stems from their remarkably enhanced toxicity. One method for achieving this is mineralization, a process that involves the complete release of all inorganic components from organic pesticides through degradation. TiO<sub>2</sub> demonstrates the capacity for photocatalytic degradation of pesticides.

Resulting radicals from this reaction subsequently interact with dissolved oxygen, generating organic peroxy radicals (ROO●), crucial for achieving total pesticide mineralization (Equations (15) and (16)) [334].



The use of pesticides in the agriculture sector has proved extremely necessary, in order to fulfill the rising food requirements driven by a significant enhancement of the population globally. While pesticides effectively enhance production and prevent agricultural losses, they come with various environmental drawbacks [335]. Similar to dyes and pharmaceuticals, pesticides pose significant threats to aquatic organisms, given their exceptionally increased biological toxicity. These substances not only cause fatalities but also lead to a notable reduction in aquatic organisms' activity [336]. Moreover, their non-biodegradable nature contributes to their accumulation within various organisms. Pesticides can induce acute and chronic health effects, ranging from immune system disruption to improper endocrine function [337]. Moreover, there has been significant attention paid to the potential carcinogenicity of pesticides [338]. Like dyes and pharmaceuticals, traditional wastewater treatment approaches are unable to thoroughly eliminate pesticides, resulting in the potential accumulation of noxious substances in various organisms within the environment [339]. Nevertheless, titanium dioxide has exhibited remarkable effectiveness in degrading pesticides, both in its pure form and when doped.

For instance, chlorpyrifos, a phosphate-based pesticide, underwent photocatalytic degradation utilizing TiO<sub>2</sub> nanoparticles. Approximately 80% of the pesticide was decomposed within 24 h, while the photocatalyst proved effective whether bacteria were present or not, although bacterial presence slightly reduced the degradation rate of the examined pesticide. The as-mentioned photocatalytic procedure necessitated UV light irradiation, as visible irradiation lacked sufficient energy for the utilization of the reaction [340]. Similarly, profenofos and quinalphos have been reduced by TiO<sub>2</sub> nanoparticles using a comparable mechanism upon UV light irradiation. The photocatalyst displayed promising reusability potential under multiple cycles without substantial activity decrease. Its performance was influenced by various factors, such as TiO<sub>2</sub> concentration, radiation duration, and system pH [341]. Additionally, titanium dioxide has demonstrated effectiveness in treating a stream, including a pesticide combination (diuron, alachlor, isoproturon and atrazine).

The efficiency of TiO<sub>2</sub> as a photocatalyst was observed in treating pure, as well as ordinary, water. However, when additional pollutants in normal water were present, there was a notable decline in TiO<sub>2</sub>'s effectiveness, attributed to the hindrance of radical formation that accelerates the photocatalytic reaction [342]. The exceptional efficacy of TiO<sub>2</sub> nanowires in atrazine degradation has been evidenced because of their significant specific surface area, as well as pore volume. These nanowires also present advantages such as cost-effectiveness in synthesis and potential reusability across multiple cycles [343].

Imidacloprid degradation by nano-TiO<sub>2</sub> particles within a cylindrical reactor has been reported as highly effective. The reactor's structure, featuring coaxial cylinders, facilitated enhanced contact among the photocatalyst and polluted water, thereby enhancing photocatalytic performance. Additionally, the reactor demonstrated applicability in both batch and continuous modes, underscoring its adaptability and effectiveness [344]. TiO<sub>2</sub> P25 has been widely recognized as a photocatalyst for pesticide elimination. In one research project, typically found pesticides and insecticides, such as malathion, fenitrothion, quinalphos, vinclozolin, dimethoate and fenarimol, have been decomposed utilizing TiO<sub>2</sub> P25 under solar light irradiation. Another commercially available form, Kronos VLP 7000, was examined but proved to be less efficient than P25, because of inferior specific surface area and pore volume attributes [345]. Additionally, TiO<sub>2</sub> P25 has demonstrated increased efficacy in removing diazinon from water, achieving >99% pesticide decomposition at a pH value equal to 6.

The reaction primarily depended on the supplied UV amount and reaction time. Additionally, TiO<sub>2</sub> concentration and aeration have been identified as improving the photocatalytic process [346]. Altering the structure of titanium dioxide nanotubes significantly improved the elimination effectiveness of simazine pesticide. The proposed approach involved structural modification by varying the anodization time, with a time equal to 10 min yielding the optimal outcomes [347].

Incorporating Fe into TiO<sub>2</sub> demonstrated exceptional performance in diazinon decomposition, achieving an optimal decomposition efficiency of ≈85%. The presence of Fe notably accelerated the reaction under UV light and ultrasonic irradiation. Ultrasonic irradiation demonstrated better degradation efficacy when used individually. However, the highest efficiency was achieved when both UV and ultrasonic irradiation were combined with Fe-TiO<sub>2</sub> [348]. Introducing cerium (Ce) doping yielded excellent outcomes in removing metolachlor, a typically used pesticide. The magnetic properties of Ce facilitated the dopant-TiO<sub>2</sub> separation. Cerium doping enhanced porosity and decreased charge carrier recombination, significantly enhancing effectiveness [349]. Ce dopant also proved effective in removing another common pesticide, glyphosate. A Ce loading of 0.45 wt.% was determined as optimal. In addition, Mn and La were studied as potential dopants towards glyphosate elimination. Among the three, Mn exhibited the optimal performance, followed by Ce and then La, all with an optimal loading of the order of 0.45 wt.%. Concentrations surpassing the optimum value led to a great efficiency loss [350].

Ce has been utilized as a dopant in the photocatalytic elimination of dicamba pesticide under visible light irradiation. An optimal loading of Ce equal to 1 wt.% led to complete degradation within 2 h, particularly effective in conditions where pH values were greater than 7, generating non-toxic by-products easily removable from water. Ce aggregation increased specific surface area and pore volume, enhancing the photocatalytic effectiveness of Ce-TiO<sub>2</sub> compared to the bare photocatalyst [351]. Boron (B) doping exhibited superior degradation of various pesticides compared to the undoped photocatalyst, significantly enhancing robustness and reusability. The presence of B atoms within the TiO<sub>2</sub> lattice contributed to improved functionality and stability of the doped photocatalyst. Combining photocatalysis with ozonation accelerated pesticide elimination [352]. Furthermore, doping TiO<sub>2</sub> with non-metals, like C, N, and F, enhanced its degradation capability, notably preventing electron and hole pair recombination under visible light. Thiamethoxam and imidacloprid insecticides were completely degraded using doped photocatalysts under different wavelengths, showing stability across multiple cycles, promising for industrial applications [353].

Finally, the method of TiO<sub>2</sub> photo-electrocatalysis has proven effective in eliminating the herbicide atrazine from water samples. Almost total elimination of the contaminant occurred within 30 min reaction time, displaying a first-order kinetics trend [354]. Atrazine removal from groundwater has been also accomplished through employing TiO<sub>2</sub>-graphite photo-electrocatalysts, exhibiting an impressive reduction effectiveness of up to 99.7% [355], slightly surpassing the efficacy observed in the earlier study.

#### 5.5. TiO<sub>2</sub>-Based Photocatalysts for Effective Elimination of Microbes from Water and Wastewater

TiO<sub>2</sub> has been studied extensively for its anti-microbial activity [356]. It can be used on surfaces or to disinfect water. When the bacteria *E. coli* suffers membrane damage, malondialdehyde is produced, due to lipid peroxidation. Bactericidal activity can be measured in this way. TiO<sub>2</sub> activated by light, can cause cell death after a short time (30 min), by damaging the cell membranes. The creation of radicals causes lipid peroxidation. The by-product malondialdehyde is also oxidated further facilitating the easy cell access [357]. Cancer cells are also vulnerable to this type of damage [358].

The efficiency of bactericidal methods depends on their effective disinfection time (EDT), representing the duration needed for complete bacterial inactivation in the absence of irradiation, and without the possibility of regrowth. In the case of TiO<sub>2</sub>, no regrowth is observed within the subsequent 60 h in the absence of irradiation, as the bacterial concentration continues to decrease in the dark [359].

Photo-induced bactericidal methods have attracted research attention. TiO<sub>2</sub> nanoparticles are very effective, due to their decreased size [360]. In order for the nanoparticles to be reused, they need to be recovered. Immobilizing them on a matrix is a good solution, but decreases their efficiency. Enhanced permeability of ions through cell membranes has been proposed as a potential disinfection method. TiO<sub>2</sub> has also been shown to degrade the toxins that are released from the dying bacterial cells [361].

Various harmful microorganisms, including *Escherichia coli*, constitute a threat to water bodies worldwide. In general, these microbes produce noxious substances upon entering the human body [362]. Temperature, water turbidity, pH, and the presence of competing microorganisms affect their lifespan [363]. While sunlight has been found efficient in inactivating a plethora of microorganisms, scaling up this method for industrial use presents significant challenges. Alternative approaches, like chlorine treatment, have been explored; however, impracticality arises from the production of noxious substances associated with these approaches [364].

Microbes in aquatic bodies, can negatively affect the fish population [365]. Infected water has also been a major factor for the spread of diseases throughout history, like cholera caused by *Vibrio cholerae*, and typhoid caused by *Salmonella typhi* [366].

In this context, it is essential to research and develop photocatalysts that are efficient and environmentally friendly. Utilizing thin films consisting of TiO<sub>2</sub> nanoparticles has demonstrated remarkable efficacy in the elimination of *E. coli* from water through photocatalysis. The swift and efficient inactivation of cells is attributed to the expansion of the cell membrane upon adsorption by titanium dioxide and illumination. The potential effects include the loss of protoplasm, speculated to result from membrane expansion and cell distortion. Additionally, acids' fast degradation further contributes to the membrane's expansion [367]. TiO<sub>2</sub> nanotubes have also demonstrated comparable anti-microbial applications in water purification, targeting organisms such as *E. coli* and *Staphylococcus aureus*. Exposure to UV irradiation for 24 h in the presence of the photocatalyst resulted in the degradation of both organisms by more than 97%. The effect was greater than that exhibited by simple TiO<sub>2</sub> P25 nanoparticles. The shape of the nanomaterial seems to be an important factor for anti-microbial capabilities [368].

Nevertheless, TiO<sub>2</sub> P25 has proven exceptionally efficient against microbes under specific parameters. *Salmonella typhimurium* and *Listeria monocytogenes* were both inactivated by the photocatalyst when exposed to UV irradiation. *Listeria* was proven to be more resistant than *Salmonella*. The mechanism seems to be membrane damage, as in other cases. The catalytic reaction was significantly influenced by the concentration of the nanoparticles, with the most favorable results obtained at a concentration equal to 1 g/L [369].

Doping of the nanoparticles has also been extensively studied. Nitrogen doping is an easy and effective way to increase the bactericidal properties. Different nitrogen containing compounds have been used and, depending on the target microorganism, the optimal chemical can differ. For example, the removal of *B. cereus* was achieved completely when triethyl amine was used. In other cases, urea was better [370]. Nitrogen doping lowers the band-gap, making the photocatalyst more effective even when irradiated with visible light. Doping with fluorine has also been investigated, yielding a comparable outcome in terms of the E<sub>g</sub>. However, a distinction was observed in the distribution of atoms. More specifically, N atoms were detected in the interstices, while F atoms were observed superficially [371].

Research has demonstrated that TiO<sub>2</sub> doped with Fe, Mn and Mg is an extremely effective method for eliminating the virus H1N1 from water. The catalytic process proved viable even in the presence of a weak source of visible light irradiation, achieving over 99% elimination effectiveness within 30 min. Additionally, elimination utilizing UV irradiation was also feasible, but it is considered less practical, since the reaction can be conducted utilizing visible irradiation [372]. Likewise, TiO<sub>2</sub> nanofibers doped with Cu exhibited impressive capabilities in removing the f2 virus and *E. coli*. The concurrent elimination of both microorganisms was demonstrated upon visible light irradiation and the reaction proved to be unaffected by pH variations. The elimination of the virus was directly correlated with the photocatalyst's con-

centration, as well as the light's intensity, showing an inverse relationship with the quantity of the virus. Nevertheless, it was observed that the elimination of the virus was more enhanced when present alone, compared to its presence alongside bacteria, indicating competition for adsorption spaces as a contributing factor [373].

Silver, which itself is considered to have anti-microbial properties, can be used to greatly enhance the TiO<sub>2</sub> efficiency. Nanowires doped with silver demonstrated superior performance to other doping elements against the bacteria *E. coli*. The processed water was determined as safe to drink, therefore this nanomaterial has potential for large scale applications [374].

Other doping agents that lower the band-gap of TiO<sub>2</sub> and make it efficient for visible light photocatalysis are manganese and cobalt. The best results were produced by co-doping, which resulted in a 99% concentration reduction for the viruses that were tested, within 20 min. Sunlight contains the UV spectrum and is superior to artificial light [375].

In general, the mode of toxicity of TiO<sub>2</sub> nanoparticles towards harmful microorganisms is depicted in Figure 12.

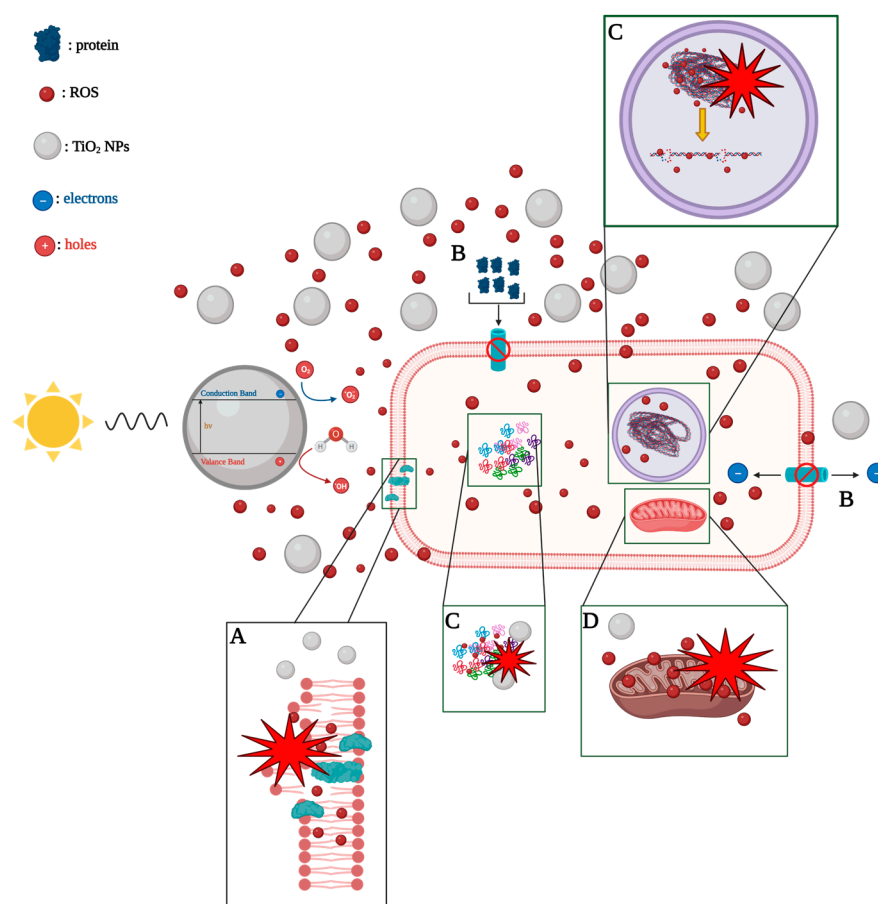


**Figure 12.** Schematic representation of the TiO<sub>2</sub> nanoparticles' toxicity mechanism towards pathogenic microorganisms. In general, the toxicity mechanism can be attributed to the following procedures: (A) infliction of cellular damage and lipid oxidation arising from the attachment of nano-particles through electrostatic interaction with the cell wall, (B) disruption of the cytoplasmic flow, due to nanoparticle hindrance of nutrient carriers, leading to (C) photocatalytic decomposition of biological macromolecules, and (D) impairment of intracellular organelles [376].

#### 5.6. TiO<sub>2</sub>-Based Photocatalysts for Effective Elimination of Hormones and Endocrine Disrupting Compounds (EDCs) from Water and Wastewater

Endocrine-disrupting chemicals (EDCs) are natural or human-made chemicals that may mimic, block, or interfere with the body's hormones, which are part of the endocrine system. These chemicals are associated with a wide array of health issues. They are found

in wastewater from some industries and from households. Drugs, pesticides and cosmetics can be a source of these chemicals, as well as living organisms [377]. They can have significant negative effects on humans, especially on the development of children [378]. It is also possible to affect the fetus in pregnant women [379]. Negative effects have also been found on aquatic life. An example of this is the feminization of fish, from high estrogen levels in their environment [380].

Hormones and some drugs are endocrine disrupting compounds. Hormones, even in very small amounts, can affect humans and other organisms [381]. Heavy metals can also affect the endocrine system. Some common chemicals found in the wastes of certain industries are phthalates, which are considered carcinogenic [382], and bisphenol, which is linked to sexual dysfunction in males [383].

It is difficult to completely remove these compounds from water, which means they often end up in the aquatic environment. It is very important to find ways to degrade these chemicals during wastewater treatment.  $\text{TiO}_2$  has shown promise as a viable and clean method to remove endocrine disrupting compounds from wastewater [384].

$\text{TiO}_2$  nanomaterials have been used for the degradation of many hormones and other similar compounds. The use of  $\text{TiO}_2$  thin films was very effective for the removal of steroidal hormones after light irradiation. Faster degradation was achieved with the addition of hydrogen peroxide [385].

Pure  $\text{TiO}_2$  nanoparticles have been used successfully for the removal of estrogens (female hormones: estrone, estradiol, estriol, estetrol) and mimic chemicals, like bisphenol A. UV light is required for efficient degradation and acidic conditions are favorable [386]. The photodegradation often has more than one stage. By-products, like hydroxylated estrones, are produced first and then they are further degraded [387]. From this class of hormones, estradiol seems to be easier to remove with pure  $\text{TiO}_2$  nanoparticles [388], while estriol and estrone require higher concentrations of the catalyst to be efficiently removed [389]. Compounds that belong to this class of chemicals have also been degraded with the use of stacked  $\text{TiO}_2$  thin films in reactors where the wastewater flows through. The removal of Bisphenol A in comparison to the other chemicals was the most challenging when using this method. The by-products produced are not as similar to estrogens, which means they are much safer [390].

Testosterone, which is a male hormone, can also be degraded by  $\text{TiO}_2$  nanoparticles. A study found that the resulting by-products are similar to those produced by natural metabolism [391]. The nanoparticles, under irradiation, can transfer electrons and also cause the formation of hydroxyl radicals in the solution. Both mechanisms are responsible for the degradation of the hormone.

Doping the nanoparticles with silver and adding hydrogen peroxide in the solution during photodegradation resulted in good performance under visible light irradiation. The test was carried out with dexamethasone as a pollutant [392].

$\text{TiO}_2$  has also been used in conjunction with phytoremediation. Phytoremediation is a technique that uses plants to clean polluted ground. By combining these two methods, researchers were able to remove the pollutant decabromodiphenyl ether. The byproducts were nontoxic. The  $\text{TiO}_2$  increased its efficiency by helping uptake by the plants [393].

Titanium dioxide has also been used in hybrid composites in an effort to synthesize a more efficient catalyst. Porphyrins are a class of organic compounds that are often used in photodynamic therapy. Researchers used cardanols, a toxic byproduct of the cashew industry, to synthesize porphyrins, that were then impregnated with  $\text{TiO}_2$  nanoparticles. Metals such as zinc and iron were also used to create metallo-porphyrins. This conjugate was used to degrade 4-nitrophenol [394].

In general, an effective way to use  $\text{TiO}_2$  nanoparticles is to immobilize them into a matrix. In this way, they can easily be used inside a recirculation reactor.  $\text{TiO}_2$ -coated clay beads were used in this way, to degrade the pollutant monocrotophos [395].

Other  $\text{TiO}_2$  nanomaterials that have been tested, are nanotubes, doped with  $\text{C}_3\text{N}_4$ . Using electro-photocatalysis, the researchers reported that the degradation of phenolic com-

pounds was much faster compared to pure TiO<sub>2</sub>. The doping lowered the band-gap [396]. Other complex nano-structures that have been synthesized are hydrogels with graphene and TiO<sub>2</sub>. The tests showed outstanding performance during photo-electrocatalysis for the degradation of bisphenol A and no significant decline in performance after 10 cycles [309,310]. The method of photo-electrocatalysis has also been used to degrade propyl paraben using TiO<sub>2</sub> nanotubes doped with WO<sub>3</sub> [397].

## 6. TiO<sub>2</sub> Nanoparticles' Fate in the Atmosphere, Aqueous Environments, and Sediments

Due to advancements in nanotechnology, the environmental impact of nanoparticles has become significant. With their increased usage and production, there is a heightened exposure of nanoparticles to the environment, encompassing the atmosphere, aqueous environments and sediments [398] (Figure 13). Sunscreens, comprising roughly a quarter of TiO<sub>2</sub> nanoparticles, represent a prominent source of these particles entering aquatic environments [399]. Upon entering water post-sunscreen application, TiO<sub>2</sub> nanoparticles are released into the surroundings, accounting for approximately 10–40% of the initially applied sunscreen, varying based on formulation viscosity [400]. In wastewater treatment plants, about 34% and 87% of TiO<sub>2</sub> nanoparticles are estimated to be removed from primary and secondary settling tanks, respectively [401]. Nevertheless, these particles may contaminate agricultural sediments and potentially seep into groundwater, because of the common use of sewage sludge as a sediment fertilizer.

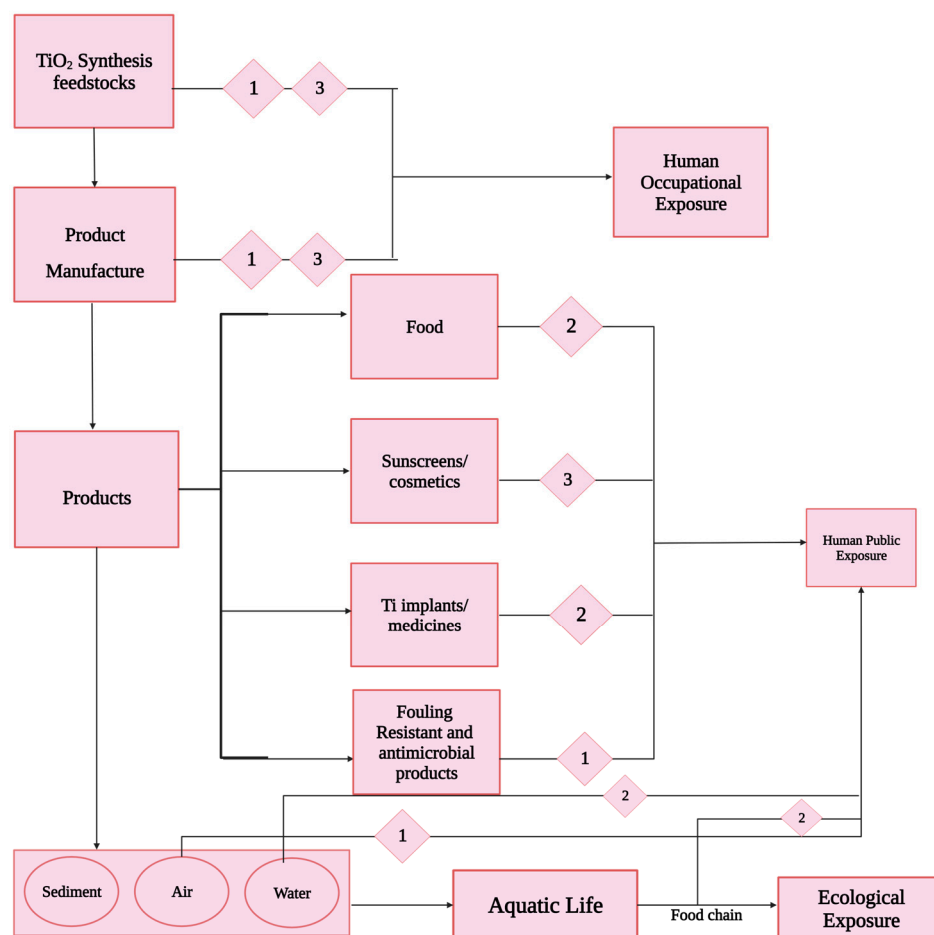


**Figure 13.** Potential scenarios involving the distribution, absorption, and repercussions of TiO<sub>2</sub> nanoparticles within an ecosystem (numbers 1, 2 and 3 stand for inhalation, ingestion and deposition, respectively).

Understanding the interaction between nanoparticles and sediments remains insufficient due to the complex nature of soil. When nanoparticles encounter sediments, they can

either be physically retained or chemically adsorbed onto the surfaces of the sediments' particles [402]. These interactions, influenced by the sediments' chemical and physical properties along with their texture, can either decrease or enhance the toxicity and availability of nanoparticles. Various parameters, like natural organic matter, salinity, ionic strength, pH values, clay content, and microbial population, impact the behavior of TiO<sub>2</sub> nanoparticles in sediments. The fate and behavior of these nanoparticles in sediments involve hetero-aggregation, homo-aggregation, and straining mechanisms [403].

## 7. Potential Toxicity of TiO<sub>2</sub> Nanoparticles

In recent times, there has been a surge in interest surrounding nanotechnology applications across diverse domains, including agriculture, medicine, pharmacy, and materials science. The utilization of TiO<sub>2</sub> nanoparticles is inevitable due to their crystal structure, size, and coating. These nanoparticles' surface charge, agglomeration, and sedimentation are influenced by their particle size, crystalline structure and coating, rendering TiO<sub>2</sub> nanoparticles highly noxious to human cells. Existing studies indicate that these nanoparticles disrupt glucose and lipid balance in mice and rats [398]. However, available data on TiO<sub>2</sub> nanoparticles' toxicity to humans remain limited, thus raising doubts about potential risks. Consequently, researchers are employing various toxicological models, like human cells, animals, and aquatic organisms, for gathering crucial information, in order to mitigate toxicity concerns (Figure 14).

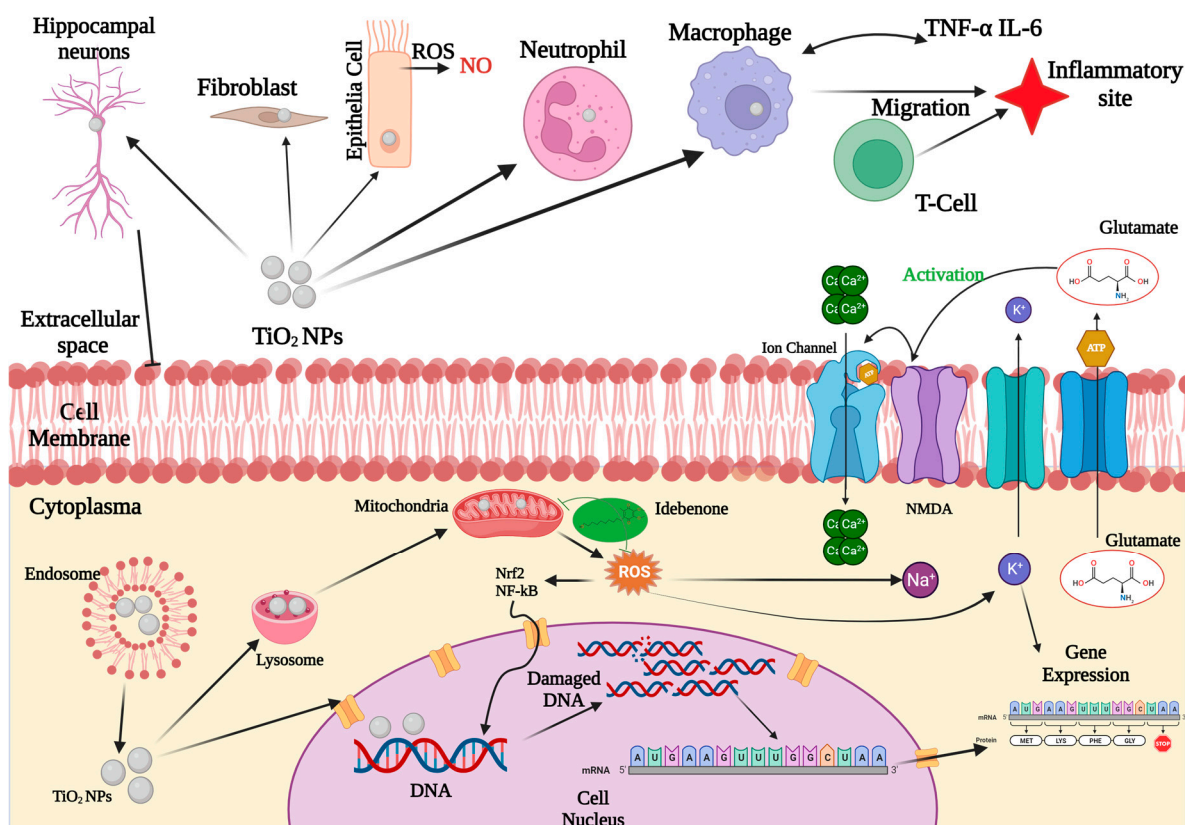


Figure 14. Illustration of TiO<sub>2</sub>'s toxicity mechanism.

Past experiments, both in laboratory settings and living organisms, have verified the detrimental effects of TiO<sub>2</sub> nanoparticles on the human body, leading to alterations in the cell cycle, nuclear constriction, and apoptosis [404,405]. Moreover, these nanoparticles have been linked to DNA damage and disruption of the small intestine epithelium, crucial for nutrient absorption [406]. Such harm can occur through multiple routes, primarily inhalation, injection, skin contact, as well as digestion and absorption [407]. Instances

in print plant facilities revealed workers experiencing respiratory issues due to exposure to polyacrylate nanoparticles combined with TiO<sub>2</sub> nanoparticles, lacking adequate protective measures [408]. Other reported clinical manifestations of TiO<sub>2</sub> toxicity include facial, hand, and forearm rashes [409], pleural effusion [410], pericardial effusions [411], hypoxemia [408], and even cases of cancer [412–414]. Studies conducting in vivo exposure tests have highlighted the accumulation of TiO<sub>2</sub> nanoparticles in various bodily organs, such as liver, heart, spleen, lungs, kidneys, digestive tract, and cardiac muscle [415,416].

### 7.1. Biodistribution and Systemic Toxicity

Nanomaterials exhibit substantial variations in composition, charge, structure and specific surface area, all impacting various organs (Figure 15) [417], and could be potentially present in organs like lungs, kidney, lymph nodes, liver, and spleen [418]. TiO<sub>2</sub> nanoparticles can move from the digestive tract to other organs or tissues, potentially causing damage to the liver and myocardium [419].

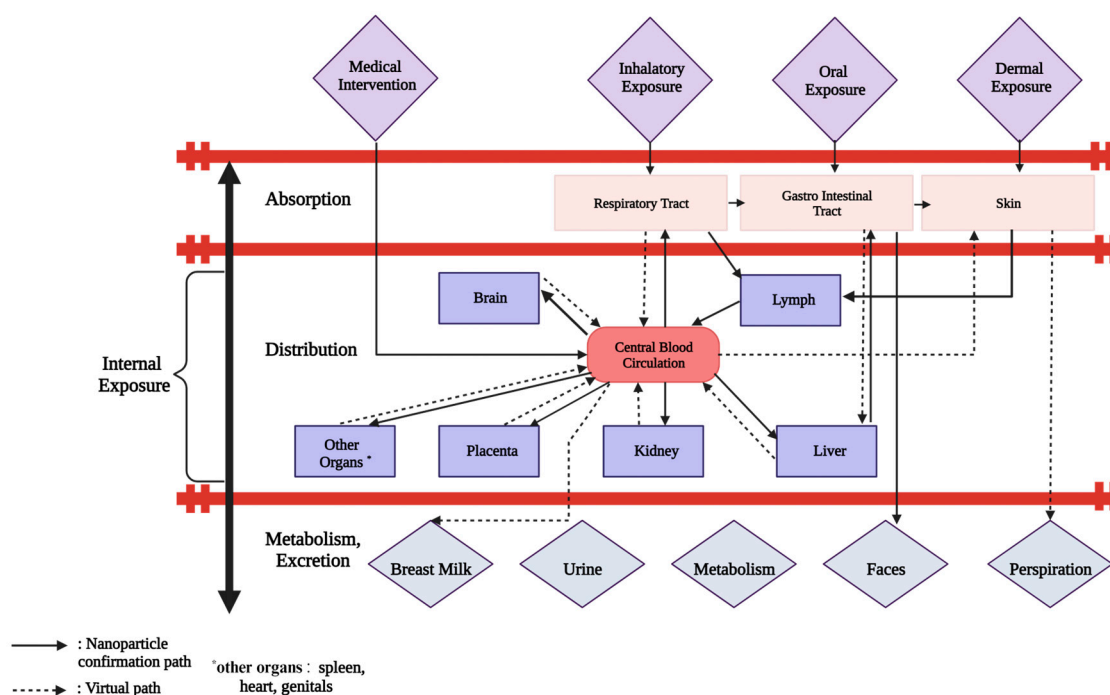


**Figure 15.** The in vivo dynamic nature of nanostructured materials.

Concerning lung toxicity, investigations suggest that the surface area might serve as the most suitable dosage indicator for TiO<sub>2</sub> nanoparticles [407]. Ultrafine TiO<sub>2</sub> nanoparticles, possessing increased quality or decreased volatility, can cause lung damage even at trace doses [420]. In experiments involving rats treated with TiO<sub>2</sub> nanoparticles, heightened inflammatory reactions have been observed, because of an enhanced surface area of the nanoparticles, in comparison to particles with a larger surface area. A few studies indicate that TiO<sub>2</sub> nanoparticles induce more substantial pulmonary inflammation than larger TiO<sub>2</sub> particles when introduced at similar mass doses [421,422]. Nevertheless, when the dosage is standardized based on surface area, the lung's response remains comparable between nanosized and fine TiO<sub>2</sub> particles. Therefore, investigations into lung toxicity demonstrate that particles of the same chemistry, but of varying sizes, are more insightful. Additionally, other studies propose that inflammatory reactions might be more intense when nanoparticles possess a larger surface area [423]. Nevertheless, numerous studies have indicated more adverse effects associated with TiO<sub>2</sub> nanoparticles [424]. These particles can lead to immunological and pathological alterations upon accumulation [425],

while, depending on their size and quantity, they can stimulate hepatic injury through changing serum biochemical factors (ALT, LDH, and BUN) [419].

Brain injury can be triggered by TiO<sub>2</sub> nanoparticles, due to their heightened susceptibility to oxidative stress [426,427]. When introduced via the nasal route, these nanoparticles can impact olfactory nerve and hippocampal neurons, leading to reduced spatial recognition memory in mice under oxidative stress conditions [428]. Additionally, disruption in the equilibrium of neurotransmitters, trace elements, and enzymes caused by TiO<sub>2</sub> nanoparticles can further impair spatial recognition memory. Various studies have demonstrated the toxic effects of these nanoparticles, which vary based on exposure duration and dosage [429–432]. TiO<sub>2</sub> nanoparticles prompt apoptosis and are able to accumulate within the brain, leading to increased levels of malondialdehyde, superoxide, 8-hydroxy-2'-deoxyguanosine, and carbonyl protein [433]. Moreover, alterations in associated genes' expression have been observed, stimulating brain microglia to disrupt mitochondrial energy production, resulting in ROS production [434,435]. Furthermore, these particles exert a noxious influence on glial cells, instigating alterations in the morphology and elevating mitochondrial membrane potential [436].

### 7.2. TiO<sub>2</sub> Nanoparticle-Induced Oxidative Stress

Oxidative stress stands as a principal mechanism behind the adverse biological impacts caused by nanoparticles [437]. This mechanism is evident through the escalation in reactive oxygen species generation, oxidative by-products, and the reduction of cellular antioxidants [438]. In the context of TiO<sub>2</sub> nanoparticles, oxidative stress is widely acknowledged as a significant mechanism, attributed to hydroxyl production, DNA damage [439], as well as elevated levels of glutathione and malondialdehyde in the liver [440]. TiO<sub>2</sub> triggers oxidative stress, generating varying quantities of hydroxyl radicals, either in the presence or absence of UV irradiation [441]. The as-mentioned •OH radicals, recognized as primary destructive agents, amplify the damage of DNA [439]. After initial exposure to UV irradiation, anatase TiO<sub>2</sub> nanoparticle sizes diminish cell viability in rats, leading to the breakage of the DNA strand and oxidative damage to the DNA [442]. This pivotal finding highlights that photo-activated TiO<sub>2</sub> nanoparticles preserve heightened cytotoxic and genotoxic potential, irrespective of the size of the nanoparticles, even if UV irradiation ceases, owing to the critical role of ROS as a signal regulator [442]. Cells' exposure to nanoparticles can disrupt cellular signaling cascades governing processes like cell proliferation, inflammation, and cell death by escalating ROS production [443]. The generation of reactive oxygen species is contingent on triggering inflammatory cascades, including the phosphorylation of Extracellular Signal-Regulated Kinase ERK1/2, Tumor Necrosis Factor alpha (TNFα), and macrophage generation. Elevated TiO<sub>2</sub> nanoparticles-induced stress results in cellular damage linked to oxidative stress and inflammatory signaling pathways' modulation [435].

### 7.3. TiO<sub>2</sub> Nanoparticles' Cellular Uptake

From a toxicological perspective, the primary attributes defining TiO<sub>2</sub> nanoparticles include their surface area, size, chemical traits, solubility, crystalline structure, and particle accumulation [444]. The uptake by cells, subcellular positioning, and ensuing toxicity are contingent upon these nanoparticle characteristics [444]. Two primary methods govern nanoparticles cell absorption: (a) active intake via endocytosis and (b) passive absorption through free diffusion [445]. When inhaled, TiO<sub>2</sub> nanoparticles can prompt alveolar macrophages towards elimination of μm-sized particles (3–6 μm), but struggle to remove TiO<sub>2</sub> nanoparticles due to their diminutive size (20 nm) [445]. Typically, phagocytosis handles particles >500 nm, while smaller particles remain in the tissue, perpetually stressing other tissues due to limitations in endocytosis [446,447]. Studies show that the uptake of TiO<sub>2</sub> nanoparticles (50 nm) through endocytosis with alveolar A549 epithelial cells is mostly confined to aggregated particles [447]. In an in vitro airway wall model, Rothen-Rutishauser and colleagues [448] observed membrane-bound aggregates (>200 nm) and

unbound aggregates within the cytoplasm. These researchers noted exceptionally high aggregated nanoparticles in both late and early endosomes. TiO<sub>2</sub> nanoparticle aggregates <200 nm could penetrate red blood cells, while larger particles remained affixed surficial to the cell [448].

#### 7.4. Potential Approaches for Addressing the Potential Toxicity of TiO<sub>2</sub> Nanoparticles

Industrial and wastewater treatment plants' (WWTPs) effluents are considered the main source of nano-TiO<sub>2</sub> entering the aquatic systems [449], thus posing a severe risk to all living biota in rivers [450], estuarine and coastal regions [451], as well as human health. For instance, Shi and his team [452] observed that the active sludge process effectively eliminated the majority of nano-TiO<sub>2</sub> from WWTPs, although the levels of Ti in the effluent remained relatively high at 27–43 µg/L. The researchers also noted total Ti concentrations in receiving waters ranging from 52 to 86 µg/L. This investigation additionally affirmed a substantial contribution from alternative sources, such as urban runoff from external paint. Westerhoff and co-researchers [453] documented nano-TiO<sub>2</sub> levels in raw sewage waters within WWTPs, ranging from 181 to 1233 µg/L. Furthermore, Sun and his team [454] disclosed nano-TiO<sub>2</sub> levels of 16 µg/L in WWTP effluents post-treatment, 170 µg/g in WWTP sludge, and 12 µg/g in solid waste. Finally, Kunhikrishnan and colleagues [455] estimated potential nano-TiO<sub>2</sub> levels of 21 ng/L in surface waters and 4 µg/L for WWTP effluents post-treatment. As a result, there is an urgent need to develop alternative approaches for water and wastewater effluents' treatment, so as to minimize, or even eliminate, the presence of nano-TiO<sub>2</sub> particles.

Photocatalytic slurry (in suspension) systems have been widely studied at laboratory scale for treatment of urban and industrial wastewaters towards the degradation of emerging organic pollutants [456]. Despite the simplicity and relevantly high efficiency of photocatalysts used in the form of dispersed powder, the practical applications of photocatalytic slurry systems are limited. This can be mainly attributed to various technical challenges, such as the potential toxicity arising from the release of some nanoparticles to water and the generation of sludge, containing nanoparticles of photocatalysts [457].

Therefore, in order to avoid the numerous drawbacks associated with the use of nano-TiO<sub>2</sub> in suspension, immobilization of photocatalyst on inert supports/substrates, such as glass, organic polymers or ceramic plates [458], in the form of thin films could significantly simplify the separation procedure and enhance applicability of the photocatalytic process. Immobilization of photocatalysts allows avoidance of the possible release of nanoparticles in water, sludge generation, and significant decrease in the cost of treatment by eliminating the photocatalyst recovery step. In a study by Valério and co-researchers [456], the relationships between photocatalysis, catalyst release and associated potential environmental hazards were assessed using zebrafish embryonic development as a proxy. Based on the acquired result, immobilized nanoparticles demonstrated the safest approach for the environment, as the process eliminated remnant additives, while preventing the release of nanoparticles.

Coating of nano-TiO<sub>2</sub> particles with ligands of different natures, like organic or inorganic species, polymers, etc., could also comprise another potential approach for preventing their release into the environment during the photocatalytic wastewater treatment. Such surface modifications of nano-TiO<sub>2</sub> have been proposed as a safer approach for the production of paints towards the photo-degradation of VOCs, in order to avoid the release of aerosolized particles and undesired organic compounds from oxidized or partially oxidized VOCs in the air [459].

## 8. Conclusions and Future Remarks

The extensive use of water in households and diverse industries has led to the pervasive contamination of available water sources and ecosystems. Numerous well-known water pollutants have been identified, highlighting their adverse impacts on both human health and aquatic life. In addition, the mechanisms employed in the photocatalytic degradation of each type of pollutant utilizing TiO<sub>2</sub> have been thoroughly reviewed. The

available synthetic approaches for the production of nano-TiO<sub>2</sub> have been also extensively studied and compared regarding their advantages and limitations. Given the toxicity-related issues that accompany the usage of nanomaterials and are attributed to their size range (1–100 nm), the toxicity of nano-TiO<sub>2</sub> structures has also been thoroughly discussed.

As an overview, it is evident from the numerous research attempts discussed within the present review that TiO<sub>2</sub>-based nanomaterials have emerged as promising and versatile candidates for addressing water and wastewater treatment challenges. Their unique photocatalytic properties, high surface area, stability, and low cost have propelled their utilization in various treatment processes. The ability of TiO<sub>2</sub> nanoparticles to efficiently degrade organic and inorganic pollutants, disinfect water from harmful pathogens, and remove heavy metal ions showcases their potential in mitigating water contamination issues. However, challenges, such as optimizing the photocatalytic efficiency under different environmental conditions, ensuring minimal nanoparticle leaching, and scaling up production for practical applications, need further research and development.

The continual advancements in nanotechnology and materials science hold immense promise for enhancing the performance and application of TiO<sub>2</sub>-based nanomaterials in water treatment. Future research directions could focus on tailoring the properties of TiO<sub>2</sub> nanoparticles, exploring novel composite materials, and assessing their long-term environmental impact to foster sustainable and efficient water treatment solutions. With concerted efforts in addressing these challenges, TiO<sub>2</sub>-based nanomaterials are poised to play a pivotal role in ensuring access to clean and safe water, contributing significantly to global water sustainability efforts.

**Author Contributions:** Conceptualization, M.-A.G. and N.L.; methodology, M.-A.G. and N.L.; validation, M.-A.G., N.L. and E.A.P.; formal analysis, M.-A.G. and N.L.; investigation, M.-A.G.; writing—original draft preparation, M.-A.G. and A.S.; writing—review and editing, M.-A.G., A.S., N.L. and E.A.P.; visualization, M.-A.G.; supervision, E.A.P. All authors have read and agreed to the published version of the manuscript.

**Funding:** This research received no external funding.

**Data Availability Statement:** No new data were created or analyzed in this study. Data sharing is not applicable to this article.

**Conflicts of Interest:** The authors declare no conflicts of interest.

## References

1. UNESCO. *The United Nations World Water Development Report 2020 Water and Climate Change*; UNESCO: Paris, France, 2020.
2. Chart, H. VTEC enteropathogenicity. *Symp. Ser. Soc. Appl. Microbiol.* **2000**, *29*, 12S–23S. [[CrossRef](#)] [[PubMed](#)]
3. Fowler, C.C.; Galán, J.E. Decoding a Salmonella typhi regulatory network that controls typhoid toxin expression within human cells. *Cell Host Microbe* **2018**, *23*, 65–76. [[CrossRef](#)]
4. Rivera-Chávez, F.; Mekalanos, J.J. Cholera toxin promotes pathogen acquisition of host-derived nutrients. *Nature* **2019**, *572*, 244–248. [[CrossRef](#)] [[PubMed](#)]
5. Chuang, C.-H.; Wang, Y.-H.; Chang, H.-J.; Chen, H.-L.; Huang, Y.-C.; Lin, T.-Y.; Ozer, E.A.; Allen, J.P.; Hauser, A.R.; Chiu, C.-H. Shanghai fever: A distinct *Pseudomonas aeruginosa* enteric disease. *Gut* **2014**, *63*, 736–743. [[CrossRef](#)] [[PubMed](#)]
6. Rajasurya, V.; Surani, S. *Legionnaires Disease in Immunocompromised Host*; IntechOpen: London, UK, 2020. [[CrossRef](#)]
7. Sansenya, T.; Masri, N.; Chankhanittha, T.; Senasu, T.; Piriyanon, J.; Mukdasai, S.; Nanan, S. Hydrothermal synthesis of ZnO photocatalyst for detoxification of anionic azo dyes and antibiotic. *J. Phys. Chem. Solids* **2022**, *160*, 110353. [[CrossRef](#)]
8. Vaez, Z.; Javanbakht, V. Synthesis, characterization and photocatalytic activity of ZSM-5/ZnO nanocomposite modified by Ag nanoparticles for methyl orange degradation. *J. Photochem. Photobiol. A* **2020**, *388*, 112064. [[CrossRef](#)]
9. Khataee, A.R.; Pons, M.N.; Zahraa, O. Photocatalytic degradation of three azo dyes using immobilized TiO<sub>2</sub> nanoparticles on glass plates activated by UV light irradiation: Influence of dye molecular structure. *J. Hazard. Mater.* **2009**, *168*, 451–457. [[CrossRef](#)]
10. Liberatore, L.; Bressan, M.; Belli, C.; Lustrato, G.; Ranalli, G. Chemical and biological combined treatments for the removal of pesticides from wastewaters. *Water Air Soil Pollut.* **2012**, *223*, 4751–4759. [[CrossRef](#)]
11. Ballesteros Martín, M.M.; Sánchez Pérez, J.A.; Casas López, J.L.; Oller, I.; Malato Rodríguez, S. Degradation of a four-pesticide mixture by combined photo-Fenton and biological oxidation. *Water Res.* **2009**, *43*, 653–660. [[CrossRef](#)]
12. Bressan, M.; Liberatore, L.; d’Alessandro, N.; Tonucci, L.; Belli, C.; Ranalli, G. Improved combined chemical and biological treatments of olive oil mill wastewaters. *J. Agric. Food Chem.* **2004**, *52*, 1228–1233. [[CrossRef](#)]

13. Tahir, M.S.; Saleem, M.; Malik, S.R.; Khan, J.R.; Siebenhofer, M. An innovative and advanced oxidation process for effluent treatment through wet tube-type electrostatic precipitation. *Chem. Eng. Process. Process Intensif.* **2012**, *52*, 16–20. [[CrossRef](#)]
14. Ben Mansour, L.; Kesentini, I. Treatment of effluents from cardboard industry by coagulation-electroflotation. *J. Hazard. Mater.* **2008**, *153*, 1067–1070. [[CrossRef](#)] [[PubMed](#)]
15. Hanay, Ö.; Hasar, H. Effect of anions on removing  $\text{Cu}^{2+}$ ,  $\text{Mn}^{2+}$  and  $\text{Zn}^{2+}$  in electrocoagulation process using aluminum electrodes. *J. Hazard. Mater.* **2011**, *189*, 572–576. [[CrossRef](#)] [[PubMed](#)]
16. Centi, G.; Perathoner, S.; Torre, T.; Verduna, M.G. Catalytic wet oxidation with  $\text{H}_2\text{O}_2$  of carboxylic acids on homogeneous and heterogeneous Fenton-type catalysts. *Catal. Today* **2000**, *55*, 61–69. [[CrossRef](#)]
17. Ghosh, P.; Samanta, A.N.; Ray, S. Reduction of COD and removal of  $\text{Zn}^{2+}$  from rayon industry wastewater by combined electro-Fenton treatment and chemical precipitation. *Desalination* **2011**, *266*, 213–217. [[CrossRef](#)]
18. Lin, S.H.; Chang, C.C. Treatment of landfill leachate by combined electro-Fenton oxidation and sequencing batch reactor method. *Water Res.* **2000**, *34*, 4243–4249. [[CrossRef](#)]
19. Ayodele, O.B.; Hameed, B.H. Synthesis of copper pillared bentonite ferrioxalate catalyst for degradation of 4-nitrophenol in visible light assisted Fenton process. *J. Ind. Eng. Chem.* **2013**, *19*, 966–974. [[CrossRef](#)]
20. Monteagudo, J.M.; Durán, A.; San Martín, I.; Aguirre, M. Effect of light source on the catalytic degradation of protocatechuic acid in a ferrioxalate-assisted photo-Fenton process. *Appl. Catal. B* **2010**, *96*, 486–495. [[CrossRef](#)]
21. John Peter, I.; Praveen, E.; Vignesh, G.; Nithiananthi, P. ZnO nanostructures with different morphology for enhanced photocatalytic activity. *Mater. Res. Express* **2017**, *4*, 124003. [[CrossRef](#)]
22. Zhang, D.E.; Ren, L.Z.; Hao, X.Y.; Pan, B.B.; Wang, M.Y.; Ma, J.J.; Li, F.; Li, S.A.; Tong, Z.W. Synthesis and photocatalytic property of multilayered  $\text{Co}_3\text{O}_4$ . *Appl. Surf. Sci.* **2015**, *355*, 547–552. [[CrossRef](#)]
23. Ani, I.J.; Akpan, U.G.; Olutoye, M.A.; Hameed, B.H. Photocatalytic degradation of pollutants in petroleum refinery wastewater by  $\text{TiO}_2$ - and  $\text{ZnO}$ -based photocatalysts: Recent development. *J. Clean. Prod.* **2018**, *205*, 930–954. [[CrossRef](#)]
24. Tanji, K.; Navio, J.A.; Chaqroune, A.; Naja, J.; Puga, F.; Hidalgo, M.C.; Kherbeche, A. Fast photodegradation of rhodamine B and caffeine using  $\text{ZnO}$ -hydroxyapatite composites under UV-light illumination. *Catal. Today* **2022**, *388–389*, 176–186. [[CrossRef](#)]
25. Lagopati, N.; Tsilibary, E.P.; Falaras, P.; Papazafiri, P.; Pavlatou, E.A.; Kotsopoulou, E.; Kitsiou, P. Effect of nanostructured  $\text{TiO}_2$  crystal phase on photoinduced apoptosis of breast cancer epithelial cells. *Int. J. Nanomed.* **2014**, *9*, 3219–3230.
26. Lagopati, N.; Kitsiou, P.; Kontos, A.; Venieratos, P.; Kotsopoulou, E.; Kontos, A.; Dionysiou, D.; Pispas, S.; Tsilibary, E.; Falaras, P. Photo-induced treatment of breast epithelial cancer cells using nanostructured titanium dioxide solution. *J. Photochem. Photobiol. A Chem.* **2010**, *214*, 215–223. [[CrossRef](#)]
27. Anitha, B.; Khadar, M.A. Anatase-rutile phase transformation and photocatalysis in peroxide gel route prepared  $\text{TiO}_2$  nanocrystals: Role of defect states. *Solid State Sci.* **2020**, *108*, 106392. [[CrossRef](#)]
28. Lagopati, N.; Kotsinas, A.; Veroutis, D.; Evangelou, K.; Papaspyropoulos, A.; Arfanis, M.; Falaras, P.; Kitsiou, P.V.; Pateras, I.; Bergonzini, A.; et al. Biological effect of silver-modified nanostructured titanium dioxide in cancer. *Cancer Genom. Proteom.* **2021**, *18* (Suppl. S3), 425–439. [[CrossRef](#)]
29. Nur, A.S.M.; Sultana, M.; Mondal, A.; Islam, S.; Robel, F.N.; Islam, A.; Sumi, M.S.A. A review on the development of elemental and codoped  $\text{TiO}_2$  photocatalysts for enhanced dye degradation under UV-vis irradiation. *J. Water Process. Eng.* **2022**, *47*, 102728. [[CrossRef](#)]
30. Kowalska, E.; Mahaney, O.O.P.; Abe, R.; Ohtani, B. Visible-light-induced photocatalysis through surface plasmon excitation of gold on titania surfaces. *Phys. Chem. Chem. Phys.* **2010**, *12*, 2344–2355. [[CrossRef](#)]
31. Akimoto, J.; Gotoh, Y.; Oosawa, Y.; Nonose, N.; Kumagai, T.; Aoki, K.; Takei, H. Topotactic oxidation of ramsdellite-type  $\text{Li}_{0.5}\text{TiO}_2$ , a new polymorph of titanium dioxide:  $\text{TiO}_2(\text{R})$ . *J. Solid State Chem.* **1994**, *113*, 27–36. [[CrossRef](#)]
32. Latroche, M.; Brohan, L.; Marchand, R.; Tournoux, M. New hollandite oxides:  $\text{TiO}_2(\text{H})$  and  $\text{K}_{0.06}\text{TiO}_2$ . *J. Solid State Chem.* **1989**, *81*, 78–82. [[CrossRef](#)]
33. Marchand, R.; Brohan, L.; Tournoux, M.  $\text{TiO}_2(\text{B})$  a new form of titanium dioxide and the potassium octatitanate  $\text{K}_2\text{Ti}_8\text{O}_{17}$ . *Mater. Res. Bull.* **1980**, *15*, 1129–1133. [[CrossRef](#)]
34. Simons, P.Y.; Dachille, F. The structure of  $\text{TiO}_2\text{II}$ , a high-pressure phase of  $\text{TiO}_2$ . *Acta Cryst.* **1967**, *23*, 334–336. [[CrossRef](#)]
35. Tang, J.; Endo, S. P–T Boundary of  $\alpha\text{-PbO}_2$  type and baddeleyite type high-pressure phases of titanium dioxide. *J. Am. Ceram. Soc.* **1993**, *76*, 796–798. [[CrossRef](#)]
36. Staun Olsen, J.; Gerward, L.; Jiang, J.Z. On the rutile/ $\alpha\text{-PbO}_2$ -type phase boundary of  $\text{TiO}_2$ . *J. Phys. Chem. Solids* **1999**, *60*, 229–233. [[CrossRef](#)]
37. Hanaor, D.A.; Sorrell, C.C. Review of the anatase to rutile phase transformation. *J. Mater. Sci.* **2011**, *46*, 855–874. [[CrossRef](#)]
38. Gamboa, J.A.; Pasquevich, D.M. Effect of chlorine atmosphere on the anatase-rutile transformation. *J. Am. Ceram. Soc.* **1992**, *75*, 2934–2938. [[CrossRef](#)]
39. Ding, X.Z.; He, Y.Z. Study of the room temperature ageing effect on structural evolution of gel-derived nanocrystalline titania powders. *J. Mater. Sci. Lett.* **1996**, *15*, 320–322. [[CrossRef](#)]
40. Muscat, J.; Swamy, V.; Harrison, N.M. First-principles calculations of the phase stability of  $\text{TiO}_2$ . *Phys. Rev. B* **2002**, *65*, 224112. [[CrossRef](#)]
41. Arlt, T.; Bermejo, M.; Blanco, M.A.; Gerward, L.; Jiang, J.Z.; Staun Olsen, J.; Recio, J.M. High-pressure polymorphs of anatase  $\text{TiO}_2$ . *Phys. Rev. B* **2000**, *61*, 14414–14419. [[CrossRef](#)]

42. Diebold, U. The surface science of titanium dioxide. *Surf. Sci. Rep.* **2003**, *48*, 53–229. [[CrossRef](#)]
43. Zhang, Q. Effects of calcination on the photocatalytic properties of nanosized TiO<sub>2</sub> powders prepared by TiCl<sub>4</sub> hydrolysis. *Appl. Catal. B* **2000**, *26*, 207–215. [[CrossRef](#)]
44. Chen, X.; Mao, S.S. Titanium dioxide nanomaterials: Synthesis, properties, modifications, and applications. *Chem. Rev.* **2007**, *107*, 2891–2959. [[CrossRef](#)]
45. Haidry, A.A.; Yucheng, W.; Fatima, Q.; Raza, A.; Zhong, L.; Chen, H.; Rutendo Mandebvu, C.; Ghani, F. Synthesis and characterization of TiO<sub>2</sub> nanomaterials for sensing environmental volatile compounds (VOCs): A review. *TrAC Trends Anal. Chem.* **2024**, *170*, 117454. [[CrossRef](#)]
46. Khataee, A.R.; Kasiri, M.B. Photocatalytic degradation of organic dyes in the presence of nanostructured titanium dioxide: Influence of the chemical structure of dyes. *J. Mol. Catal. A Chem.* **2010**, *328*, 8–26. [[CrossRef](#)]
47. Alves Junior, R.; Alves, H.P.A.; Cartaxo, J.M.; Rodrigues, A.M.; Neves, G.A.; Menezes, R.R. Use of nanostructured and modified TiO<sub>2</sub> as a gas sensing agent. *Ceramica* **2021**, *67*, 316–326. [[CrossRef](#)]
48. Kumara, G.W.C.; Hakkoum, H.; Comini, E. Recent advancements in TiO<sub>2</sub> nanostructures: Sustainable synthesis and gas sensing. *Nanomaterials* **2023**, *13*, 1424. [[CrossRef](#)]
49. Covaliu-Mierlă, C.I.; Matei, E.; Stoian, O.; Covaliu, L.; Constandache, A.-C.; Iovu, H.; Paraschiv, G. TiO<sub>2</sub>-Based nanofibrous membranes for environmental protection. *Membranes* **2022**, *12*, 236. [[CrossRef](#)]
50. Wendt, S.; Sprunger, P.T.; Lira, E.; Madsen, G.K.; Li, Z.; Hansen, J.Ø.; Matthiesen, J.; Blekinge-Rasmussen, A.; Laegsgaard, E.; Hammer, B.; et al. The role of interstitial sites in the Ti<sub>3d</sub> defect state in the band gap of titania. *Science* **2008**, *320*, 1755–1759. [[CrossRef](#)]
51. Tisdale, W.A.; Williams, K.J.; Timp, B.A.; Norris, D.J.; Aydil, E.S.; Zhu, X.Y. Hot-electron transfer from semiconductor nanocrystals. *Science* **2010**, *328*, 1543–1547. [[CrossRef](#)] [[PubMed](#)]
52. Raj, V.B.; Singh, H.; Nimal, A.T.; Sharma, M.U.; Gupta, V. Oxide thin films (ZnO, TeO<sub>2</sub>, SnO<sub>2</sub>, and TiO<sub>2</sub>) based surface acoustic wave (SAW) E-nose for the detection of chemical warfare agents. *Sensor. Actuators B Chem.* **2013**, *178*, 636–647. [[CrossRef](#)]
53. Skubal, L.R.; Meshkov, N.K.; Vogt, M.C. Detection and identification of gaseous organics using a TiO<sub>2</sub> sensor. *J. Photochem. Photobiol. Chem.* **2002**, *148*, 103–108. [[CrossRef](#)]
54. Tomer, V.K.; Duhan, S. Ordered mesoporous Ag-doped TiO<sub>2</sub>/SnO<sub>2</sub> nanocomposite based highly sensitive and selective VOC sensors. *J. Mater. Chem. A Mater.* **2016**, *4*, 1033–1043. [[CrossRef](#)]
55. Memon, S.F.; Wang, R.; Strunz, B.; Chowdhry, B.S.; Pembroke, J.T.; Lewis, E. A Review of optical fibre ethanol sensors: Current state and future prospects. *Sensors* **2022**, *22*, 950. [[CrossRef](#)]
56. Subha, P.P.; Vikas, L.S.; Jayaraj, M.K. Solution-processed CuO/TiO<sub>2</sub> heterojunction for enhanced room temperature ethanol sensing applications. *Phys. Scripta* **2018**, *93*, 055001. [[CrossRef](#)]
57. Shannon, R.D.; Pask, J.A. Kinetics of the anatase-rutile transformation. *J. Am. Ceram. Soc.* **1965**, *48*, 391–398. [[CrossRef](#)]
58. Batzill, M.; Morales, E.H.; Diebold, U. Influence of nitrogen doping on the defect formation and surface properties of TiO<sub>2</sub> rutile and anatase. *Phys. Rev. Lett.* **2006**, *96*, 026103. [[CrossRef](#)] [[PubMed](#)]
59. Oskam, G.; Nellore, A.; Penn, R.L.; Searson, P.C. The growth kinetics of TiO<sub>2</sub> nanoparticles from titanium (IV) alkoxide at high water/titanium ratio. *J. Phys. Chem. B* **2003**, *107*, 1734–1738. [[CrossRef](#)]
60. Zhang, H.; Banfield, J. Thermodynamic analysis of phase stability of nanocrystalline titania. *J. Mater. Chem.* **1998**, *8*, 2073–2076. [[CrossRef](#)]
61. Bin, X.L.; Li, J.L.; Yang, B.; Yu, Y. Ti<sup>3+</sup> in the surface of titanium dioxide: Generation, properties and photocatalytic application. *J. Nanomater.* **2012**, *2012*, 831524. [[CrossRef](#)]
62. Janotti, A.; Varley, J.B.; Rinke, P.; Umezawa, N.; Kresse, G.; Van De Walle, C.G. Hybrid functional studies of the oxygen vacancy in TiO<sub>2</sub>. *Phys. Rev. B Condens. Matter.* **2010**, *81*, 085212. [[CrossRef](#)]
63. Cronmeyer, D.C. Infrared absorption of reduced rutile TiO<sub>2</sub> single crystals. *Phys. Rev.* **1959**, *113*, 1222. [[CrossRef](#)]
64. Reddy, K.M.; Manorama, S.V.; Reddy, A.R. Bandgap studies on anatase titanium dioxide nanoparticles. *Mater. Chem. Phys.* **2003**, *78*, 239–245. [[CrossRef](#)]
65. Nakamura, I.; Negishi, N.; Kutsuna, S.; Ihara, T.; Sugihara, S.; Takeuchi, K. Role of oxygen vacancy in the plasma-treated TiO<sub>2</sub> photocatalyst with visible light activity for NO removal. *J. Mol. Catal. Chem.* **2000**, *161*, 205–212. [[CrossRef](#)]
66. Amiri, V.; Roshan, H.; Mirzaei, A.; Neri, G.; Ayeshe, A.I. Nanostructured metal oxide-based acetone gas sensors: A review. *Sensors* **2020**, *20*, 3096. [[CrossRef](#)]
67. Raghu, A.V.; Karuppanan, K.K.; Nampootheri, J.; Pullithadathil, B. Wearable, flexible ethanol gas sensor based on TiO<sub>2</sub> nanoparticles-grafted 2D-titanium carbide nanosheets. *ACS Appl. Nano Mater.* **2019**, *2*, 1152–1163. [[CrossRef](#)]
68. Nunes, D.; Fortunato, E.; Martins, R. Flexible nanostructured TiO<sub>2</sub>-based gas and UV sensors: A review. *Discov. Mater.* **2022**, *2*, 2. [[CrossRef](#)]
69. Tian, X.; Cui, X.; Lai, T.; Ren, J.; Yang, Z.; Xiao, M.; Wang, B.; Xiao, X.; Wang, Y. Gas sensors based on TiO<sub>2</sub> nanostructured materials for the detection of hazardous gases: A review. *Nano Mater. Sci.* **2021**, *3*, 390–403. [[CrossRef](#)]
70. Fujishima, A.; Rao, T.N.; Tryk, D.A. Titanium dioxide photocatalysis. *J. Photochem. Photobiol. C Photochem. Rev.* **2000**, *1*, 1–21. [[CrossRef](#)]
71. Shafei, A.; Salarpour, M.E.; Sheibani, S. Effect of intermediate ball milling on the synthesis of Cu-doped TiO<sub>2</sub> nano-photocatalyst by sol-gel method. *J. Sol-Gel. Sci. Technol.* **2019**, *92*, 173–185. [[CrossRef](#)]

72. Zhou, R.; Lin, S.; Zong, H.; Huang, T.; Li, F.; Pan, J.; Cui, J. Continuous synthesis of Ag/TiO<sub>2</sub> nanoparticles with enhanced photocatalytic activity by pulsed laser ablation. *J. Nanomater.* **2017**, *2017*, 4604159. [[CrossRef](#)]
73. Gupta, V.; Sarkar, S.; Aftenieva, O.; Tsuda, T.; Kumar, L.; Schletz, D.; Schultz, J.; Kiriy, A.; Fery, A.; Vogel, N.; et al. Nanoimprint lithography facilitated plasmonic-photon coupling for enhanced photoconductivity and photocatalysis. *Adv. Funct. Mater.* **2021**, *31*, 2105054. [[CrossRef](#)]
74. Vahl, A.; Veziroglu, S.; Henkel, B.; Strunskus, T.; Polonskyi, O.; Aktas, O.C.; Faupel, F. Pathways to tailor photocatalytic performance of TiO<sub>2</sub> thin films deposited by reactive magnetron sputtering. *Materials* **2019**, *12*, 2840. [[CrossRef](#)]
75. Zhang, B.; He, X.; Ma, X.; Chen, Q.; Liu, G.; Zhou, Y.; Ma, D.; Cui, C.; Ma, J.; Xin, Y. In situ synthesis of ultrafine TiO<sub>2</sub> nanoparticles modified g-C<sub>3</sub>N<sub>4</sub> heterojunction photocatalyst with enhanced photocatalytic activity. *Sep. Purif. Technol.* **2020**, *247*, 116932. [[CrossRef](#)]
76. Gour, A.; Jain, N.K. Advances in green synthesis of nanoparticles. *Artif. Cells Nanomed. Biotechnol.* **2019**, *47*, 844–851. [[CrossRef](#)] [[PubMed](#)]
77. Iravani, S. Green synthesis of metal nanoparticles using plants. *Green Chem.* **2011**, *13*, 2638–2650. [[CrossRef](#)]
78. Vanlalveni, C.; Lallianrawna, S.; Biswas, A.; Selvaraj, M.; Changmai, B.; Rokhum, S.L. Green synthesis of silver nanoparticles using plant extracts and their antimicrobial activities: A review of recent literature. *RSC Adv.* **2021**, *11*, 2804–2837. [[CrossRef](#)] [[PubMed](#)]
79. Mathur, P.; Jha, S.; Ramteke, S.; Jain, N.K. Pharmaceutical aspects of silver nanoparticles. *Artif. Cells Nanomed. Biotechnol.* **2017**, *46*, 115–126. [[CrossRef](#)]
80. Mahy, J.G.; Lejeune, L.; Haynes, T.; Lambert, S.D.; Marcilli, R.H.M.; Fustin, C.-A.; Hermans, S. Eco-friendly colloidal aqueous sol-gel process for TiO<sub>2</sub> synthesis: The peptization method to obtain crystalline and photoactive materials at low temperature. *Catalysts* **2021**, *11*, 768. [[CrossRef](#)]
81. Song, M.; Yang, Y.; Xiang, M.; Zhu, Q.; Zhao, H. Synthesis of nano-sized TiC powders by designing chemical vapor deposition system in a fluidized bed reactor. *Powder Technol.* **2021**, *380*, 256–264. [[CrossRef](#)]
82. Esparza-Contro, C.; Berthomé, G.; Renou, G.; Robaut, F.; Coindeau, S.; Vachey, C.; Cambin, J.; Mantel, M.; Latu-Romain, L. Microstructures of titanium oxide thin films grown continuously on stainless steel wires by PVD in an inverted cylindrical magnetron: Towards an industrial process. *Surf. Coat. Technol.* **2020**, *389*, 125643. [[CrossRef](#)]
83. Ramakrishnan, V.M.; Natarajan, M.; Santhanam, A.; Asokan, V.; Velauthapillai, D. Size controlled synthesis of TiO<sub>2</sub> nanoparticles by modified solvothermal method towards effective photo catalytic and photovoltaic applications. *Mater. Res. Bull.* **2018**, *97*, 351–360. [[CrossRef](#)]
84. Horti, N.C.; Kamatagi, M.D.; Patil, N.R.; Nataraj, S.K.; Sannaikar, M.S.; Inamdar, S.R. Synthesis and photoluminescence properties of titanium oxide (TiO<sub>2</sub>) nanoparticles: Effect of calcination temperature. *Optik* **2019**, *194*, 163070. [[CrossRef](#)]
85. Andronic, L.; Enesca, A. Black TiO<sub>2</sub> synthesis by chemical reduction methods for photocatalysis applications. *Front. Chem.* **2020**, *8*, 565489. [[CrossRef](#)]
86. Xiang, L.; Liu, X.; Yang, C.; Lei, Q.; Zhao, J.; Zhao, X. Ultrafast synthesis of anatase TiO<sub>2</sub> microspheres doped with rare-earth by one-step microwave method. *Inorg. Chem. Commun.* **2021**, *127*, 108532. [[CrossRef](#)]
87. Leong, C.Y.; Lo, Y.S.; Koh, P.W.; Lee, S.L. Synthesis of titanium dioxide nanotubes with different N-containing ligands via hydrothermal method. *Sci. Technol. Indones.* **2021**, *6*, 67–73. [[CrossRef](#)]
88. Hussain, I.; Singh, N.B.; Singh, A.; Singh, H.; Singh, S.C. Green synthesis of nanoparticles and its potential application. *Biotechnol. Lett.* **2015**, *38*, 545–560. [[CrossRef](#)]
89. Robert, D.; Weber, J.V. Titanium dioxide synthesis by sol gel methods and evaluation of their photocatalytic activity. *J. Mater. Sci. Lett.* **1999**, *18*, 97–98. [[CrossRef](#)]
90. Jayaseelan, C.; Rahuman, A.A.; Roopan, S.M.; Kirthi, A.V.; Venkatesan, J.; Kim, S.K.; Iyappan, M.; Siva, C. Biological approach to synthesize TiO<sub>2</sub> nanoparticles using *Aeromonas hydrophila* and its antibacterial activity. *Spectrochim. Acta A Mol. Biomol. Spectrosc.* **2013**, *15*, 82–89. [[CrossRef](#)]
91. Nadeem, M.; Tungmunnithum, D.; Hano, C.; Abbasi, B.H.; Hashmi, S.S.; Ahmad, W.; Zahir, A. The current trends in the green syntheses of titanium oxide nanoparticles and their applications. *Green Chem. Lett. Rev.* **2018**, *11*, 492–502. [[CrossRef](#)]
92. Subhapiya, S.; Gomathipriya, P. Green synthesis of titanium dioxide (TiO<sub>2</sub>) nanoparticles by *Trigonella foenum-graecum* extract and its antimicrobial properties. *Microb. Pathog.* **2018**, *116*, 215–220. [[CrossRef](#)] [[PubMed](#)]
93. Edmundson, M.C.; Capeness, M.; Horsfall, L. Exploring the potential of metallic nanoparticles within synthetic biology. *New Biotechnol.* **2014**, *31*, 572–578. [[CrossRef](#)] [[PubMed](#)]
94. Macwan, D.P.; Dave, P.N.; Chaturvedi, S. A review on nano-TiO<sub>2</sub> sol-gel type syntheses and its applications. *J. Mater. Sci.* **2011**, *46*, 3669–3686. [[CrossRef](#)]
95. Zhang, X.Y.; Li, H.P.; Cui, X.L.; Lin, Y. Graphene/TiO<sub>2</sub> nanocomposites: Synthesis, characterization and application in hydrogen evolution from water photocatalytic splitting. *J. Mater. Chem.* **2010**, *20*, 2801–2806. [[CrossRef](#)]
96. Antonelli, D.M.; Ying, J.Y. Synthesis of hexagonally packed mesoporous TiO<sub>2</sub> by a modified sol-gel method. *Angew Chem. Int.* **1995**, *34*, 2014–2017. [[CrossRef](#)]
97. Barringer, E.A.; Bowen, H.K. Formation, packing, and sintering of monodisperse TiO<sub>2</sub> powders. *J. Am. Ceram. Soc.* **1982**, *65*, C199–C201. [[CrossRef](#)]
98. Yu, H.F.; Wang, S.M. Effects of water content and pH on gel-derived TiO<sub>2</sub>-SiO<sub>2</sub>. *J. Non-Cryst. Solids* **2000**, *261*, 260–267. [[CrossRef](#)]

99. Matijević, E.; Budnik, M.; Meites, L. Preparation and mechanism of formation of titanium dioxide hydrosols of narrow size distribution. *J. Colloid Interface Sci.* **1977**, *61*, 302–311. [[CrossRef](#)]
100. Castrejón-Sánchez, V.H.; López, R.; Ramón-González, M.; Enríquez-Pérez, Á.; Camacho-López, M.; Villa-Sánchez, G. Annealing control on the anatase/rutile ratio of nanostructured titanium dioxide obtained by sol-gel. *Crystals* **2019**, *9*, 22. [[CrossRef](#)]
101. Kim, D.J.; Hahn, S.H.; Oh, S.H.; Kim, E.J. Influence of calcination temperature on structural and optical properties of TiO<sub>2</sub> thin films prepared by sol-gel dip coating. *Mater. Lett.* **2002**, *57*, 355–360. [[CrossRef](#)]
102. Acharyulu, N.P.S.; Srinivasu, C.; Babavali, S.K.F. Synthesis of carbon nano spherical structures and nano composite oxide [TiO<sub>2</sub>/SnO<sub>2</sub> (2:1)] hollow spheres by hydrothermal method and study of characterization with photo catalytic activity. *Mater. Today Proc.* **2020**, *27*, 1282–1288. [[CrossRef](#)]
103. Trinh, T.T.; Giang, N.T.H.; Huong, L.M.; Thinh, D.B.; Dat, N.M.; Trinh, D.N.; Hai, N.D.; Oanh, D.T.Y.; Nam, H.M.; Phong, M.T.; et al. Hydrothermal synthesis of titanium dioxide/graphene aerogel for photodegradation of methylene blue in aqueous solution. *J. Sci. Adv. Mater. Devices* **2022**, *7*, 100433. [[CrossRef](#)]
104. Paaianen, J.; Pettilä, L.; Lönnrot, S.; Heikkilä, M.; Hatanpää, T.; Ritala, M.; Koivula, R. Electroblown titanium dioxide and titanium dioxide/silicon dioxide submicron fibers with and without titania nanorod layer for strontium(II) uptake. *Chem. Eng. J. Adv.* **2023**, *13*, 100434. [[CrossRef](#)]
105. Hashemi, M.M.; Nikfarjam, A.; Hajghassem, H.; Salehifar, N. Hierarchical dense array of ZnO nanowires spatially grown on ZnO/TiO<sub>2</sub> nanofibers and their ultraviolet activated gas sensing properties. *J. Phys. Chem. C* **2020**, *124*, 322–335. [[CrossRef](#)]
106. Singh, A.K.; Bhowmik, B. A highly stable room temperature titania nanostructure-based thin film transistor (TFT) alcohol sensor. *Sens. Diagn.* **2023**, *2*, 225–235. [[CrossRef](#)]
107. Prathan, A.; Sanglao, J.; Wang, T.; Bhoomanee, C.; Ruankham, P.; Gardchareon, A.; Wongratanaphisan, D. Controlled structure and growth mechanism behind hydrothermal growth of TiO<sub>2</sub> nanorods. *Sci. Rep.* **2020**, *10*, 8065. [[CrossRef](#)]
108. Ibrahim, S.A.; Anwar, M.K.; Ainuddin, A.R.; Hariri, A.; Rus, A.Z.M.; Kamdi, Z.; Yunus, M.Z.; Harun, Z. Synthesis and characterization of visible light active Fe-TiO<sub>2</sub> using hydrothermal method. *Int. J. Integr. Eng.* **2019**, *11*, 80–85. [[CrossRef](#)]
109. Reilly, K.; Adeli, B.; Fang, B.; Wilkinson, D.P.; Taghipour, F. Advanced titanium dioxide fluidizable nanowire photocatalysts. *RSC Adv.* **2022**, *12*, 4240–4252. [[CrossRef](#)]
110. Hameed, H.G.; Abdulrahman, N.A. Synthesis of TiO<sub>2</sub> nanoparticles by hydrothermal method and characterization of their antibacterial activity: Investigation of the impact of magnetism on the photocatalytic properties of the nanoparticles. *Phys. Chem. Res.* **2023**, *11*, 771–782.
111. Ahn, K.H.; Park, Y.B.; Park, D.W. Kinetic and mechanistic study on the chemical vapor deposition of titanium dioxide thin films by in situ FT-IR using TTIP. *Surf. Coat. Technol.* **2003**, *171*, 198–204. [[CrossRef](#)]
112. Djerdj, I.; Tonejc, A.M.; Bijelić, M.; Vraneša, V.; Turković, A. Transmission electron microscopy studies of nanostructured TiO<sub>2</sub> films on various substrates. *Vacuum* **2005**, *80*, 371–378. [[CrossRef](#)]
113. Astinchap, B.; Ghanbaripour, H.; Amuzgar, R. Multifractal study of TiO<sub>2</sub> thin films deposited by MO-CVD method: The role of precursor amount and substrate temperature. *Optik* **2020**, *222*, 165384. [[CrossRef](#)]
114. Zhang, Q.; Li, C. Pure anatase phase titanium dioxide films prepared by mist chemical vapor deposition. *Nanomaterials* **2018**, *8*, 827. [[CrossRef](#)]
115. Ghufraan, M.; Uddin, G.M.; Khan, A.A.; Hussein, H.; Khurshid, K.; Arafat, S.M. Comparative Experimental Investigation of Mechanical Properties and Adhesion of Low Temperature PVD Coated TiO<sub>2</sub> Thin Films. In *Advances in Manufacturing II. Manufacturing; Lecture Notes in Mechanical Engineering*; Gapiński, B., Szostak, M., Ivanov, V., Eds.; Springer: Cham, Switzerland, 2019. [[CrossRef](#)]
116. Artoshina, O.V.; Rossouw, A.; Semina, V.K.; Nechaev, A.N.; Apel, P.Y. Structural and physicochemical properties of titanium dioxide thin films obtained by reactive magnetron sputtering, on the surface of track-etched membranes. *Pet. Chem.* **2015**, *55*, 759–768. [[CrossRef](#)]
117. Supriadi, S.; Suharno, B.; Nugraha, N.K.; Yasinta, A.O.; Annur, D. Adhesiveness of TiO<sub>2</sub> PVD coating on electropolished stainless steel 17-4 PH orthodontic bracket. *Mater. Res. Express* **2019**, *6*, 094003. [[CrossRef](#)]
118. Maziarz, W. TiO<sub>2</sub>/SnO<sub>2</sub> and TiO<sub>2</sub>/CuO thin film nano-heterostructures as gas sensors. *Appl. Surf. Sci.* **2019**, *480*, 361–370. [[CrossRef](#)]
119. Costa, O.Y.A.; Raaijmakers, J.M.; Kuramae, E.E. Microbial extracellular polymeric substances: Ecological function and impact on soil aggregation. *Front. Microbiol.* **2018**, *9*, 1636. [[CrossRef](#)] [[PubMed](#)]
120. Mughal, B.; Zaidi, S.Z.J.; Zhang, X.; Hassan, S.U. Biogenic nanoparticles: Synthesis, characterisation and applications. *Appl. Sci.* **2021**, *11*, 2598. [[CrossRef](#)]
121. Salem, N.F.A.; Abouelkheir, S.S.; Yousif, A.M.; Meneses-Brassea, B.P.; Sabry, S.A.; Ghazlan, H.A.; El-Gendy, A.A. Large scale production of superparamagnetic iron oxide nanoparticles by the haloarchaeon Halobiforma sp. N1 and their potential in localized hyperthermia cancer therapy. *Nanotechnology* **2020**, *32*, 09LT01. [[CrossRef](#)] [[PubMed](#)]
122. Bahrulolum, H.; Nooraei, S.; Javanshir, N.; Tarrahimofrad, H.; Mirbagheri, V.S.; Easton, A.J.; Ahmadian, G. Green synthesis of metal nanoparticles using microorganisms and their application in the agrifood sector. *J. Nanobiotechnol.* **2021**, *19*, 86. [[CrossRef](#)] [[PubMed](#)]
123. Mukherjee, S.; Nethi, S.K. Biological Synthesis of Nanoparticles Using Bacteria. In *Nanotechnology for Agriculture*; Panpatte, D.G., Jhala, Y.K., Eds.; Springer: Singapore, 2019; pp. 37–51. [[CrossRef](#)]

124. Babitha, S.; Korrapati, P.S. Biosynthesis of titanium dioxide nanoparticles using a probiotic from coal fly ash effluent. *Mater. Res. Bull.* **2013**, *48*, 4738–4742. [[CrossRef](#)]
125. Salman, J.A.S.; Ibrahim, K.H.; Ali, F.A. Effect of culture media on biosynthesis of titanium dioxide nanoparticles using *Lactobacillus crispatus*. *Int. J. Adv. Res.* **2014**, *2*, 1014–1021.
126. Órdenes-Aenishanslins, N.A.; Saona, L.A.; Durán-Toro, V.M.; Monrás, J.P.; Bravo, D.M.; Pérez-Donoso, J.M. Use of titanium dioxide nanoparticles biosynthesized by *Bacillus mycoides* in quantum dot sensitized solar cells. *Microb. Cell Fact.* **2014**, *13*, 90. [[CrossRef](#)] [[PubMed](#)]
127. Sunkar, S.; Nachiyar, C.V.; Lerensha, R.; Renugadevi, K. Biogenesis of TiO<sub>2</sub> nanoparticles using endophytic *Bacillus cereus*. *J. Nanopart. Res.* **2014**, *16*, 2681. [[CrossRef](#)]
128. Suriyaraj, S.P.; Selvakumar, R. Room temperature biosynthesis of crystalline TiO<sub>2</sub> nanoparticles using *Bacillus licheniformis* and studies on the effect of calcination on phase structure and optical properties. *RSC Adv.* **2014**, *4*, 39619–39624. [[CrossRef](#)]
129. Dheeba, B.; Marikani, K.; Rajarathinam, K.; Nageswari, K.; Kannan, K. Biosynthesis and characterization of intracellular TiO<sub>2</sub> nanoparticles by *Lactobacillus* sp: And its potential application in decolourization of methyl orange dyes. *Int. J. Pharm. Pharmaceut. Sci.* **2015**, *7*, 225–229.
130. Jha, A.K.; Prasad, K.; Kulkarni, A.R. Synthesis of TiO<sub>2</sub> nanoparticles using microorganisms. *Colloids Surf. B Biointerfaces* **2009**, *71*, 226–229. [[CrossRef](#)]
131. Taran, M.; Rad, M.; Alavi, M. Biosynthesis of TiO<sub>2</sub> and ZnO nanoparticles by *Halomonas elongata* IBRC-M 10214 in different conditions of medium. *Bioimpacts* **2018**, *8*, 81–89. [[CrossRef](#)]
132. Ağçeli, G.K.; Hammachi, H.; Kodal, S.P.; Cihangir, N.; Aksu, Z. A novel approach to synthesize TiO<sub>2</sub> nanoparticles: Biosynthesis by using *Streptomyces* sp. HC1. *J. Inorg. Organomet. Polym.* **2020**, *30*, 3221–3229. [[CrossRef](#)]
133. Bansal, V.; Rautaray, D.; Bharde, A.; Ahire, K.; Sanyal, A.; Ahmad, A.; Sastry, M. Fungus-mediated biosynthesis of silica and titania particles. *J. Mater. Chem.* **2005**, *15*, 2583. [[CrossRef](#)]
134. Rajakumar, G.; Rahuman, A.A.; Roopan, S.M.; Khanna, V.G.; Elango, G.; Kamaraj, C.; Zahir, A.A.; Velayutham, K. Fungus-mediated biosynthesis and characterization of TiO<sub>2</sub> nanoparticles and their activity against pathogenic bacteria. *Spectrochim. Acta A Mol. Biomol. Spectrosc.* **2012**, *91*, 23–29. [[CrossRef](#)] [[PubMed](#)]
135. Yadav, A.; Kon, K.; Kratosova, G.; Duran, N.; Ingle, A.P.; Rai, M. Fungi as an efficient mycosystem for the synthesis of metal nanoparticles: Progress and key aspects of research. *Biotechnol. Lett.* **2015**, *37*, 2099–2120. [[CrossRef](#)]
136. Chinnaperumal, K.; Govindasamy, B.; Paramasivam, D.; Dilipkumar, A.; Dhayalan, A.; Vadivel, A.; Sengodan, K.; Pachiappan, P. Bio-pesticidal effects of *Trichoderma viride* formulated titanium dioxide nanoparticle and their physiological and biochemical changes on *Helicoverpa armigera* (Hub.). *Pestic. Biochem. Physiol.* **2018**, *149*, 26–36. [[CrossRef](#)]
137. Rehman, S.; Jermy, R.; Mousa Asiri, S.; Shah, M.A.; Farooq, R.; Ravinayagam, V.; Azam Ansari, M.; Alsalem, Z.; Al Jindan, R.; Reshi, Z.; et al. Using *Fomitopsis pinicola* for bioinspired synthesis of titanium dioxide and silver nanoparticles, targeting biomedical applications. *RSC Adv.* **2020**, *10*, 32137–32147. [[CrossRef](#)] [[PubMed](#)]
138. Arya, S.; Sonawane, H.; Math, S.; Tambade, P.; Chaskar, M.; Shinde, D. Biogenic titanium nanoparticles (TiO<sub>2</sub> NPs) from *Trichoderma citrinoviride* extract: Synthesis, characterization and antibacterial activity against extremely drugresistant *Pseudomonas aeruginosa*. *Int. Nano Lett.* **2020**, *11*, 35–42. [[CrossRef](#)]
139. Peiris, M.; Gunasekara, T.; Jayaweera, P.M.; Fernando, S. TiO<sub>2</sub> nanoparticles from baker's yeast: A potent antimicrobial. *J. Microbiol. Biotechnol.* **2018**, *28*, 1664–1670. [[CrossRef](#)]
140. Sumerel, J.L.; Yang, W.; Kisailus, D.; Weaver, J.C.; Choi, J.H.; Morse, D.E. Biocatalytically templated synthesis of titanium dioxide. *Chem. Mater.* **2003**, *15*, 4804–4809. [[CrossRef](#)]
141. Johnson, J.M.; Kinsinger, N.; Sun, C.; Li, D.; Kisailus, D. Urease-mediated room-temperature synthesis of nanocrystalline titanium dioxide. *J. Am. Chem. Soc.* **2012**, *134*, 13974–13977. [[CrossRef](#)]
142. Nabi, G.; Aain, Q.; Khalid, N.R.; Tahir, M.B.; Rafique, M.; Rizwan, M.; Hussain, S.; Iqbal, T.; Majid, A. A Review on novel eco-friendly green approach to synthesis TiO<sub>2</sub> nanoparticles using different extracts. *J. Inorg. Organomet. Polym.* **2018**, *28*, 1552–1564. [[CrossRef](#)]
143. Ovais, M.; Khalil, A.T.; Islam, N.U.; Ahmad, I.; Ayaz, M.; Saravanan, M.; Shinwari, K.Z.; Mukherjee, S. Role of plant phytochemicals and microbial enzymes in biosynthesis of metallic nanoparticles. *Appl. Microbiol. Biotechnol.* **2018**, *102*, 6799–6814. [[CrossRef](#)] [[PubMed](#)]
144. Sundrarajan, M.; Gowri, S. Green synthesis of titanium dioxide nanoparticles by *Nyctanthes arbor-tristis* leaves extract. *Chalco-genide Lett.* **2011**, *8*, 447–451.
145. Sethy, N.K.; Arif, Z.; Mishra, P.K.; Kumar, P. Green synthesis of TiO<sub>2</sub> nanoparticles from *Syzygium cumini* extract for photo-catalytic removal of lead (Pb) in explosive industrial wastewater. *Green Process. Syn.* **2020**, *9*, 171–181. [[CrossRef](#)]
146. Koca, F.D.; Duman, F. Genotoxic and cytotoxic activity of green synthesized TiO<sub>2</sub> nanoparticles. *Appl. Nanosci.* **2018**, *9*, 815–823. [[CrossRef](#)]
147. Pushpamalini, T.; Keerthana, M.; Sangavi, R.; Nagaraj, A.; Kamaraj, P. Comparative analysis of green synthesis of TiO<sub>2</sub> nanoparticles using four different leaf extract. *Mater. Today Proceed.* **2021**, *40*, S180–S184. [[CrossRef](#)]
148. Rao, K.G.; Ashok, C.; Rao, K.V.; Chakra, C.S.; Tambur, P. Green synthesis of TiO<sub>2</sub> nanoparticles using Aloe Vera extract. *Int. J. Adv. Res. Phys. Sci.* **2015**, *2*, 28–34.

149. Rajkumari, J.; Magdalane, C.M.; Siddhardha, B.; Madhavan, J.; Ramalingam, G.; Al-Dhabi, N.A.; Arasu, M.V.; Ghilan, A.K.M.; Duraipandiayan, V.; Kaviyarasu, K. Synthesis of titanium oxide nanoparticles using *Aloe barbadensis* mill and evaluation of its antibiofilm potential against *Pseudomonas aeruginosa* PAO1. *J. Photochem. Photobiol. B* **2019**, *201*, 111667. [CrossRef] [PubMed]
150. Hameed, R.S.; Fayyad, R.J.; Nuaman, R.S.; Hamdan, N.T.; Maliki, S.A.J. Synthesis and characterization of a novel titanium nanoparticles using banana peel extract and investigate its antibacterial and insecticidal activity. *J. Pure Appl. Microbiol.* **2019**, *13*, 2241–2249. [CrossRef]
151. Ali, O.M.; Hasanin, M.S.; Suleiman, W.B.; Helal, E.E.H.; Hashem, A.H. Green biosynthesis of titanium dioxide quantum dots using watermelon peel waste: Antimicrobial, antioxidant, and anticancer activities. *Biomass Convers. Biorefin.* **2022**. [CrossRef]
152. Madadi, Z.; Soltanieh, M.; Lotfabad, T.B.; Nazari, S. Green synthesis of titanium dioxide nanoparticles with *Glycyrrhiza glabra* and their photocatalytic activity. *Asian J. Green Chem.* **2019**, *4*, 256–268. [CrossRef]
153. Bekele, E.T.; Gonfa, B.A.; Zelekew, O.A.; Belay, H.H.; Sabir, F.K. Synthesis of titanium oxide nanoparticles using root extract of *Kniphofia foliosa* as a template, characterization, and its application on drug resistance bacteria. *J. Nanomater.* **2020**, *2020*, 2817037. [CrossRef]
154. Al-Shabib, N.A.; Husain, F.M.; Qais, F.A.; Ahmad, N.; Khan, A.; Alyousef, A.A.; Arshad, M.; Noor, S.; Khan, J.M.; Alam, P.; et al. Phyto-mediated synthesis of porous titanium dioxide nanoparticles from *Withania somnifera* root extract: Broad-spectrum attenuation of biofilm and cytotoxic properties against HepG2 cell lines. *Front. Microbiol.* **2020**, *11*, 1680. [CrossRef]
155. Marimuthu, S.; Rahuman, A.A.; Jayaseelan, C.; Kirthi, A.V.; Santhoshkumar, T.; Velayutham, K.; Bagavan, A.; Kamaraj, C.; Elango, G.; Iyappan, M.; et al. Acaricidal activity of synthesized titanium dioxide nanoparticles using *Calotropis gigantea* against *Rhipicephalus microplus* and *Haemaphysalis bispinosa*. *Asian Pac. J. Trop. Med.* **2013**, *6*, 682–688. [CrossRef]
156. Aravind, M.; Amalanathan, M.; Mary, M.S.M. Synthesis of TiO<sub>2</sub> nanoparticles by chemical and green synthesis methods and their multifaceted properties. *Appl. Sci.* **2021**, *3*, 409. [CrossRef]
157. Devikala, S.; Abisharani, J.M.; Bharath, M. Biosynthesis of TiO<sub>2</sub> nanoparticles from *Caesalpinia pulcherrima* flower extracts. *Mater. Today Proceed.* **2021**, *40*, S185–S188. [CrossRef]
158. Mohamed, H.H.; Alomair, N.A.; Akhtar, S.; Youssef, T.E. Eco-friendly synthesized  $\alpha$ -Fe<sub>2</sub>O<sub>3</sub>/TiO<sub>2</sub> heterojunction with enhanced visible light photocatalytic activity. *J. Photochem. Photobiol. A Chem.* **2019**, *382*, 111951. [CrossRef]
159. Aslam, M.; Abdullah, A.Z.; Rafatullah, M.; Fawad, A. *Abelmoschus esculentus* (Okra) seed extract for stabilization of the biosynthesized TiO<sub>2</sub> photocatalyst used for degradation of stable organic substance in water. *Environ. Sci. Pollut. Res.* **2022**, *29*, 41053–41064. [CrossRef]
160. Sunny, N.E.; Mathew, S.S.; Venkat Kumar, S.; Saravanan, P.; Rajeshkannan, R.; Rajasimman, M.; Vasseghian, Y. Effect of green synthesized nano-titanium synthesized from *Trachyspermum ammi* extract on seed germination of *Vigna radiate*. *Chemosphere* **2022**, *300*, 134600. [CrossRef] [PubMed]
161. Arun, J.; Nachiappan, S.; Rangarajan, G.; Alagappan, R.P.; Gopinath, K.P.; Lichtfouse, E. Synthesis and application of titanium dioxide photocatalysis for energy, decontamination and viral disinfection: A review. *Environ. Chem. Lett.* **2023**, *21*, 339–362. [CrossRef] [PubMed]
162. Nasirian, M.; Mehrvar, M. Photocatalytic degradation of aqueous Methyl Orange using nitrogen-doped TiO<sub>2</sub> photocatalyst prepared by novel method of ultraviolet-assisted thermal synthesis. *J. Environ. Sci.* **2018**, *66*, 81–93. [CrossRef] [PubMed]
163. Kubiak, A.; Bielan, Z.; Bartkowiak, A.; Gabała, E.; Piasecki, A.; Zalas, M.; Zielińska-Jurek, A.; Janczarek, M.; Siwińska-Ciesielczyk, K.; Jesionowski, T. Synthesis of titanium dioxide via surfactant-assisted microwave method for photocatalytic and dye-sensitized solar cells applications. *Catalysts* **2020**, *10*, 586. [CrossRef]
164. Jiao, J.; Wei, Y.; Zhao, Z.; Zhong, W.; Liu, J.; Li, J.; Duan, A.; Jiang, G. Synthesis of 3D ordered macroporous TiO<sub>2</sub>-supported Au nanoparticle photocatalysts and their photocatalytic performances for the reduction of CO<sub>2</sub> to methane. *Catal. Today* **2015**, *258*, 319–326. [CrossRef]
165. Kubiak, A.; Wojciechowska, W.; Kurc, B.; Pigłowska, M.; Synoradzki, K.; Gabała, E.; Moszyński, D.; Szybowicz, M.; Siwińska-Ciesielczyk, K.; Jesionowski, T. Highly crystalline TiO<sub>2</sub>-MoO<sub>3</sub> composite materials synthesized via a template-assisted microwave method for electrochemical application. *Crystals* **2020**, *10*, 493. [CrossRef]
166. Coromelci, C.; Neamtu, M.; Ignat, M.; Samoila, P.; Zaltariov, M.F.; Palamaru, M. Ultrasound assisted synthesis of heterostructured TiO<sub>2</sub>/ZnFe<sub>2</sub>O<sub>4</sub> and TiO<sub>2</sub>/ZnFe<sub>1.98</sub>La<sub>0.02</sub>O<sub>4</sub> systems as tunable photocatalysts for efficient organic pollutants removal. *Ceram. Int.* **2022**, *48*, 4829–4840. [CrossRef]
167. López-Mayán, J.J.; del-Ángel-Monroy, S.; Peña-Vázquez, E.; Barciela-Alonso, M.C.; Bermejo-Barrera, P.; Moreda-Piñeiro, A. Titanium dioxide nanoparticles assessment in seaweeds by single particle inductively coupled plasma-mass spectrometry. *Talanta* **2022**, *236*, 122856. [CrossRef] [PubMed]
168. Mauchauffé, R.; Kang, S.; Moon, S.Y. Fast formation of amorphous titanium dioxide thin films using a liquid-assisted plasma-enhanced deposition process in open air. *Surf. Coat. Technol.* **2019**, *376*, 84–89. [CrossRef]
169. Guo, C.; Kong, M. Fabrication of ultralow stress TiO<sub>2</sub>/SiO<sub>2</sub> optical coatings by plasma ion-assisted deposition. *Coatings* **2020**, *10*, 720. [CrossRef]
170. Sugahara, T.; Alipour, L.; Hirose, Y.; Ekubaru, Y.; Nakamura, J.; Ono, H.; Harada, N.; Suganuma, K. Formation of metal-organic decomposition derived nanocrystalline structure titanium dioxide by heat sintering and photosintering methods for advanced coating process, and its volatile organic compounds' gas-sensing properties. *ACS Appl. Electron. Mater.* **2020**, *2*, 1670–1678. [CrossRef]

171. Xin, J.H.; Daoud, W.A.; Kong, Y.Y. A new approach to UV-blocking treatment for cotton fabrics. *Textil. Res. J.* **2004**, *74*, 97–100. [CrossRef]
172. Martinez, U.; Hammer, B. Adsorption properties versus oxidation states of rutile TiO<sub>2</sub>. *J. Chem. Phys.* **2011**, *134*, 194703. [CrossRef]
173. Mendive, C.B.; Hansmann, D.; Bredow, T.; Bahnemann, D. New insights into the mechanism of TiO<sub>2</sub> photocatalysis: Thermal processes beyond the electron–hole creation. *J. Phys. Chem. C* **2011**, *115*, 19676–19685. [CrossRef]
174. Boroski, M.; Rodrigues, A.C.; Garcia, J.C.; Sampaio, L.C.; Nozaki, J.; Hioka, N. Combined electrocoagulation and TiO<sub>2</sub> photo-assisted treatment applied to wastewater effluents from pharmaceutical and cosmetic industries. *J. Hazard. Mater.* **2009**, *162*, 448–454. [CrossRef]
175. Yao, J.; Chen, H.; Jiang, F.; Jiao, Z.; Jin, M. Titanium dioxide and cadmium sulfide co-sensitized graphitic carbon nitride nanosheets composite photocatalysts with superior performance in phenol degradation under visible-light irradiation. *J. Colloid Interface Sci.* **2017**, *490*, 154–162. [CrossRef]
176. Chong, M.N.; Jin, B.; Chow, C.W.K.; Saint, C. Recent developments in photocatalytic water treatment technology: A review. *Water Res.* **2010**, *44*, 2997–3027. [CrossRef] [PubMed]
177. Wang, D.; Li, Y.; Li Puma, G.; Wang, C.; Wang, P.; Zhang, W.; Wang, Q. Mechanism and experimental study on the photocatalytic performance of Ag/AgCl@chiral TiO<sub>2</sub> nanofibers photocatalyst: The impact of wastewater components. *J. Hazard. Mater.* **2015**, *285*, 277–284. [CrossRef] [PubMed]
178. Andreozzi, R.; Caprio, V.; Insola, A.; Marotta, R. Advanced oxidation processes (AOP) for water purification and recovery. *Catal. Today* **1999**, *53*, 51–59. [CrossRef]
179. Prasse, C.; Stalter, D.; Schulte-Oehlmann, U.; Oehlmann, J.; Ternes, T.A. Spoilt for choice: A critical review on the chemical and biological assessment of current wastewater treatment technologies. *Water Res.* **2015**, *87*, 237–270. [CrossRef] [PubMed]
180. Prieto-Rodríguez, L.; Oller, I.; Klamerth, N.; Agüera, A.; Rodríguez, E.M.; Malato, S. Application of solar AOPs and ozonation for elimination of micropollutants in municipal wastewater treatment plant effluents. *Water Res.* **2013**, *47*, 1521–1528. [CrossRef]
181. Keen, O.S.; McKay, G.; Mezyk, S.P.; Linden, K.G.; Rosario-Ortiz, F.L. Identifying the factors that influence the reactivity of effluent organic matter with hydroxyl radicals. *Water Res.* **2014**, *50*, 408–419. [CrossRef]
182. Kudo, A.; Miseki, Y. Heterogeneous photocatalyst materials for water splitting. *Chem. Soc. Rev.* **2009**, *38*, 253–278. [CrossRef]
183. Prihod'ko, R.V.; Soboleva, N.M. Photocatalysis: Oxidative processes in water treatment. *J. Chem.* **2013**, *2013*, 168701. [CrossRef]
184. Kümmerer, K. Antibiotics in the aquatic environment—A review—part I. *Chemosphere* **2009**, *75*, 417–434. [CrossRef]
185. Rasouli, S.; Rezaei, N.; Hamed, H.; Zendejboudi, S.; Duan, X. Superhydrophobic and superoleophilic membranes for oil-water separation application: A comprehensive review. *Mater. Des.* **2021**, *204*, 109599. [CrossRef]
186. Zareei Pour, F.; Sabzehmeidani, M.M.; Karimi, H.; Madadi Avargani, V.; Ghaedi, M. Superhydrophobic–superoleophilic electrospun nanofibrous membrane modified by the chemical vapor deposition of dimethyl dichlorosilane for efficient oil-water separation. *J. Appl. Polym. Sci.* **2019**, *136*, 47621. [CrossRef]
187. Ahmadpour, N.; Sayadi, M.H.; Sobhani, S.; Hajiani, M. A potential natural solar light active photocatalyst using magnetic ZnFe<sub>2</sub>O<sub>4</sub>@TiO<sub>2</sub>/Cu nanocomposite as a high performance and recyclable platform for degradation of naproxen from aqueous solution. *J. Clean. Prod.* **2020**, *268*, 122023. [CrossRef]
188. Kumar, A.; Kumar, A.; Sharma, G.; Al-Muhtaseb, A.H.; Naushad, M.; Ghfar, A.A.; Stadler, F.J. Quaternary magnetic BiOCl/g-C<sub>3</sub>N<sub>4</sub>/Cu<sub>2</sub>O/Fe<sub>3</sub>O<sub>4</sub> nano-junction for visible light and solar powered degradation of sulfamethoxazole from aqueous environment. *Chem. Eng. J.* **2018**, *334*, 462–478. [CrossRef]
189. Ahmadpour, N.; Sayadi, M.H.; Sobhani, S.; Hajiani, M. Photocatalytic degradation of model pharmaceutical pollutant by novel magnetic TiO<sub>2</sub>@ZnFe<sub>2</sub>O<sub>4</sub>/Pd nanocomposite with enhanced photocatalytic activity and stability under solar light irradiation. *J. Environ. Manag.* **2020**, *271*, 110964. [CrossRef]
190. Naushad, M. Surfactant assisted nano-composite cation exchanger: Development, characterization and applications for the removal of toxic Pb<sup>2+</sup> from aqueous medium. *Chem. Eng. J.* **2014**, *235*, 100–108. [CrossRef]
191. Sayadi, M.H.; Ahmadpour, N.; Homaeigohar, S. Photocatalytic and antibacterial properties of Ag-CuFe<sub>2</sub>O<sub>4</sub>@WO<sub>3</sub> magnetic nanocomposite. *Nanomaterials* **2021**, *11*, 298. [CrossRef]
192. Liu, F.; Liang, J.; Chen, L.; Tong, M.; Liu, W. Photocatalytic removal of diclofenac by Ti doped BiOI microspheres under visible light irradiation: Kinetics, mechanism, and pathways. *J. Mol. Liq.* **2019**, *275*, 807–814. [CrossRef]
193. Comber, S.; Gardner, M.; Sörme, P.; Ellor, B. The removal of pharmaceuticals during wastewater treatment: Can it be predicted accurately? *Sci. Total Environ.* **2019**, *676*, 222–230. [CrossRef]
194. Awfa, D.; Ateia, M.; Fujii, M.; Johnson, M.S.; Yoshimura, C. Photodegradation of pharmaceuticals and personal care products in water treatment using carbonaceous-TiO<sub>2</sub> composites: A critical review of recent literature. *Water Res.* **2018**, *142*, 26–45. [CrossRef]
195. Mudgal, S.; De Toni, A.; Lockwood, S.; Sales, K.; Backhaus, T.; Sorensen, B.H. Study on the environmental risks of medicinal products. In *BIO Intelligence Service*; European Commission: Brussels, Belgium, 2013; Available online: <https://hal.science/hal-03859880> (accessed on 12 January 2024).
196. Sheng, C.; Agwu Nnanna, A.G.; Liu, Y.; Vargo, J.D. Removal of trace pharmaceuticals from water using coagulation and powdered activated carbon as pretreatment to ultrafiltration membrane system. *Sci. Total Environ.* **2016**, *550*, 1075–1083. [CrossRef]
197. Bai, X.; Acharya, K. Removal of trimethoprim, sulfamethoxazole, and triclosan by the green alga *Nannochloris* sp. *J. Hazard. Mater.* **2016**, *315*, 70–75. [CrossRef]

198. Williams, R.T.; Cook, J.C. Exposure to pharmaceuticals present in the environment. *Ther. Innov. Regul. Sci.* **2007**, *41*, 133–141. [[CrossRef](#)]
199. Oluwole, A.O.; Omotola, E.O.; Olatunji, O.S. Pharmaceuticals and personal care products in water and wastewater: A review of treatment processes and use of photocatalyst immobilized on functionalized carbon in AOP degradation. *BMC Chem.* **2020**, *14*, 62. [[CrossRef](#)] [[PubMed](#)]
200. Kümmerer, K.; Steger-Hartmann, T.; Meyer, M. Biodegradability of the anti-tumour agent ifosfamide and its occurrence in hospital effluents and communal sewage. *Water Res.* **1997**, *31*, 2705–2710. [[CrossRef](#)]
201. Kumar, A.; Sharma, G.; Naushad, M.; Ahamad, T.; Cataluña Veses, R.; Stadler, F.J. Highly visible active Ag<sub>2</sub>CrO<sub>4</sub>/Ag/BiFeO<sub>3</sub>@RGO nano-junction for photoreduction of CO<sub>2</sub> and photocatalytic removal of ciprofloxacin and bromate ions: The triggering effect of Ag and RGO. *Chem. Eng. J.* **2019**, *370*, 148–165. [[CrossRef](#)]
202. Layton, A.; Gregory, B.; Seward, J.; Schultz, T.; Sayler, G. Mineralization of steroidal hormones by biosolids in wastewater treatment systems in Tennessee USA. *Environ. Sci. Technol.* **2000**, *34*, 3925–3931. [[CrossRef](#)]
203. Kokkinos, P.; Venieri, D.; Mantzavinos, D. Advanced oxidation processes for water and wastewater viral disinfection. a systematic review. *Food Environ. Virol.* **2021**, *13*, 283–302. [[CrossRef](#)] [[PubMed](#)]
204. Kanakaraju, D.; Glass, B.D.; Oelgemöller, M. Titanium dioxide photocatalysis for pharmaceutical wastewater treatment. *Environ. Chem. Lett.* **2014**, *12*, 27–47. [[CrossRef](#)]
205. Zhang, Y.; Zhou, Z.; Chen, T.; Wang, H.; Lu, W. Graphene TiO<sub>2</sub> nanocomposites with high photocatalytic activity for the degradation of sodium pentachlorophenol. *J. Environ. Sci.* **2014**, *26*, 2114–2122. [[CrossRef](#)]
206. Sharma, G.; Alothman, Z.A.; Kumar, A.; Sharma, S.; Kumar Ponnusamy, S.; Naushad, M. Fabrication and characterization of a nanocomposite hydrogel for combined photocatalytic degradation of a mixture of malachite green and fast green dye. *Nanotechnol. Environ. Eng.* **2017**, *2*, 4. [[CrossRef](#)]
207. Akter, S.; Islam, S.; Kabir, H.; Shaikh, A.A.; Gafur, A. UV/TiO<sub>2</sub> photodegradation of metronidazole, ciprofloxacin and sulfamethoxazole in aqueous solution: An optimization and kinetic study. *Arab. J. Chem.* **2022**, *15*, 103900. [[CrossRef](#)]
208. Sharma, M.; Yadav, A.; Mandal, M.K.; Dubey, K.K. TiO<sub>2</sub> based photocatalysis: A valuable approach for the removal of pharmaceuticals from aquatic environment. *Int. J. Environ. Sci. Technol.* **2023**, *20*, 4569–4584. [[CrossRef](#)]
209. Manasa, M.; Chandewar, P.R.; Mahalingam, H. Photocatalytic degradation of ciprofloxacin & norfloxacin and disinfection studies under solar light using boron & cerium doped TiO<sub>2</sub> catalysts synthesized by green EDTA-citrate method. *Catal. Today* **2020**, *375*, 522–536. [[CrossRef](#)]
210. Suwannaruang, T.; Kidkhunthod, P.; Chanlek, N.; Soontaranon, S.; Wantala, K. High anatase purity of nitrogen-doped TiO<sub>2</sub> nanorice particles for the photocatalytic treatment activity of pharmaceutical wastewater. *Appl. Surf. Sci.* **2019**, *478*, 1–14. [[CrossRef](#)]
211. Martins, P.; Kappert, S.; Nga Le, H.; Sebastian, V.; Kühn, K.; Alves, M.; Pereira, L.; Cuniberti, G.; Melle-Franco, M.; Lanceros-Méndez, S. Enhanced photocatalytic activity of Au/TiO<sub>2</sub> nanoparticles against ciprofloxacin. *Catalysts* **2020**, *10*, 234. [[CrossRef](#)]
212. Cabrera-Reina, A.; Martínez-Piernas, A.B.; Bertakis, Y.; Xekoukoulotakis, N.P.; Agüera, A.; Sánchez-Pérez, J.A. Ti photocatalysis under natural solar radiation for the degradation of the carbapenem antibiotics imipenem and meropenem in aqueous solutions at pilot plant scale. *Water Res.* **2019**, *166*, 115037. [[CrossRef](#)] [[PubMed](#)]
213. Truppi, A.; Petronella, F.; Placido, T.; Margiotta, V.; Lasorella, G.; Giotta, L.; Giannini, C.; Sibillano, T.; Murgolo, S.; Mascolo, G.; et al. Gram-scale synthesis of UV-vis light active plasmonic photocatalytic nanocomposite based on TiO<sub>2</sub>/Au nanorods for degradation of pollutants in water. *Appl. Catal. B Environ.* **2019**, *243*, 604–613. [[CrossRef](#)]
214. Gómez-Avilés, A.; Peñas-Garzón, M.; Bedia, J.; Rodriguez, J.J.; Bolver, C. C-modified TiO<sub>2</sub> using lignin as carbon precursor for the solar photocatalytic degradation of acetaminophen. *Chem. Eng. J.* **2019**, *358*, 1574–1582. [[CrossRef](#)]
215. Peñas-Garzón, M.; Gómez-Avilés, A.; Bolver, C.; Rodriguez, J.J.; Bedia, J. Degradation pathways of emerging contaminants using TiO<sub>2</sub>-activated carbon heterostructures in aqueous solution under simulated solar light. *Chem. Eng. J.* **2020**, *392*, 124867. [[CrossRef](#)]
216. Murgolo, S.; Moreira, I.S.; Piccirillo, C.; Castro, P.M.L.; Ventrella, G.; Coccozza, C.; Mascolo, G. Photocatalytic degradation of diclofenac by hydroxyapatite–TiO<sub>2</sub> composite material: Identification of transformation products and assessment of toxicity. *Materials* **2018**, *11*, 1779. [[CrossRef](#)]
217. Czech, B.; Tyszczyk-Rotko, K. Visible-light-driven photocatalytic removal of acetaminophen from water using a novel MWCNT-TiO<sub>2</sub>-SiO<sub>2</sub> photocatalysts. *Separ. Purif. Technol.* **2018**, *206*, 343–355. [[CrossRef](#)]
218. Payan, A.; Akbar Isari, A.; Gholizade, N. Catalytic decomposition of sulfamethazine antibiotic and pharmaceutical wastewater using Cu-TiO<sub>2</sub>@functionalized SWCNT ternary porous nanocomposite: Influential factors, mechanism, and pathway studies. *Chem. Eng. J.* **2019**, *361*, 1121–1141. [[CrossRef](#)]
219. Abdelraheem, W.H.M.; Nadagouda, M.N.; Dionysiou, D.D. Solar light-assisted remediation of domestic wastewater by N,B-TiO<sub>2</sub> nanoparticles for potable reuse. *Appl. Catal. B Environ.* **2020**, *269*, 118807. [[CrossRef](#)]
220. Carbuloni, C.F.; Savoia, J.E.; Santos, J.S.P.; Pereira, C.A.A.; Marques, R.G.; Ribeiro, V.A.S.; Ferrari, A.M. Degradation of metformin in water by TiO<sub>2</sub>-ZrO<sub>2</sub> photocatalysis. *J. Environ. Manag.* **2020**, *262*, 110347. [[CrossRef](#)]
221. Escudeiro de Oliveira, M.; Barroso, B.L.; de Almeida, J.; Moraes, M.L.L.; de Arruda Rodrigues, C. Photoelectrocatalytic degradation of 17 $\alpha$ -ethinylestradiol and estrone under UV and visible light using nanotubular oxide arrays grown on Ti-0.5wt%W. *Environ. Res.* **2020**, *191*, 110044. [[CrossRef](#)] [[PubMed](#)]

222. Gurung, K.; Ncibi, M.C.; Thangaraj, S.K.; Jänis, J.; Seyedsalehi, M.; Sillanpää, M. Removal of pharmaceutically active compounds (PhACs) from real membrane bioreactor (MBR) effluents by photocatalytic degradation using composite Ag<sub>2</sub>O/P-25 photocatalyst. *Separ. Purif. Technol.* **2019**, *215*, 317–328. [[CrossRef](#)]
223. Gomathi Devi, L.; Kavitha, R. A review on plasmonic metal TiO<sub>2</sub> composite for generation, trapping, storing and dynamic vectorial transfer of photogenerated electrons across the Schottky junction in a photocatalytic system. *Appl. Surf. Sci.* **2016**, *360*, 601–622. [[CrossRef](#)]
224. Yin, X.; Que, W.; Liao, Y.; Xie, H.; Fei, D. Ag-TiO<sub>2</sub> nanocomposites with improved photocatalytic properties prepared by a low temperature process in polyethylene glycol. *Colloids Surf. A* **2012**, *410*, 153–158. [[CrossRef](#)]
225. Fei, J.; Li, J. Controlled preparation of porous TiO<sub>2</sub>-Ag nanostructures through supramolecular assembly for plasmon-enhanced photocatalysis. *Adv. Mater.* **2015**, *27*, 314–319. [[CrossRef](#)] [[PubMed](#)]
226. Hou, W.; Cronin, S.B. A review of surface plasmon resonance-enhanced photocatalysis. *Adv. Funct. Mater.* **2013**, *23*, 1612–1619. [[CrossRef](#)]
227. Wang, T.; Wang, H.-J.; Lin, J.-S.; Yang, J.-L.; Zhang, F.-L.; Lin, X.-M.; Zhang, Y.-J.; Jin, S.; Li, J.-F. Plasmonic photocatalysis: Mechanism, applications and perspectives. *Chin. J. Struct. Chem.* **2023**, *42*, 100066. [[CrossRef](#)]
228. Kaur, R.; Pal, B. Co-catalysis effect of different morphological facets of as prepared Ag nanostructures for the photocatalytic oxidation reaction by Ag-TiO<sub>2</sub> aqueous slurry. *Mater. Chem. Phys.* **2013**, *143*, 393–399. [[CrossRef](#)]
229. Gang, R.; Xia, Y.; Xu, L.; Zhang, L.; Ju, S.; Wang, Z.; Koppala, S. Size controlled Ag decorated TiO<sub>2</sub> plasmonic photocatalysts for tetracycline degradation under visible light. *Surf. Interfaces* **2022**, *31*, 102018. [[CrossRef](#)]
230. Litter, M.I. Mechanisms of removal of heavy metals and arsenic from water by TiO<sub>2</sub>-heterogeneous photocatalysis. *Pure Appl. Chem.* **2015**, *87*, 557–567. [[CrossRef](#)]
231. Zhang, D.; Zhang, C.L.; Zhou, P. Preparation of porous nano-calcium titanate microspheres and its adsorption behavior for heavy metal ion in water. *J. Hazard. Mater.* **2011**, *186*, 971–977. [[CrossRef](#)]
232. Shaheen, N.; Irfan, N.M.; Khan, I.N.; Islam, S.; Islam, M.S.; Ahmed, M.K. Presence of heavy metals in fruits and vegetables: Health risk implications in Bangladesh. *Chemosphere* **2016**, *152*, 431–438. [[CrossRef](#)]
233. Khan, A.; Khan, S.; Khan, M.A.; Qamar, Z.; Waqas, M. The uptake and bioaccumulation of heavy metals by food plants, their effects on plants nutrients, and associated health risk: A review. *Environ. Sci. Pollut. Res.* **2015**, *22*, 13772–13799. [[CrossRef](#)]
234. Kyung, H.; Lee, J.; Choi, W. Simultaneous and synergistic conversion of dyes and heavy metal ions in aqueous TiO<sub>2</sub> suspensions under visible-light illumination. *Environ. Sci. Technol.* **2005**, *39*, 2376–2382. [[CrossRef](#)]
235. Mahdavi, S.; Jalali, M.; Afkhami, A. Heavy metals removal from aqueous solutions using TiO<sub>2</sub>, MgO, and Al<sub>2</sub>O<sub>3</sub> nanoparticles. *Chem. Eng. Commun.* **2013**, *200*, 448–470. [[CrossRef](#)]
236. Poursani, A.S.; Nilchi, A.; Hassani, A.; Shariat, S.M.; Nouri, J. The synthesis of nano TiO<sub>2</sub> and its use for removal of lead ions from aqueous solution. *J. Water Resour. Protect.* **2016**, *8*, 438–448. [[CrossRef](#)]
237. Luo, T.; Cui, J.; Hu, S.; Huang, Y.; Jing, C. Arsenic removal and recovery from copper smelting wastewater using TiO<sub>2</sub>. *Environ. Sci. Technol.* **2010**, *44*, 9094–9098. [[CrossRef](#)]
238. Yan, M.; Zeng, G.; Li, X.; Zhao, C.; Yang, G.; Gong, J.; Chen, G.; Tang, L.; Huang, D. Titanium dioxide nanotube arrays with silane coupling agent modification for heavy metal reduction and persistent organic pollutant degradation. *New J. Chem.* **2017**, *41*, 4377–4389. [[CrossRef](#)]
239. Skubal, L.R.; Meshkov, N.K. Reduction and removal of mercury from water using arginine-modified TiO<sub>2</sub>. *J. Photochem. Photobiol. A Chem.* **2002**, *148*, 211–214. [[CrossRef](#)]
240. Zhang, F.-S.; Nriagu, J.O.; Itoh, H. Photocatalytic removal and recovery of mercury from water using TiO<sub>2</sub>-modified sewage sludge carbon. *J. Photochem. Photobiol. A Chem.* **2004**, *167*, 223–228. [[CrossRef](#)]
241. Dou, B.; Chen, H. Removal of toxic mercury(II) from aquatic solutions by synthesized TiO<sub>2</sub> nanoparticles. *Desalination* **2011**, *269*, 260–265. [[CrossRef](#)]
242. Xu, S.; Du, A.J.; Liu, J.; Ng, J.; Sun, D.D. Highly efficient CuO incorporated TiO<sub>2</sub> nanotube photocatalyst for hydrogen production from water. *Int. J. Hydrogen Energy* **2011**, *36*, 6538–6545. [[CrossRef](#)]
243. Xu, S.C.; Pan, S.S.; Xu, Y.; Luo, Y.Y.; Zhang, Y.X.; Li, G.H. Efficient removal of Cr (VI) from wastewater under sunlight by Fe(II)-doped TiO<sub>2</sub> spherical shell. *J. Hazard. Mater.* **2014**, *283*, 7–13. [[CrossRef](#)] [[PubMed](#)]
244. Chen, Z.; Li, Y.; Guo, M.; Xu, F.; Wang, P.; Du, Y.; Na, P. One-pot synthesis of Mn-doped TiO<sub>2</sub> grown on graphene and the mechanism for removal of Cr(VI) and Cr (III). *J. Hazard. Mater.* **2016**, *310*, 188–198. [[CrossRef](#)]
245. Gullipilli, S.; Rupakula, R.B. Adsorption studies of Cr(VI) and Cu(II) metal ions from aqueous solutions by synthesized Ag and Mg co-doped TiO<sub>2</sub> nanoparticles. *Separ. Sci. Technol.* **2018**, *54*, 2983–2992. [[CrossRef](#)]
246. Eddy, D.R.; Rahayu, I.; Wyantuti, S.; Hartati, Y.W.; Firdaus, M.L.; Bahti, H.H. Photocatalytic activity of gadolinium doped TiO<sub>2</sub> particles for decreasing heavy metal chromium (VI) concentration. *J. Phys. Conf. Ser.* **2018**, *1080*, 012013. [[CrossRef](#)]
247. Luo, Z.; Qu, L.; Jia, J.; Wang, J.; Jiang, S.; Wu, Z.; Wu, X. TiO<sub>2</sub>/EDTA-rich carbon composites: Synthesis, characterization and visible-light-driven photocatalytic reduction of Cr(VI). *Chin. Chem. Lett.* **2018**, *29*, 547–550. [[CrossRef](#)]
248. Kobayashi, Y.; Kanasaki, R.; Nozaki, T.; Shoji, R.; Sato, K. Improving effect of MnO<sub>2</sub> addition on TiO<sub>2</sub>-photocatalytic removal of lead ion from water. *J. Water Environ. Technol.* **2017**, *15*, 35–42. [[CrossRef](#)]
249. Zhang, Y.; Hu, H.; Chang, M.; Chen, D.; Zhang, M.; Wu, L.; Li, X. Nonuniform doping outperforms uniform doping for enhancing the photocatalytic efficiency of Au-doped TiO<sub>2</sub> nanotubes in organic dye degradation. *Ceram. Int.* **2017**, *43*, 9053–9059. [[CrossRef](#)]

250. Zhang, Y.; Hu, Z.; Cui, X.; Yao, W.; Duan, T.; Zhu, W. Capture of Cs<sup>+</sup> and Sr<sup>2+</sup> from aqueous solutions by using Cr doped TiO<sub>2</sub> nanotubes. *J. Nanosci. Nanotechnol.* **2017**, *17*, 3943–3950. [[CrossRef](#)]
251. Garza-Arévalo, J.I.; García-Montes, I.; Reyes, M.H.; Guzmán-Mar, J.L.; Rodríguez-González, V.; Reyes, L.H. Fe doped TiO<sub>2</sub> photocatalyst for the removal of As (III) under visible radiation and its potential application on the treatment of As-contaminated groundwater. *Mater. Res. Bull.* **2016**, *73*, 145–152. [[CrossRef](#)]
252. Seema, K.M.; Mamba, B.B.; Njuguna, J.; Bakhtizin, R.Z.; Mishra, A.K. Removal of lead (II) from aqueous waste using (CD-PCL-TiO<sub>2</sub>) bio-nanocomposites. *Int. J. Biol. Macromol.* **2018**, *109*, 136–142. [[CrossRef](#)] [[PubMed](#)]
253. Zhao, Y.; Chang, W.; Huang, Z.; Feng, X.; Ma, L.; Qi, X.; Li, Z. Enhanced removal of toxic Cr(VI) in tannery wastewater by photoelectrocatalysis with synthetic TiO<sub>2</sub> hollow spheres. *Appl. Surf. Sci.* **2017**, *405*, 102–110. [[CrossRef](#)]
254. Wang, Q.; Zheng, Q.; Jin, R.; Gao, S.; Yuan, Q.; Rong, W.; Wang, R. Photoelectrocatalytic removal of organic dyes and Cr(VI) ions using Ag<sub>3</sub>PO<sub>4</sub> nanoparticles sensitized TiO<sub>2</sub> nanotube arrays. *Mater. Chem. Phys.* **2017**, *199*, 209–215. [[CrossRef](#)]
255. Hang, Y.; Yin, H.; Ji, Y.; Liu, Y.; Lu, Z.; Wang, A.; Shen, L.; Yin, H. Adsorption performances of naked and 3-aminopropyl triethoxysilane-modified mesoporous TiO<sub>2</sub> hollow nanospheres for Cu<sup>2+</sup>, Cd<sup>2+</sup>, Pb<sup>2+</sup>, Cr(VI) ions. *J. Nanosci. Nanotechnol.* **2017**, *17*, 5539–5549. [[CrossRef](#)]
256. Abbas, K.K.; Al-Ghaban, A.M.H.A. Enhanced solar light photoreduction of innovative TiO<sub>2</sub> nanospherical shell by reduced graphene oxide for removal silver ions from aqueous media. *J. Environ. Chem. Eng.* **2019**, *7*, 103168. [[CrossRef](#)]
257. Gan, W.; Shang, X.; Li, X.H.; Zhang, J.; Fu, X. Achieving high adsorption capacity and ultrafast removal of methylene blue and Pb<sup>2+</sup> by graphene-like TiO<sub>2</sub>@C. *Colloids Surf. A* **2019**, *561*, 218–225. [[CrossRef](#)]
258. Ajmal, A.; Majeed, I.; Malik, R.N.; Idriss, H.; Nadeem, M.A. Principles and mechanisms of photocatalytic dye degradation on TiO<sub>2</sub>-based photocatalysts: A comparative overview. *RSC Adv.* **2014**, *4*, 37003–37026. [[CrossRef](#)]
259. Konstantinou, I.K.; Albanis, T.A. TiO<sub>2</sub>-assisted photocatalytic degradation of azo dyes in aqueous solution: Kinetic and mechanistic investigations: A review. *Appl. Catal. B Environ.* **2004**, *49*, 1–14. [[CrossRef](#)]
260. Zhang, F.; Zhao, J.; Shen, T.; Hidaka, H.; Pelizzetti, E.; Serpone, N. TiO<sub>2</sub>-assisted photodegradation of dye pollutants II. Adsorption and degradation kinetics of eosin in TiO<sub>2</sub> dispersions under visible light irradiation. *Appl. Catal. B Environ.* **1998**, *15*, 147–156. [[CrossRef](#)]
261. Sakthivel, S.; Neppolian, B.; Shankar, M.V.; Arabindoo, B.; Palanichamy, M.; Murugesan, V. Solar photocatalytic degradation of azo dye: Comparison of photocatalytic efficiency of ZnO and TiO<sub>2</sub>. *Sol. Energy Mater. Sol. Cells* **2003**, *77*, 65–82. [[CrossRef](#)]
262. Chen, C.; Li, X.; Ma, W.; Zhao, J.; Hidaka, H.; Serpone, N. Effect of transition metal ions on the TiO<sub>2</sub>-assisted photodegradation of dyes under visible irradiation: A probe for the interfacial electron transfer process and reaction mechanism. *J. Phys. Chem. B* **2002**, *106*, 318–324. [[CrossRef](#)]
263. Gola, D.; Malik, A.; Namburath, M.; Ahammad, S.Z. Removal of industrial dyes and heavy metals by *Beauveria bassiana*: FTIR, SEM, TEM and AFM investigations with Pb(II). *Environ. Sci. Pollut. Res.* **2018**, *25*, 20486–20496. [[CrossRef](#)] [[PubMed](#)]
264. Chung, K.T. Azo dyes and human health: A review. *J. Environ. Sci. Health Part C Environ. Carcinog. Ecotoxicol. Rev.* **2016**, *34*, 233–261. [[CrossRef](#)] [[PubMed](#)]
265. Raman, C.D.; Kanmani, S. Textile dye degradation using nano zero valent iron: A review. *J. Environ. Manag.* **2016**, *177*, 341–355. [[CrossRef](#)] [[PubMed](#)]
266. Chandra, R.; Mukhopadhyay, S.; Nath, M. TiO<sub>2</sub>@ZIF-8: A novel approach of modifying micro-environment for enhanced photo-catalytic dye degradation and high usability of TiO<sub>2</sub> nanoparticles. *Mater. Lett.* **2016**, *164*, 571–574. [[CrossRef](#)]
267. Dariani, R.S.; Esmaeili, A.; Mortezaali, A.; Dehghanpour, S. Photocatalytic reaction and degradation of methylene blue on TiO<sub>2</sub> nano-sized particles. *Optik* **2016**, *127*, 7143–7154. [[CrossRef](#)]
268. Singh, R.; Kumari, P.; Chavan, P.D.; Datta, S.; Dutta, S. Synthesis of solvothermal derived TiO<sub>2</sub> nanocrystals supported on ground nano egg shell waste and its utilization for the photocatalytic dye degradation. *Opt. Mater.* **2017**, *73*, 377–383. [[CrossRef](#)]
269. Ljubas, D.; Smoljanić, G.; Juretić, H. Degradation of Methyl Orange and Congo Red dyes by using TiO<sub>2</sub> nanoparticles activated by the solar and the solar-like radiation. *J. Environ. Manag.* **2015**, *161*, 83–91. [[CrossRef](#)] [[PubMed](#)]
270. Zulfiqar, M.; Chowdhury, S.; Sufian, S.; Omar, A.A. Enhanced photocatalytic activity of Orange II in aqueous solution using solvent-based TiO<sub>2</sub> nanotubes: Kinetic, equilibrium and thermodynamic studies. *J. Clean. Prod.* **2018**, *203*, 848–859. [[CrossRef](#)]
271. Pol, R.; Guerrero, M.; García-Lecina, E.; Altube, A.; Rossinyol, E.; Garroni, S.; Baró, M.D.; Pons, J.; Sort, J.; Pellicer, E. Ni-, Pt- and (Ni/Pt)-doped TiO<sub>2</sub> nanophotocatalysts: A smart approach for sustainable degradation of Rhodamine B dye. *Appl. Catal. B Environ.* **2016**, *181*, 270–278. [[CrossRef](#)]
272. Gnanasekaran, L.; Hemamalini, R.; Saravanan, R.; Ravichandran, K.; Gracia, F.; Gupta, V.K. Intermediate state created by dopant ions (Mn, Co and Zr) into TiO<sub>2</sub> nanoparticles for degradation of dyes under visible light. *J. Mol. Liq.* **2016**, *223*, 652–659. [[CrossRef](#)]
273. Kerkez-Kuyumcu, Ö.; Kibar, E.; Dayioğlu, K.; Gedik, F.; Akin, A.N.; Özkara Aydinoglu, S. A comparative study for removal of different dyes over M/TiO<sub>2</sub> (M ¼ Cu, Ni, Co, Fe, Mn and Cr) photocatalysts under visible light irradiation. *J. Photochem. Photobiol. A Chem.* **2015**, *311*, 176–185. [[CrossRef](#)]
274. Kaur, N.; Kaur, S.; Singh, V. Preparation, characterization and photocatalytic degradation kinetics of Reactive Red dye 198 using N, Fe codoped TiO<sub>2</sub> nanoparticles under visible light. *Desalin. Water Treat.* **2016**, *57*, 9237–9246. [[CrossRef](#)]
275. Sood, S.; Umar, A.; Kumar Mehta, S.; Sinha, A.S.K.; Kansal, S.K. Efficient photocatalytic degradation of brilliant green using Sr-doped TiO<sub>2</sub> nanoparticles. *Ceram. Int.* **2015**, *41*, 3533–3540. [[CrossRef](#)]

276. Brindha, A.; Sivakumar, T. Visible active N, S co-doped TiO<sub>2</sub>/graphene photocatalysts for the degradation of hazardous dyes. *J. Photochem. Photobiol. A Chem.* **2017**, *340*, 146–156. [[CrossRef](#)]
277. McManamon, C.; O'Connell, J.; Delaney, P.; Rasappa, S.; Holmes, J.D.; Morris, M.A. A facile route to synthesis of S-doped TiO<sub>2</sub> nanoparticles for photocatalytic activity. *J. Mol. Catal. A Chem.* **2015**, *406*, 51–57. [[CrossRef](#)]
278. Shao, J.; Sheng, W.; Wang, M.; Li, S.; Chen, J.; Zhang, Y.; Cao, S. In situ synthesis of carbon-doped TiO<sub>2</sub> single-crystal nanorods with a remarkably photocatalytic efficiency. *Appl. Catal. B Environ.* **2017**, *209*, 311–319. [[CrossRef](#)]
279. Zhang, Q.; Fu, Y.; Wu, Y.; Zhang, Y.N.; Zuo, T. Low-cost Y-doped TiO<sub>2</sub> nanosheets film with highly reactive {001} facets from CRT waste and enhanced photocatalytic removal of Cr(VI) and methyl orange. *ACS Sustain. Chem. Eng.* **2016**, *4*, 1794–1803. [[CrossRef](#)]
280. Li, Q.; Zong, L.; Li, C.; Yang, J. Reprint of photocatalytic reduction of CO<sub>2</sub> on MgO/TiO<sub>2</sub> nanotube films. *Appl. Surf. Sci.* **2014**, *319*, 16–20. [[CrossRef](#)]
281. Dahl, M.; Liu, Y.; Yin, Y. Composite titanium dioxide nanomaterials. *Chem. Rev.* **2014**, *114*, 9853–9889. [[CrossRef](#)] [[PubMed](#)]
282. Anwar, D.I.; Mulyadi, D. Synthesis of Fe-TiO<sub>2</sub> composite as a photocatalyst for degradation of methylene blue. *Procedia Chem* **2015**, *17*, 49–54. [[CrossRef](#)]
283. Lei, P.; Wang, F.; Gao, X.; Ding, Y.; Zhang, S.; Zhao, J.; Liu, S.; Yang, M. Immobilization of TiO<sub>2</sub> nanoparticles in polymeric substrates by chemical bonding for multi-cycle photodegradation of organic pollutants. *J. Hazard. Mater.* **2012**, *227–228*, 185–194. [[CrossRef](#)]
284. Talebi, S.; Chaibakhsh, N.; Moradi-Shoeili, Z. Application of nanoscale ZnS/TiO<sub>2</sub> composite for optimized photocatalytic decolorization of a textile dye. *J. Appl. Res. Technol.* **2017**, *15*, 378–385. [[CrossRef](#)]
285. Hui, C.; Lei, Z.; Xitang, W.; Shujing, L.; Zhongxing, L. Preparation of nanoporous TiO<sub>2</sub>/SiO<sub>2</sub> composite with rice husk as template and its photocatalytic property. *Rare Met. Mater. Eng.* **2015**, *44*, 1607–1611. [[CrossRef](#)]
286. Li, J.; Zhen, D.; Sui, G.; Zhang, C.; Deng, Q.; Jia, L. Nanocomposite of Cu-TiO<sub>2</sub>-SiO<sub>2</sub> with high photoactive performance for degradation of rhodamine B dye in aqueous wastewater. *J. Nanosci. Nanotechnol.* **2012**, *12*, 6265–6270. [[CrossRef](#)]
287. Liu, J.; Liu, J.; Shi, F.; Hu, S.; Jiang, S.; Liu, S.; Liu, D.; Tian, X. F/W codoped TiO<sub>2</sub>-SiO composite aerogels with improved visible light-driven photocatalytic activity. *J. Solid State Chem.* **2019**, *275*, 8–15. [[CrossRef](#)]
288. Shao, L.; Liu, H.; Zeng, W.; Zhou, C.; Li, D.; Wang, L.; Lan, Y.; Xu, F.; Liu, G. Immobilized and photocatalytic performances of PDMS-SiO<sub>2</sub>-chitosan@TiO<sub>2</sub> composites on pumice under simulated sunlight irradiation. *Appl. Surf. Sci.* **2019**, *478*, 1017–1026. [[CrossRef](#)]
289. Tang, Y.; Di, W.; Zhai, X.; Yang, R.; Qin, W. NIR-responsive photocatalytic activity and mechanism of NaYF<sub>4</sub>:Yb,Tm@TiO<sub>2</sub> core-shell nanoparticles. *ACS Catal.* **2013**, *3*, 405–412. [[CrossRef](#)]
290. Djellabi, R.; Ghorab, M.F.; Cerrato, G.; Morandi, S.; Gatto, S.; Oldani, V.; Di Michele, A.; Bianchi, C.L. Photoactive TiO<sub>2</sub>-montmorillonite composite for degradation of organic dyes in water. *J. Photochem. Photobiol. A Chem.* **2015**, *295*, 57–63. [[CrossRef](#)]
291. Alagarasi, A.; Rajalakshmi, P.U.; Shanthi, K.; Selvam, P. Solar light photocatalytic activity of mesoporous nanocrystalline TiO<sub>2</sub>, SnO<sub>2</sub>, and TiO<sub>2</sub>-SnO<sub>2</sub> composites. *Mater. Today Sustain.* **2019**, *5*, 100016. [[CrossRef](#)]
292. Magdalane, C.M.; Kanimozhi, K.; Arularasu, M.V.; Ramalingam, G.; Kaviyarasu, K. Self-cleaning mechanism of synthesized SnO<sub>2</sub>/TiO<sub>2</sub> nanostructure for photocatalytic activity application for waste water treatment. *Surf. Interfaces* **2019**, *17*, 100346. [[CrossRef](#)]
293. Li, Y.; Zhang, W.; Li, L.; Yi, C.; Lv, H.; Song, Q. Litchi-like CdS/CdTiO<sub>3</sub>-TiO<sub>2</sub> composite: Synthesis and enhanced photocatalytic performance for crystal violet degradation and hydrogen production. *RSC Adv.* **2016**, *6*, 51374–51386. [[CrossRef](#)]
294. Hamdy, M.S.; Saputera, W.H.; Groenen, E.J.; Mul, G. A novel TiO<sub>2</sub> composite for photocatalytic wastewater treatment. *J. Catal.* **2014**, *310*, 75–83. [[CrossRef](#)]
295. Rahimi, B.; Jafari, N.; Abdolahnejad, A.; Farrokhzadeh, H.; Ebrahimi, A. Application of efficient photocatalytic process using a novel BiVO<sub>4</sub>/TiO<sub>2</sub>-NaY zeolite composite for removal of acid orange 10 dye in aqueous solutions: Modeling by response surface methodology (RSM). *J. Environ. Chem. Eng.* **2019**, *7*, 103253. [[CrossRef](#)]
296. Saleh, R.; Taufik, A.; Prakoso, S.P. Fabrication of Ag<sub>2</sub>O/TiO<sub>2</sub> composites on nanographene platelets for the removal of organic pollutants: Influence of oxidants and inorganic anions. *Appl. Surf. Sci.* **2019**, *480*, 697–708. [[CrossRef](#)]
297. Visa, M.; Isac, L.; Duta, A. New fly ash TiO<sub>2</sub> composite for the sustainable treatment of wastewater with complex pollutants load. *Appl. Surf. Sci.* **2015**, *339*, 62–68. [[CrossRef](#)]
298. Jaseela, P.K.; Garvasis, J.; Joseph, A. Selective adsorption of methylene blue (MB) dye from aqueous mixture of MB and methyl orange (MO) using mesoporous titania (TiO<sub>2</sub>)-poly vinyl alcohol (PVA) nanocomposite. *J. Mol. Liq.* **2019**, *286*, 110908. [[CrossRef](#)]
299. Yun, J.; Jin, D.; Lee, Y.S.; Kim, H. Photocatalytic treatment of acidic waste water by electrospun composite nanofibers of pH-sensitive hydrogel and TiO<sub>2</sub>. *Mater. Lett.* **2010**, *64*, 2431–2434. [[CrossRef](#)]
300. Cheng, H.; Hu, M.; Zhai, Q.; Li, S.; Jiang, Y. Polydopamine tethered CPO/HRPTiO<sub>2</sub> nano-composites with high bio-catalytic activity, stability and reusability: Enzyme-photo bifunctional synergistic catalysis in water treatment. *Chem. Eng. J.* **2018**, *347*, 703–710. [[CrossRef](#)]
301. Saleh, T.A.; Gupta, V.K. Photo-catalyzed degradation of hazardous dye methyl orange by use of a composite catalyst consisting of multi-walled carbon nanotubes and titanium dioxide. *J. Colloid Interface Sci.* **2012**, *371*, 101–106. [[CrossRef](#)]
302. Rajamanickam, D.; Shanthi, M. Photocatalytic degradation of an azo dye Sunset Yellow under UV-A light using TiO<sub>2</sub>/CAC composite catalysts. *Spectrochim. Acta Part A Mol. Biomol. Spectrosc.* **2014**, *128*, 100–108. [[CrossRef](#)]

303. Hassan, M.E.; Liu, G.; Omer, E.O.M.; Goja, A.M.; Acharya, S. Silver embedded C-TiO<sub>2</sub> exhibits improved photocatalytic properties with potential application in waste water treatment. *Arab. J. Chem.* **2018**, *12*, 1134–1140. [[CrossRef](#)]
304. Xu, C.; Cui, A.; Xu, Y.; Fu, X. Graphene oxide-TiO<sub>2</sub> composite filtration membranes and their potential application for water purification. *Carbon* **2013**, *62*, 465–471. [[CrossRef](#)]
305. Ahmed, A.S.; Ahamad, T.; Ahmad, N.; Khan, M.Z. Removal enhancement of acid navy blue dye by GO-TiO<sub>2</sub> nanocomposites synthesized using sonication method. *Mater. Chem. Phys.* **2019**, *238*, 121906. [[CrossRef](#)]
306. Mohamed, H.H.; Alsanea, A.A. TiO<sub>2</sub>/carbon dots decorated reduced graphene oxide composites from waste car bumper and TiO<sub>2</sub> nanoparticles for photocatalytic applications. *Arab. J. Chem.* **2018**, *13*, 3082–3091. [[CrossRef](#)]
307. Ranjith, R.; Renganathan, V.; Chen, S.M.; Selvan, N.S.; Rajam, P.S. Green synthesis of reduced graphene oxide supported TiO<sub>2</sub>/Co<sub>3</sub>O<sub>4</sub> nanocomposite for photocatalytic degradation of methylene blue and crystal violet. *Ceram. Int.* **2019**, *45*, 12926–12933. [[CrossRef](#)]
308. Monga, D.; Basu, S. Enhanced photocatalytic degradation of industrial dye by g-C<sub>3</sub>N<sub>4</sub>/TiO<sub>2</sub> nanocomposite: Role of shape of TiO<sub>2</sub>. *Adv. Powder Technol.* **2019**, *30*, 1089–1098. [[CrossRef](#)]
309. Zhang, J.J.; Fang, S.S.; Mei, J.Y.; Zheng, G.P.; Zheng, X.C.; Guan, X.X. High-efficiency removal of rhodamine B dye in water using g-C<sub>3</sub>N<sub>4</sub> and TiO<sub>2</sub> co-hybridized 3D graphene aerogel composites. *Separ. Purif. Technol.* **2018**, *194*, 96–103. [[CrossRef](#)]
310. Zhang, Y.; Cui, W.; An, W.; Liu, L.; Liang, Y.; Zhu, Y. Combination of photoelectrocatalysis and adsorption for removal of bisphenol A over TiO<sub>2</sub>-graphene hydrogel with 3D network structure. *Appl. Catal. B Environ.* **2018**, *221*, 36–46. [[CrossRef](#)]
311. Chi, L.; Qian, Y.; Guo, J.; Wang, X.; Arandiyani, H.; Jiang, Z. Novel g-C<sub>3</sub>N<sub>4</sub>/TiO<sub>2</sub>/PAA/PTFE ultrafiltration membrane enabling enhanced antifouling and exceptional visible-light photocatalytic self-cleaning. *Catal. Today* **2019**, *335*, 527–537. [[CrossRef](#)]
312. Daneshvar, N.; Salari, D.; Niaei, A.; Rasoulifard, M.H.; Khataee, A.R. Immobilization of TiO<sub>2</sub> nanopowder on glass beads for the photocatalytic decolorization of an azo dye C.I. Direct Red 23. *J. Environ. Sci. Health* **2005**, *40*, 1605–1617. [[CrossRef](#)] [[PubMed](#)]
313. Cunha, D.L.; Kuznetsov, A.; Achete, C.A.; Machado, A.E.d.H.; Marques, M. Immobilized TiO<sub>2</sub> on glass spheres applied to heterogeneous photocatalysis: Photoactivity, leaching and regeneration process. *PeerJ* **2018**, *6*, e4464. [[CrossRef](#)] [[PubMed](#)]
314. Abbasi, Z.; Farrokhnia, A.; García-López, E.I.; Zargar Shoushtari, M. Codeposition of Fe<sub>3</sub>O<sub>4</sub> nanoparticles sandwiched between g-C<sub>3</sub>N<sub>4</sub> and TiO<sub>2</sub> nanosheets: Structure, characterization and high photocatalytic activity for efficiently degradation of dye pollutants. *Phys. Chem. Res.* **2019**, *7*, 65–80. [[CrossRef](#)]
315. Gu, W.; Lu, F.; Wang, C.; Kuga, S.; Wu, L.; Huang, Y.; Wu, M. Face-to-Face interfacial assembly of ultrathin g-C<sub>3</sub>N<sub>4</sub> and anatase TiO<sub>2</sub> nanosheets for enhanced solar photocatalytic activity. *ACS Appl. Mater. Interfaces* **2017**, *9*, 28674–28684. [[CrossRef](#)] [[PubMed](#)]
316. Qiu, J.; Liu, F.; Yue, C.; Ling, C.; Li, A. A recyclable nanosheet of Mo/N-doped TiO<sub>2</sub> nanorods decorated on carbon nanofibers for organic pollutants degradation under simulated sunlight irradiation. *Chemosphere* **2019**, *215*, 280–293. [[CrossRef](#)]
317. Khan, M.A.; Mutahir, S.; Wang, F.; Lei, W.; Xia, M. Sensitization of TiO<sub>2</sub> nanosheets with Cu-biphenylamine framework to enhance photocatalytic degradation performance of toxic organic contaminants: Synthesis, mechanism and kinetic studies. *Nanotechnology* **2018**, *29*, 375605. [[CrossRef](#)]
318. Nair, A.K.; Jagadeesh Babu, P.E. Ag-TiO<sub>2</sub> nanosheet embedded photocatalytic membrane for solar water treatment. *J. Environ. Chem. Eng.* **2017**, *5*, 4128–4133. [[CrossRef](#)]
319. Du, F.; Zuo, X.; Yang, Q.; Yang, B.; Li, G.; Ding, Z.; Wu, M.; Ma, Y.; Jin, S.; Zhu, K. Facile assembly of TiO<sub>2</sub> nanospheres/SnO<sub>2</sub> quantum dots composites with excellent photocatalyst activity for the degradation of methyl orange. *Ceram. Int.* **2016**, *42*, 12778–12782. [[CrossRef](#)]
320. Wang, H.; Xiao, L.; Wang, C.; Lin, B.; Lyu, S.; Chu, X.; Chi, Y.; Yang, X.; Wang, X. Pd/TiO<sub>2</sub> nanospheres with three-dimensional hyperstructure for enhanced photodegradation of organic dye. *Chem. Res.* **2019**, *35*, 667–673. [[CrossRef](#)]
321. Ghaforyan, H.; Ghaffary, T.; Pincak, R.; Ebrahimzadeh, M. Effects of ultrasound waves intensity on the removal of Congo Red color from the textile industry wastewater by Fe<sub>3</sub>O<sub>4</sub>@TiO<sub>2</sub> core-shell nanospheres. *arXiv* **2017**, arXiv:1708.04683. [[CrossRef](#)]
322. Tetteh, E.K.; Rathilal, S.; Asante-Sackey, D.; Chollom, M.N. Prospects of synthesized magnetic TiO<sub>2</sub>-based membranes for wastewater treatment: A review. *Materials* **2021**, *14*, 3524. [[CrossRef](#)]
323. Cao, J.; Song, X.Z.; Kang, X.; Dai, Z.; Tan, Z. One-pot synthesis of oleic acid modified monodispersed mesoporous TiO<sub>2</sub> nanospheres with enhanced visible light photocatalytic performance. *Adv. Powder Technol.* **2018**, *29*, 1925–1932. [[CrossRef](#)]
324. Liu, D.; Tian, R.; Wang, J.; Nie, E.; Piao, X.; Li, X.; Sun, Z. Photoelectrocatalytic degradation of methylene blue using F doped TiO<sub>2</sub> photoelectrode under visible light irradiation. *Chemosphere* **2017**, *185*, 574–581. [[CrossRef](#)] [[PubMed](#)]
325. Nurdin, M.; Azis, T.; Maulidiyah, M.; Aladin, A.; Hafid, N.A.; Salim, L.O.A.; Wibowo, D. Photocurrent responses of metanil yellow and remazol red B organic dyes by using TiO<sub>2</sub>/Ti electrode. *IOP Conf. Ser. Mater. Sci. Eng.* **2018**, *367*, 12048. [[CrossRef](#)]
326. Yilmaz, P.; Lacerda, A.M.; Larrosa, I.; Dunn, S. Photoelectrocatalysis of rhodamine B and solar hydrogen production by TiO<sub>2</sub> and Pd/TiO<sub>2</sub> catalyst systems. *Electrochim. Acta* **2017**, *231*, 641–649. [[CrossRef](#)]
327. Likodimos, V. Photonic crystal-assisted visible light activated TiO<sub>2</sub> photocatalysis. *Appl. Catal. B Environ.* **2018**, *230*, 269–303. [[CrossRef](#)]
328. Lu, Y.; Yu, H.; Chen, S.; Quan, X.; Zhao, H. Integrating plasmonic nanoparticles with TiO<sub>2</sub> photonic crystal for enhancement of visible-light-driven photocatalysis. *Environ. Sci. Technol.* **2012**, *46*, 1724–1730. [[CrossRef](#)]
329. Liao, G.; Chen, S.; Quan, X.; Chen, H.; Zhang, Y. Photonic crystal coupled TiO<sub>2</sub>/polymer hybrid for efficient photocatalysis under visible light irradiation. *Environ. Sci. Technol.* **2010**, *44*, 3481–3485. [[CrossRef](#)] [[PubMed](#)]

330. Wang, Y.; Li, P.; Chen, S.L.; Wang, A.J. Dual-bandgap effect of photonic crystals on TiO<sub>2</sub> photocatalytic activity in ultraviolet and visible light regions. *Catal. Surv.* **2019**, *23*, 23–32. [[CrossRef](#)]
331. Geng, Z.; Zhang, Y.; Yuan, X.; Huo, M.; Zhao, Y.; Lu, Y.; Qiu, Y. Incorporation of Cu<sub>2</sub>O nanocrystals into TiO<sub>2</sub> photonic crystal for enhanced UV-visible light driven photocatalysis. *J. Alloys Compd.* **2015**, *644*, 734–741. [[CrossRef](#)]
332. Chen, H.; Chen, S.; Quan, X.; Zhang, Y. Structuring a TiO<sub>2</sub>-based photonic crystal photocatalyst with Schottky junction for efficient photocatalysis. *Environ. Sci. Technol.* **2010**, *44*, 451–455. [[CrossRef](#)]
333. Li, Y.; Chang, Y.; Liu, F.T.; Zhao, Y.; Wang, J.; Wang, C.W. Photonic crystal structural-induced Cu<sub>3</sub>SnS<sub>4</sub>/Ti<sup>3+</sup>-TiO<sub>2</sub> p-n coaxial heterojunction arrays for light-driven H<sub>2</sub> production and pollutant degradation. *Mater. Des.* **2017**, *133*, 426–434. [[CrossRef](#)]
334. Vela, N.; Pérez-Lucas, G.; Fenoll, J.; Navarro, S. Recent overview on the abatement of pesticide residues in water by photocatalytic treatment using TiO<sub>2</sub>. In *Application of Titanium Dioxide*; IntechOpen: London, UK, 2017. [[CrossRef](#)]
335. Liu, Y.; Liu, F.; Pan, X.; Li, J. Protecting the environment and public health from pesticides. *Environ. Sci. Technol.* **2012**, *46*, 5658–5659. [[CrossRef](#)]
336. Shuman-Goodier, M.E.; Propper, C.R. A meta-analysis synthesizing the effects of pesticides on swim speed and activity of aquatic vertebrates. *Sci. Total Environ.* **2016**, *565*, 758–766. [[CrossRef](#)]
337. Blair, A.; Ritz, B.; Wesseling, C.; Beane Freeman, L. Pesticides and human health. *Occup. Environ. Med.* **2015**, *72*, 81–82. [[CrossRef](#)]
338. Alavanja, M.C.R.; Bonner, M.R. Occupational pesticide exposures and cancer risk: A review. *J. Toxicol. Environ. Health Part B* **2012**, *15*, 238–263. [[CrossRef](#)]
339. Vanraes, P.; Ghodbane, H.; Davister, D.; Wardenier, N.; Nikiforov, A.; Verheust, Y.P.; Van Hulle, S.W.H.; Hamdaoui, O.; Vandamme, J.; Van Durme, J.; et al. Removal of several pesticides in a falling water film DBD reactor with activated carbon textile: Energy efficiency. *Water Res.* **2017**, *116*, 1–12. [[CrossRef](#)]
340. Farner Budaraz, J.; Cooper, E.M.; Gardner, C.; Hodzic, E.; Ferguson, P.L.; Gunsch, C.K.; Wiesner, M.R. Chlorpyrifos degradation via photoreactive TiO<sub>2</sub> nanoparticles: Assessing the impact of a multi-component degradation scenario. *J. Hazard. Mater.* **2019**, *372*, 61–68. [[CrossRef](#)]
341. Amalraj, A.; Thirumalaisamy, S.; Rajeswari, A.; Pius, A. Photocatalytic degradation of quinalphos and profenofos pesticides using UV irradiated TiO<sub>2</sub> nanoparticles—a kinetic study. *Mater. Focus* **2016**, *5*, 377–384. [[CrossRef](#)]
342. Cruz, M.; Gomez, C.; Duran-Valle, C.J.; Pastrana-Martínez, L.M.; Faria, J.L.; Silva, A.M.T.; Faraldos, M.; Bahamonde, A. Bare TiO<sub>2</sub> and graphene oxide TiO<sub>2</sub> photocatalysts on the degradation of selected pesticides and influence of the water matrix. *Appl. Surf. Sci.* **2017**, *416*, 1013–1021. [[CrossRef](#)]
343. Zhang, Y.; Han, C.; Zhang, G.; Dionysiou, D.D.; Nadagouda, M.N. PEG-assisted synthesis of crystal TiO<sub>2</sub> nanowires with high specific surface area for enhanced photocatalytic degradation of atrazine. *Chem. Eng. J.* **2015**, *268*, 170–179. [[CrossRef](#)]
344. Ahmari, H.; Heris, S.Z.; Khayyat, M.H. The effect of titanium dioxide nanoparticles and UV irradiation on photocatalytic degradation of Imidaclopride. *Environ. Technol.* **2018**, *39*, 536–547. [[CrossRef](#)] [[PubMed](#)]
345. Vela, N.; Calín, M.; Yáñez-Gascón, M.J.; Garrido, I.; Pérez-Lucas, G.; Fenoll, J.; Navarro, S. Photocatalytic oxidation of six pesticides listed as endocrine disruptor chemicals from wastewater using two different TiO<sub>2</sub> samples at pilot plant scale under sunlight irradiation. *J. Photochem. Photobiol. A Chem.* **2018**, *353*, 271–278. [[CrossRef](#)]
346. Kalantary, R.R.; Dadban Shahamat, Y.; Farzadkia, M.; Esrafil, A.; Asgharnia, H. Photocatalytic degradation and mineralization of diazinon in aqueous solution using nano-TiO<sub>2</sub> (Degussa, P25): Kinetic and statistical analysis. *Desalin. Water Treat.* **2015**, *55*, 555–563. [[CrossRef](#)]
347. Suhaimy, S.H.M.; Lai, C.W.; Tajuddin, H.A.; Samsudin, E.M.; Johan, M.R. Impact of TiO<sub>2</sub> nanotubes' morphology on the photocatalytic degradation of simazine pollutant. *Materials* **2018**, *11*, 66. [[CrossRef](#)]
348. Tabasideh, S.; Maleki, A.; Shahmoradi, B.; Ghahremani, E.; McKay, G. Sonophotocatalytic degradation of diazinon in aqueous solution using iron-doped TiO<sub>2</sub> nanoparticles. *Separ. Purif. Technol.* **2017**, *189*, 186–192. [[CrossRef](#)]
349. Mermana, J.; Sutthivaiyakit, P.; Blaise, C.; Gagné, F.; Charnsethikul, S.; Kidkhunthod, P.; Sutthivaiyakit, S. Photocatalysis of S-metolachlor in aqueous suspension of magnetic cerium-doped mTiO<sub>2</sub> core-shell under simulated solar light. *Environ. Sci. Pollut. Res.* **2017**, *24*, 4077–4092. [[CrossRef](#)] [[PubMed](#)]
350. Umar, K.; Aris, A.; Ahmad, H.; Parveen, T.; Jaafar, J.; Majid, Z.A.; Reddy, A.V.B.; Talib, J. Synthesis of visible light active doped TiO<sub>2</sub> for the degradation of organic pollutants-methylene blue and glyphosate. *J. Anal. Sci. Technol.* **2016**, *7*, 29. [[CrossRef](#)]
351. Maddila, S.; Oseghe, E.O.; Jonnalagadda, S.B. Photocatalyzed ozonation by Ce doped TiO<sub>2</sub> catalyst degradation of pesticide Dicamba in water. *J. Chem. Technol. Biotechnol.* **2016**, *91*, 385–393. [[CrossRef](#)]
352. Quiñones, D.H.; Rey, A.; Álvarez, P.M.; Beltrán, F.J.; Li Puma, G. Boron doped TiO<sub>2</sub> catalysts for photocatalytic ozonation of aqueous mixtures of common pesticides: Diuron, o-phenylphenol, MCPA and terbuthylazine. *Appl. Catal. B Environ.* **2014**, *178*, 74–81. [[CrossRef](#)]
353. Joseph, A.I.J.; Thiripuranthagan, S. Non-metal doped titania photocatalysts for the degradation of neonicotinoid insecticides under visible light irradiation. *J. Nanosci. Nanotechnol.* **2018**, *18*, 3158–3164. [[CrossRef](#)] [[PubMed](#)]
354. Komtchou, S.; Dirany, A.; Drogui, P.; Deegan, N.; El Khakani, M.A.; Robert, D.; Lafrance, P. Degradation of atrazine in aqueous solution with electrophotocatalytic process using TiO<sub>2-x</sub> photoanode. *Chemosphere* **2016**, *157*, 79–88. [[CrossRef](#)] [[PubMed](#)]
355. Turan, N.B.; Sari Erkan, H.; Çağlak, A.; Bakırdere, S.; Engin, G.O. Optimization of atrazine removal from synthetic groundwater by electrooxidation process using titanium dioxide and graphite electrodes. *Separ. Sci. Technol.* **2019**, *55*, 3036–3045. [[CrossRef](#)]

356. Matsunaga, T.; Tomoda, R.; Nakajima, T.; Wake, H. Photoelectrochemical sterilization of microbial cells by semiconductor powders. *FEMS Microbiol. Lett.* **1985**, *29*, 211–214. Available online: <https://www.sciencedirect.com/science/article/pii/0378109785903003> (accessed on 12 January 2024). [CrossRef]
357. Maness, P.-C.; Smolinski, S.; Blake, D.M.; Huang, Z.; Wolfrum, E.J.; Jacoby, W.A. Bactericidal activity of photocatalytic TiO<sub>2</sub> reaction toward an understanding of its killing mechanism. *Appl. Environ. Microbiol.* **1999**, *65*, 4094–4098. [CrossRef]
358. Cai, R.; Hashimoto, K.; Itoh, K.; Kubota, Y.; Fujishima, A. Photokilling of malignant cells with ultrafine TiO<sub>2</sub> powder. *Bull. Chem. Soc. Jpn.* **1991**, *64*, 1268–1273. [CrossRef]
359. Karunakaran, C. Solar Photocatalytic Disinfection of Bacteria. In *New and Future Developments in Catalysis*; Suib, S.L., Ed.; Elsevier B.V.: Amsterdam, The Netherlands, 2013. [CrossRef]
360. Prasad, G.K.; Ramacharyulu, P.V.R.K.; Merwyn, S.; Agarwal, G.S.; Srivastava, A.R.; Beer Singh, G.P.R.; Vijayaraghavan, R. Photocatalytic inactivation of spores of *Bacillus anthracis* using titania nanomaterials. *J. Hazard. Mater.* **2011**, *185*, 977–982. [CrossRef] [PubMed]
361. Nasser, A.M.; Paulman, H.; Sela, O.; Ktaitzer, T.; Cikurel, H.; Zuckerman, I.; Meir, A.; Aharoni, A.; Adin, A. UV disinfection of wastewater effluents for unrestricted irrigation. *Water Sci. Technol.* **2006**, *54*, 83–88. [CrossRef] [PubMed]
362. Egli, T.; Köster, W.; Meile, L. Pathogenic microbes in water and food: Changes and challenges. *FEMS Microbiol. Rev.* **2002**, *26*, 111–112. [CrossRef] [PubMed]
363. Laxma Reddy, P.V.; Kavitha, B.; Kumar Reddy, P.A.; Kim, K.H. TiO<sub>2</sub>-based photocatalytic disinfection of microbes in aqueous media: A review. *Environ. Res.* **2017**, *154*, 296–303. [CrossRef] [PubMed]
364. Mahmood, M.A.; Baruah, S.; Anal, A.K.; Dutta, J. Heterogeneous photocatalysis for removal of microbes from water. *Environ. Chem. Lett.* **2012**, *10*, 145–151. [CrossRef]
365. Leung, T.L.F.; Bates, A.E. More rapid and severe disease outbreaks for aquaculture at the tropics: Implications for food security. *J. Appl. Ecol.* **2013**, *50*, 215–222. [CrossRef]
366. Ashbolt, N.J. Microbial contamination of drinking water and disease outcomes in developing regions. *Toxicology* **2004**, *198*, 229–238. [CrossRef] [PubMed]
367. Joost, U.; Juganson, K.; Visnapuu, M.; Mortimer, M.; Kahru, A.; Nõmmiste, E.; Joost, U.; Kisand, V.; Ivask, A. Photocatalytic antibacterial activity of nano-TiO<sub>2</sub> (anatase)-based thin films: Effects on *Escherichia coli* cells and fatty acids. *J. Photochem. Photobiol. B Biol.* **2015**, *142*, 178–185. [CrossRef]
368. Podporska-Carroll, J.; Panaitescu, E.; Quilty, B.; Wang, L.; Menon, L.; Pillai, S.C. Antimicrobial properties of highly efficient photocatalytic TiO<sub>2</sub> nanotubes. *Appl. Catal. B Environ.* **2015**, *176–177*, 70–75. [CrossRef]
369. Long, M.; Wang, J.; Zhuang, H.; Zhang, Y.; Wu, H.; Zhang, J. Performance and mechanism of standard nano-TiO<sub>2</sub> (P-25) in photocatalytic disinfection of foodborne microorganisms-*Salmonella typhimurium* and *Listeria monocytogenes*. *Food Control* **2014**, *39*, 68–74. [CrossRef]
370. Makropoulou, T.; Panagiotopoulou, P.; Venieri, D. N-doped TiO<sub>2</sub> photocatalysts for bacterial inactivation in water. *J. Chem. Technol. Biotechnol.* **2018**, *93*, 2518–2526. [CrossRef]
371. Milosevic, I.; Jayaprakash, A.; Greenwood, B.; van Driel, B.; Rtimi, S.; Bowen, P. Synergistic effect of fluorinated and N doped TiO<sub>2</sub> nanoparticles leading to different microstructure and enhanced photocatalytic bacterial inactivation. *Nanomaterials* **2017**, *7*, 391. [CrossRef]
372. Choi, S.Y.; Cho, B. Extermination of influenza virus H1N1 by a new visible-light induced photocatalyst under fluorescent light. *Virus Res.* **2018**, *248*, 71–73. [CrossRef]
373. Zheng, X.; Shen, Z.; Cheng, C.; Shi, L.; Cheng, R.; Yuan, D. Photocatalytic disinfection performance in virus and virus/bacteria system by Cu-TiO<sub>2</sub> nanofibers under visible light. *Environ. Pollut.* **2018**, *237*, 452–459. [CrossRef]
374. Rao, G.; Brastad, K.S.; Zhang, Q.; Robinson, R.; He, Z.; Li, Y. Enhanced disinfection of *Escherichia coli* and bacteriophage MS2 in water using a copper and silver loaded titanium dioxide nanowire membrane. *Front. Environ. Sci. Eng.* **2016**, *10*, 11. [CrossRef]
375. Venieri, D.; Gounaki, I.; Binas, V.; Zachopoulos, A.; Kiriakidis, G.; Mantzavinos, D. Inactivation of MS2 coliphage in sewage by solar photocatalysis using metal-doped TiO<sub>2</sub>. *Appl. Catal. B Environ.* **2015**, *178*, 54–64. [CrossRef]
376. De Pasquale, I.; Lo Porto, C.; Dell'Edera, M.; Petronella, F.; Agostiano, A.; Curri, M.L.; Comparelli, R. Photocatalytic TiO<sub>2</sub>-based nanostructured materials for microbial inactivation. *Catalysts* **2020**, *10*, 1382. [CrossRef]
377. Tijani, J.O.; Fatoba, O.O.; Petrik, L.F. A review of pharmaceuticals and endocrinedisrupting compounds: Sources, effects, removal, and detections. *Water. Air. Soil Pollut.* **2013**, *224*, 1770. [CrossRef]
378. Burkhardt-Holm, P. Endocrine disruptors and water quality: A state-of-the-art review. *Int. J. Water Resour. Dev.* **2010**, *26*, 477–493. [CrossRef]
379. Monneret, C. What is an endocrine disruptor? *Comptes Rendus Biol.* **2017**, *340*, 403–405. [CrossRef]
380. Tetreault, G.R.; Bennett, C.J.; Shires, K.; Knight, B.; Servos, M.R.; McMaster, M.E. Intersex and reproductive impairment of wild fish exposed to multiple municipal wastewater discharges. *Aquat. Toxicol.* **2011**, *104*, 278–290. [CrossRef]
381. Tabata, A.; Kashiwada, S.; Ohnishi, Y.; Ishikawa, H.; Miyamoto, N.; Itoh, M.; Magara, Y. Estrogenic influences of estradiol-17 beta, p-nonylphenol and bis-phenol-A on Japanese medaka (*Oryzias latipes*) at detected environmental concentrations. *Water Sci. Technol.* **2001**, *43*, 109–116. [CrossRef]

382. Villeneuve, S.; Cyr, D.; Lynge, E.; Orsi, L.; Sabroe, S.; Merletti, F.; Gorini, G.; Morales Suarez Varela, M.; Ahrens, W.; Baumgardt-Elms, C.; et al. Occupation and occupational exposure to endocrine disrupting chemicals in male breast cancer: A case-control study in Europe. *Occup. Environ. Med.* **2010**, *67*, 837–844. [[CrossRef](#)]
383. Li, D.; Zhou, Z.; Qing, D.; He, Y.; Wu, T.; Miao, M.; Wang, J.; Weng, X.; Ferber, J.R.; Herrinton, L.J.; et al. Occupational exposure to bisphenol-A (BPA) and the risk of self-reported male sexual dysfunction. *Hum. Reprod.* **2009**, *25*, 519–527. [[CrossRef](#)]
384. Tong, A.Y.C.; Braund, R.; Warren, D.S.; Peake, B.M. TiO<sub>2</sub>-assisted photodegradation of pharmaceuticals—A review. *Cent. Eur. J. Chem.* **2012**, *10*, 989–1027. [[CrossRef](#)]
385. AlAani, H.; Hashem, S.; Karabet, F. Photocatalytic (UV-A/TiO<sub>2</sub>) and photolytic (UV-A) degradation of steroid hormones: Ethinyl estradiol, levonorgestrel, and progesterone. *Int. J. Chem. Res.* **2017**, *10*, 1061–1070.
386. Arlos, M.J.; Liang, R.; Hatat-Fraile, M.M.; Bragg, L.M.; Zhou, N.Y.; Servos, M.R.; Andrews, S.A. Photocatalytic decomposition of selected estrogens and their estrogenic activity by UV-LED irradiated TiO<sub>2</sub> immobilized on porous titanium sheets via thermal-chemical oxidation. *J. Hazard. Mater.* **2016**, *318*, 541–550. [[CrossRef](#)]
387. Sornalingam, K.; McDonagh, A.; Zhou, J.L.; Johir, M.A.H.; Ahmed, M.B. Photocatalysis of estrone in water and wastewater: Comparison between Au-TiO<sub>2</sub> nanocomposite and TiO<sub>2</sub>, and degradation by-products. *Sci. Total Environ.* **2018**, *610–611*, 521–530. [[CrossRef](#)]
388. Zatloukalová, K.; Obalová, L.; Koči, K.; Čapek, L.; Matěj, Z.; Šnajdhaufová, H.; Ryczkowski, J.; Słowik, G. Photocatalytic degradation of endocrine disruptor compounds in water over immobilized TiO<sub>2</sub> photocatalysts. *Iran. J. Chem. Chem. Eng. IJCCCE* **2017**, *36*, 29–38. [[CrossRef](#)]
389. Ramírez-Sánchez, I.M.; Tuberty, S.; Hambourger, M.; Bandala, E.R. Resource efficiency analysis for photocatalytic degradation and mineralization of estriol using TiO<sub>2</sub> nanoparticles. *Chemosphere* **2017**, *184*, 1270–1285. [[CrossRef](#)]
390. Solcova, O.; Spacilova, L.; Maleterova, Y.; Morozova, M.; Ezechias, M.; Kresinova, Z. Photocatalytic water treatment on TiO<sub>2</sub> thin layers. *Desalin. Water Treat.* **2016**, *57*, 11631–11638. [[CrossRef](#)]
391. Ruokolainen, M.; Gul, T.; Permentier, H.; Sikanen, T.; Kostiaainen, R.; Kotiaho, T. Comparison of TiO<sub>2</sub> photocatalysis, electrochemically assisted Fenton reaction and direct electrochemistry for simulation of phase I metabolism reactions of drugs. *Eur. J. Pharmaceut. Sci.* **2016**, *83*, 36–44. [[CrossRef](#)]
392. Pazoki, M.; Parsa, M.; Farhadpour, R. Removal of the hormones dexamethasone (DXM) by Ag doped on TiO<sub>2</sub> photocatalysis. *J. Environ. Chem. Eng.* **2016**, *4*, 4426–4434. [[CrossRef](#)]
393. Chow, K.L.; Man, Y.B.; Tam, N.F.Y.; Liang, Y.; Wong, M.H. Removal of decabromodiphenyl ether (BDE-209) using a combined system involving TiO<sub>2</sub> photocatalysis and wetland plants. *J. Hazard. Mater.* **2017**, *322*, 263–269. [[CrossRef](#)]
394. Vasapollo, G.; Mele, G.; Del Sole, R.; Pio, I.; Li, J.; Mazzetto, S.E. Use of novel cardanol-porphyrin hybrids and their TiO<sub>2</sub>-based composites for the photodegradation of 4-Nitrophenol in water. *Molecules* **2011**, *16*, 5769–5784. [[CrossRef](#)]
395. Sraw, A.; Kaur, T.; Pandey, Y.; Sobti, A.; Wanchoo, R.K.; Toor, A.P. Fixed bed recirculation type photocatalytic reactor with TiO<sub>2</sub> immobilized clay beads for the degradation of pesticide polluted water. *J. Environ. Chem. Eng.* **2018**, *6*, 7035–7043. [[CrossRef](#)]
396. Wang, H.; Liang, Y.; Liu, L.; Hu, J.; Cui, W. Highly ordered TiO<sub>2</sub> nanotube arrays wrapped with g-C<sub>3</sub>N<sub>4</sub> nanoparticles for efficient charge separation and increased photoelectrocatalytic degradation of phenol. *J. Hazard. Mater.* **2018**, *344*, 369–380. [[CrossRef](#)]
397. Martins, A.S.; Nuñez, L.; Lanza, M.R.d.V. Enhanced photoelectrocatalytic performance of TiO<sub>2</sub> nanotube array modified with WO<sub>3</sub> applied to the degradation of the endocrine disruptor propyl paraben. *J. Electroanal. Chem.* **2017**, *802*, 33–39. [[CrossRef](#)]
398. Baranowska-Wójcik, E.; Szwajgier, D.; Oleszczuk, P.; Winiarska-Mieczan, A. Effects of titanium dioxide nanoparticles exposure on human health—a review. *Biol. Trace Elem. Res.* **2020**, *193*, 118–129. [[CrossRef](#)]
399. Heilgeist, S.; Sekine, R.; Sahin, O.; Stewart, R.A. Finding Nano: Challenges involved in monitoring the presence and fate of engineered titanium dioxide nanoparticles in aquatic environments. *Water* **2021**, *13*, 734. [[CrossRef](#)]
400. Jeon, S.-K.; Kim, E.-J.; Lee, J.; Lee, S. Potential risks of TiO<sub>2</sub> and ZnO nanoparticles released from sunscreens into outdoor swimming pools. *J. Hazard. Mater.* **2016**, *317*, 312–318. [[CrossRef](#)]
401. Choi, S.; Johnston, M.; Wang, G.-S.; Huang, C.P. A seasonal observation on the distribution of engineered nanoparticles in municipal wastewater treatment systems exemplified by TiO<sub>2</sub> and ZnO. *Sci. Total Environ.* **2018**, *625*, 1321–1329. [[CrossRef](#)]
402. Reddy, P.V.L.; Hernandez-Viezcás, J.A.; Peralta-Videa, J.R.; Gardea-Torresdey, J.L. Lessons learned: Are engineered nanomaterials toxic to terrestrial plants? *Sci. Total Environ.* **2016**, *568*, 470–479. [[CrossRef](#)]
403. Thiagarajan, V.; Ramasubbu, S. Fate and behaviour of TiO<sub>2</sub> nanoparticles in the soil: Their impact on staple food crops. *Water Air Soil Pollut.* **2021**, *232*, 274. [[CrossRef](#)]
404. Liu, R.; Zhang, X.; Pu, Y.; Yin, L.; Li, Y.; Zhang, X.; Liang, G.; Li, X.; Zhang, J. Small-sized titanium dioxide nanoparticles mediate immune toxicity in rat pulmonary alveolar macrophages in vivo. *J. Nanosci. Nanotechnol.* **2010**, *10*, 5161–5169. [[CrossRef](#)]
405. Acar, M.; Bulut, Z.; Ateş, A.; Nami, B.; Koçak, N.; Yıldız, B. Titanium dioxide nanoparticles induce cytotoxicity and reduce mitotic index in human amniotic fluid-derived cells. *Hum. Exp. Toxicol.* **2015**, *34*, 74–82. [[CrossRef](#)]
406. Biola-Clier, M.; Gaillard, J.-C.; Rabilloud, T.; Armengaud, J.; Carriere, M. Titanium dioxide nanoparticles alter the cellular phosphoproteome in A549 Cells. *Nanomaterials* **2020**, *10*, 185. [[CrossRef](#)]
407. Shi, H.; Magaye, R.; Castranova, V.; Zhao, J. Titanium dioxide nanoparticles: A review of current toxicological data. *Part. Fibre Toxicol.* **2013**, *10*, 15. [[CrossRef](#)]
408. Song, Y.; Li, X.; Du, X. Exposure to nanoparticles is related to pleural effusion, pulmonary fibrosis and granuloma. *Eur. Respir. J.* **2009**, *34*, 559–567. [[CrossRef](#)]

409. Lu, N.; Zhu, Z.; Zhao, X.; Tao, R.; Yang, X.; Gao, Z. Nano titanium dioxide photocatalytic protein tyrosine nitration: A potential hazard of TiO<sub>2</sub> on skin. *Biochem. Biophys. Res. Commun.* **2008**, *370*, 675–680. [[CrossRef](#)]
410. Mercer, R.R.; Scabillon, J.; Wang, L.; Kisin, E.; Murray, A.R.; Schwegler-Berry, D.; Shvedova, A.A.; Castranova, V. Alteration of deposition pattern and pulmonary response as a result of improved dispersion of aspirated single-walled carbon nanotubes in a mouse model. *Am. J. Physiol. Lung Cell Mol. Physiol.* **2008**, *294*, L87–L97. [[CrossRef](#)]
411. Hamilton, R.F., Jr.; Buford, M.C.; Wood, M.B.; Arnone, B.; Morandi, M.; Holian, A. Engineered carbon nanoparticles alter macrophage immune function and initiate airway hyper-responsiveness in the BALB/c mouse model. *Nanotoxicology* **2007**, *1*, 104–117. [[CrossRef](#)]
412. Boffetta, P.; Gaborieau, V.; Nadon, L.; Parent, M.F.; Weiderpass, E.; Siemiatycki, J. Exposure to titanium dioxide and risk of lung cancer in a population-based study from Montreal. *Scand. J. Work Environ. Health* **2001**, *27*, 227–232. [[CrossRef](#)]
413. Behnam, M.A.; Emami, F.; Sobhani, Z.; Dehghanian, A.R. The application of titanium dioxide (TiO<sub>2</sub>) nanoparticles in the photo-thermal therapy of melanoma cancer model. *Iran J. Basic Med. Sci.* **2018**, *21*, 1133–1139. [[CrossRef](#)]
414. Fujiwara, R.; Luo, Y.; Sasaki, T.; Fujii, K.; Ohmori, H.; Kuniyasu, H. Cancer therapeutic effects of titanium dioxide nanoparticles are associated with oxidative stress and cytokine induction. *Pathobiology* **2015**, *82*, 243–251. [[CrossRef](#)]
415. Bahadar, H.; Maqbool, F.; Niaz, K.; Abdollahi, M. Toxicity of nanoparticles and an overview of current experimental models. *Iran Biomed. J.* **2016**, *20*, 1–11. [[CrossRef](#)]
416. Song, B.; Zhang, Y.; Liu, J.; Feng, X.; Zhou, T.; Shao, L. Is neurotoxicity of metallic nanoparticles the cascades of oxidative stress? *Nanoscale Res. Lett.* **2016**, *11*, 291. [[CrossRef](#)]
417. McClements, D.J.; Xiao, H.; Demokritou, P. Physicochemical and colloidal aspects of food matrix effects on gastrointestinal fate of ingested inorganic nanoparticles. *Adv. Colloid Interface Sci.* **2017**, *246*, 165–180. [[CrossRef](#)]
418. Patri, A.; Umbreit, T.; Zheng, J.; Nagashima, K.; Goering, P.; Francke-Carroll, S.; Gordon, E.; Weaver, J.; Miller, T.; Sadrieh, N.; et al. Energy dispersive X-ray analysis of titanium dioxide nanoparticle distribution after intravenous and subcutaneous injection in mice. *J. Appl. Toxicol.* **2009**, *29*, 662–672. [[CrossRef](#)]
419. Wang, J.; Zhou, G.; Chen, C.; Yu, H.; Wang, T.; Ma, Y.; Jia, G.; Gao, Y.; Li, B.; Sun, J.; et al. Acute toxicity and biodistribution of different sized titanium dioxide particles in mice after oral administration. *Toxicol. Lett.* **2007**, *168*, 176–185. [[CrossRef](#)]
420. Wang, Y.; Cui, H.; Zhou, J.; Li, F.; Wang, J.; Chen, M.; Liu, Q. Cytotoxicity, DNA damage, and apoptosis induced by titanium dioxide nanoparticles in human non-small cell lung cancer A549 cells. *Environ. Sci. Pollut. Res. Int.* **2015**, *22*, 5519–5530. [[CrossRef](#)]
421. Sager, T.M.; Kommineni, C.; Castranova, V. Pulmonary response to intratracheal instillation of ultrafine versus fine titanium dioxide: Role of particle surface area. *Part. Fibre Toxicol.* **2008**, *5*, 17. [[CrossRef](#)]
422. Oberdörster, G.; Oberdörster, E.; Oberdörster, J. Nanotoxicology: An emerging discipline evolving from studies of ultrafine particles. *Environ. Health Perspect.* **2005**, *113*, 823–839. [[CrossRef](#)]
423. Warheit, D.B.; Webb, T.R.; Reed, K.L.; Frerichs, S.; Sayes, C.M. Pulmonary toxicity study in rats with three forms of ultrafine-TiO<sub>2</sub> particles: Differential responses related to surface properties. *Toxicology* **2007**, *230*, 90–104. [[CrossRef](#)]
424. Nemmar, A.; Melghit, K.; Al-Salam, S.; Zia, S.; Dhanasekaran, S.; Attoub, S.; Al-Amri, I.; Ali, B.H. Acute respiratory and systemic toxicity of pulmonary exposure to rutile Fe-doped TiO<sub>2</sub> nanorods. *Toxicology* **2011**, *279*, 167–175. [[CrossRef](#)]
425. Li, N.; Duan, Y.; Hong, M.; Zheng, L.; Fei, M.; Zhao, X.; Wang, J.; Cui, Y.; Liu, H.; Cai, J.; et al. Spleen injury and apoptotic pathway in mice caused by titanium dioxide nanoparticles. *Toxicol. Lett.* **2010**, *195*, 161–168. [[CrossRef](#)]
426. Kreyling, W.G.; Holzwarth, U.; Haberl, N.; Kozempel, J.; Hirn, S.; Wenk, A.; Schleh, C.; Schäffler, M.; Lipka, J.; Semmler-Behnke, M.; et al. Quantitative biokinetics of titanium dioxide nanoparticles after intravenous injection in rats: Part 1. *Nanotoxicology* **2017**, *11*, 434–442. [[CrossRef](#)]
427. Kreyling, W.G.; Holzwarth, U.; Schleh, C.; Kozempel, J.; Wenk, A.; Haberl, N.; Hirn, S.; Schäffler, M.; Lipka, J.; Semmler-Behnke, M.; et al. Quantitative biokinetics of titanium dioxide nanoparticles after oral application in rats: Part 2. *Nanotoxicology* **2017**, *11*, 443–453. [[CrossRef](#)]
428. Wang, J.; Chen, C.; Liu, Y.; Jiao, F.; Li, W.; Lao, F.; Li, Y.; Li, B.; Ge, C.; Zhou, G.; et al. Potential neurological lesion after nasal instillation of TiO<sub>2</sub> nanoparticles in the anatase and rutile crystal phases. *Toxicol. Lett.* **2008**, *183*, 72–80. [[CrossRef](#)]
429. Czajka, M.; Sawicki, K.; Sikorska, K.; Popek, S.; Kruszewski, M.; Kapka-Skrzypczak, L. Toxicity of titanium dioxide nanoparticles in central nervous system. *Toxicol. Vitro* **2015**, *29*, 1042–1052. [[CrossRef](#)]
430. Grissa, I.; Guezguez, S.; Ezzi, L.; Chakroun, S.; Sallem, A.; Kerkeni, E.; Elghoul, J.; El Mir, L.; Mehdi, M.; Cheikh, H.B.; et al. The effect of titanium dioxide nanoparticles on neuroinflammation response in rat brain. *Environ. Sci. Pollut. Res. Int.* **2016**, *23*, 20205–20213. [[CrossRef](#)]
431. Valentini, X.; Deneufbourg, P.; Paci, P.; Rugira, P.; Laurent, S.; Frau, A.; Stanicki, D.; Ris, L.; Nonclercq, D. Morphological alterations induced by the exposure to TiO<sub>2</sub> nanoparticles in primary cortical neuron cultures and in the brain of rats. *Toxicol. Rep.* **2018**, *5*, 878–889. [[CrossRef](#)]
432. Li, X.; Xu, S.; Zhang, Z.; Schluesener, H.J. Apoptosis induced by titanium dioxide nanoparticles in cultured murine microglia N9 cells. *Chin. Sci. Bull.* **2009**, *54*, 3830–3836. [[CrossRef](#)]

433. Ze, Y.; Hu, R.; Wang, X.; Sang, X.; Ze, X.; Li, B.; Su, J.; Wang, Y.; Guan, N.; Zhao, X.; et al. Neurotoxicity and gene-expressed profile in brain-injured mice caused by exposure to titanium dioxide nanoparticles. *J. Biomed. Mater. Res. A* **2014**, *102*, 470–478. [[CrossRef](#)]
434. Long, T.C.; Saleh, N.; Tilton, R.D.; Lowry, G.V.; Veronesi, B. Titanium dioxide (P25) produces reactive oxygen species in immortalized brain microglia (BV2): Implications for nanoparticle neurotoxicity. *Environ. Sci. Technol.* **2006**, *40*, 4346–4352. [[CrossRef](#)]
435. Gurr, J.R.; Wang, A.S.; Chen, C.H.; Jan, K.Y. Ultrafine titanium dioxide particles in the absence of photoactivation can induce oxidative damage to human bronchial epithelial cells. *Toxicology* **2005**, *213*, 66–73. [[CrossRef](#)]
436. Huerta-García, E.; Pérez-Arizti, J.A.; Márquez-Ramírez, S.G.; Delgado-Buenrostro, N.L.; Chirino, Y.I.; Iglesias, G.G.; López-Marure, R. Titanium dioxide nanoparticles induce strong oxidative stress and mitochondrial damage in glial cells. *Free Radic. Biol. Med.* **2014**, *73*, 84–94. [[CrossRef](#)]
437. Kohen, R.; Nyska, A. Invited review: Oxidation of biological systems: Oxidative stress phenomena, antioxidants, redox reactions, and methods for their quantification. *Toxicol. Pathol.* **2002**, *30*, 620–650. [[CrossRef](#)]
438. Hou, J.; Wang, L.; Wang, C.; Zhang, S.; Liu, H.; Li, S.; Wang, X. Toxicity and mechanisms of action of titanium dioxide nanoparticles in living organisms. *J. Environ. Sci.* **2019**, *75*, 40–53. [[CrossRef](#)]
439. Reeves, J.F.; Davies, S.J.; Dodd, N.J.; Jha, A.N. Hydroxyl radicals (\*OH) are associated with titanium dioxide (TiO<sub>2</sub>) nanoparticle-induced cytotoxicity and oxidative DNA damage in fish cells. *Mutat. Res.* **2008**, *640*, 113–122. [[CrossRef](#)]
440. Rajapakse, K.; Drobne, D.; Valant, J.; Vodovnik, M.; Levart, A.; Marinsek-Logar, R. Acclimation of *Tetrahymena thermophila* to bulk and nano-TiO<sub>2</sub> particles by changes in membrane fatty acids saturation. *J. Hazard. Mater.* **2012**, *221–222*, 199–205. [[CrossRef](#)]
441. Uchino, T.; Tokunaga, H.; Ando, M.; Utsumi, H. Quantitative determination of OH radical generation and its cytotoxicity induced by TiO<sub>2</sub>-UVA treatment. *Toxicol. In Vitro* **2002**, *16*, 629–635. [[CrossRef](#)]
442. Petković, J.; Kuzma, T.; Rade, K.; Novak, S.; Filipič, M. Pre-irradiation of anatase TiO<sub>2</sub> particles with UV enhances their cytotoxic and genotoxic potential in human hepatoma HepG2 cells. *J. Hazard. Mater.* **2011**, *196*, 145–152. [[CrossRef](#)]
443. Barthel, A.; Klotz, L.O. Phosphoinositide 3-kinase signaling in the cellular response to oxidative stress. *Biol. Chem.* **2005**, *386*, 207–216. [[CrossRef](#)]
444. Xia, T.; Kovoichich, M.; Brant, J.; Hotze, M.; Sempf, J.; Oberley, T.; Sioutas, C.; Yeh, J.I.; Wiesner, M.R.; Nel, A.E. Comparison of the abilities of ambient and manufactured nanoparticles to induce cellular toxicity according to an oxidative stress paradigm. *Nano Lett.* **2006**, *6*, 1794–1807. [[CrossRef](#)]
445. Geiser, M.; Casaulta, M.; Kupferschmid, B.; Schulz, H.; Semmler-Behnke, M.; Kreyling, W. The role of macrophages in the clearance of inhaled ultrafine titanium dioxide particles. *Am. J. Respir. Cell Mol. Biol.* **2008**, *38*, 371–376. [[CrossRef](#)]
446. Aderem, A.; Underhill, D.M. Mechanisms of phagocytosis in macrophages. *Annu. Rev. Immunol.* **1999**, *17*, 593–623. [[CrossRef](#)]
447. Liu, X.; Sui, B.; Sun, J. Size- and shape-dependent effects of titanium dioxide nanoparticles on the permeabilization of the blood-brain barrier. *J. Mater. Chem. B* **2017**, *5*, 9558–9570. [[CrossRef](#)]
448. Rothen-Rutishauser, B.M.; Schürch, S.; Haenni, B.; Kapp, N.; Gehr, P. Interaction of fine particles and nanoparticles with red blood cells visualized with advanced microscopic techniques. *Environ. Sci. Technol.* **2006**, *40*, 4353–4359. [[CrossRef](#)]
449. Stone, V.; Nowack, B.; Baun, A.; van den Brink, N.; von der Kammer, F.; Dusinska, M.; Handy, R.; Hankin, S.; Hassellöv, M.; Jøner, E.; et al. Nanomaterials for environmental studies: Classification, reference material issues, and strategies for physico-chemical characterization. *Sci. Total Environ.* **2010**, *408*, 1745–1754. [[CrossRef](#)]
450. Li, L.; Sillanpää, M.; Risto, M. Influences of water properties on the aggregation and deposition of engineered titanium dioxide nanoparticles in natural waters. *Environ. Pollut.* **2016**, *219*, 132–138. [[CrossRef](#)]
451. Skrabal, S.A.; Terry, C.M. Distributions of dissolved titanium in porewaters of estuarine and coastal marine sediments. *Mar. Chem.* **2002**, *77*, 109–122. [[CrossRef](#)]
452. Shi, X.H.; Jiang, P.; Wang, H.Y.; Zhang, S.H.; Ji, T.; Liu, W.J.; Zhou, H.Y. The redshifted hydrogen Balmer and metastable He I absorption line system in mini-FeLoBAL quasar SDSS J112526.12+002901.3: A parsec-scale accretion inflow? *Astrophys. J.* **2016**, *829*, 96. [[CrossRef](#)]
453. Westerhoff, P.; Song, G.; Hristovski, K.; Kiser, M.A. Occurrence and removal of titanium at full scale wastewater treatment plants: Implications for TiO<sub>2</sub> nanomaterials. *J. Environ. Monit.* **2011**, *13*, 1195–1203. [[CrossRef](#)]
454. Sun, J.; Guo, L.H.; Zhang, H.; Zhao, L. UV irradiation induced transformation of TiO<sub>2</sub> nanoparticles in water: Aggregation and photoreactivity. *Environ. Sci. Technol.* **2014**, *48*, 11962–11968. [[CrossRef](#)]
455. Kunhikrishnan, A.; Shon, H.K.; Bolan, N.S.; El Saliby, I.; Vigneswaran, S. Sources, Distribution, Environmental Fate, and Ecological Effects of Nanomaterials in Wastewater Streams. *Crit. Rev. Environ. Sci. Technol.* **2015**, *45*, 277–318. [[CrossRef](#)]
456. Valério, A.; Sárria, M.P.; Rodríguez-Lorenzo, L.; Hotza, D.; Espiña, B.; Gómez González, S.Y. Are TiO<sub>2</sub> nanoparticles safe for photocatalysis in aqueous media? *Nanoscale Adv.* **2020**, *2*, 4951–4960. [[CrossRef](#)]
457. Rueda-Marquez, J.J.; Levchuk, I.; Fernández Ibañez, P.; Sillanpää, M. A critical review on application of photocatalysis for toxicity reduction of real wastewaters. *J. Clean. Prod.* **2020**, *258*, 120694. [[CrossRef](#)]

- 
458. Miranda-García, N.; Suárez, S.; Maldonado, M.I.; Malato, S.; Sánchez, B. Regeneration approaches for TiO<sub>2</sub> immobilized photocatalyst used in the elimination of emerging contaminants in water. *Catal. Today* **2014**, *230*, 27–34. [[CrossRef](#)]
459. Laisney, J.; Rosset, A.; Bartolomei, V.; Predoi, D.; Truffier-Boutry, D.; Artous, S.; Bergé, V.; Brochardd, G.; Michaud-Soret, I. TiO<sub>2</sub> nanoparticles coated with bio-inspired ligands for the safer-by-design development of photocatalytic paints. *Environ. Sci. Nano* **2021**, *8*, 297–310. [[CrossRef](#)]

**Disclaimer/Publisher’s Note:** The statements, opinions and data contained in all publications are solely those of the individual author(s) and contributor(s) and not of MDPI and/or the editor(s). MDPI and/or the editor(s) disclaim responsibility for any injury to people or property resulting from any ideas, methods, instructions or products referred to in the content.